Development of Catalytic PolyHIPEs using MOFs for the Hydrolysis of Dipeptides

Toby Daniel Watts

(tdw23@kent.ac.uk)

Declaration

I declare that this thesis is my own work, and has been written in my own words. Appropriate care has been taken to accurately reference the works of others where necessary.

Signed –

Toby Daniel Watts

27th November 2019

Number of pages: 139

School of Chemistry and Forensics

Acknowledgements

Firstly, I would like to thank Dr. Simon Holder for giving me the opportunity to carry out this project. I would also like to thank him for his constant dedication to the progression of the project, his advice and extensive knowledge on all things related to my work. I would also like to thank Dr. Ewan Clark, who was my secondary supervisor during this project, for his help with any synthetic struggles and advice on NMR related problems.

I would like to thank Dr. Alex Wright for his initial help with synthesis and constant advice on any issues, whether synthetic or analytical, taking time away from his work to look for a solution. Additionally, Professor Anna Corrias for her expert knowledge of TGA, and more specifically the more problematic Surfer porosimeter, throughout the many issues with the piece of equipment she always found a solution. Thanks also goes to all the other academics and technical staff who have helped me throughout the past year.

Next, I would like to thank the individuals, who have been working with me every day over the past year: Aaron, Alex, Anna, Athina, Giada, Jed and Matt. Their advice and support on work related problems and their friendship throughout is much appreciated and attributed to a much more enjoyable work environment.

I would like to thank Tora who has supported and motivated me throughout to stay on track and for giving me another focus outside of studying.

Finally and most importantly, I would like to thank my family and specifically my parents for their unconditional support throughout the whole of my university studies and for the encouragement to achieve my goals.

Abstract

Metal Organic Frameworks (MOFs) are materials that have shown impressive catalytic activity in a variety of reactions. Poly high internal phase emulsions (PolyHIPEs) are highly porous templated networks that have shown the ability to store active catalysts within their pores. This work looks at the use of MOFs and polyHIPE-MOFs in the hydrolysis of diglycine in water and water/THF.

MOF-808 is known to be one of the most effective MOFs in catalysis and has been used in a number of reactions. Therefore, it was decided that MOF-808 was the main focus in the hydrolysis studies, and would be subsequently embedded in the polyHIPE. The hydrolysis studies proved that MOF-808 was an extremely effective catalyst under a number of different conditions.

The superabsorbent swelling ability of the polyHIPE made up of styrene and divinylbenzene was important in the hydrolysis studies, as the polymer was only effective when a 50:50 mixture of d-THF and D_2O was used. This was evident from the swelling studies of the polyHIPE, which showed a major difference from 100 % water to a 50:50 mix with THF. This was due to the water being absorbed onto the surface of the polymer, but it was unable to absorb inside the polymer where the active catalyst was stored.

The other MOFs used in this study showed varying levels of success in the hydrolysis of diglycine, although compared to MOF-808 the percentage conversion to glycine was extremely low. The MOFs used were mainly zirconium based although a titanium and bimetallic (Zr-Ti) MOF were used to compare the effect of metal centres. The zirconium, titanium and bimetallic equivalent MOFs varied in there catalytic activity, the titanium MOF showed the least conversion, there was a slight increase in conversion for the zirconium MOF and a significant increase for the bimetallic MOF. This was due to the large surface areas and porosity from the titanium metal centre and the stability provided by the zirconium metal centre.

List of Abbreviations

<	Less than
>	Greater than
AIBN	Azobisisobutyronitrile
bdc	1,4 benzenedicarboxylic acid
BET	Brunauer-Emmett-Teller
btc	1,3,5 benzenetricarboxylic acid
C	Celsius
Cu	Copper
CWA	Chemical Warfare Agent
D_2O	Deuterium oxide
DMF	N,N,Dimethylformamide
DMNP	Methyl paraoxon
d-THF	Deuterated tetrahydrofuran
DUT	Dresden University of Technology
DVB	Divinylbenzene
FT-IR	Fourier transform-infra-red spectroscopy
gly-gly	Diglycine
g	Gram
HIPE	High internal-phase emulsion
HKUST	Hong Kong University of Science and Technology

IR	Infra-red
K	Kelvin
MIL	Materials Institute Lavoisier
ml	Millilitre
mM	Millimolar
mmol	Millimol
MOF	Metal-Organic Framework
ndc	Naphthalenedicarboxylic acid
NHC	N-Heterocyclic carbene
NMR	Nuclear magnetic resonance
NNU	Nanjing Normal University
NU	Northwestern University
PCN	Porous coordination network
ppm	Parts per million
PTFE	Polytetrafluoroethylene
PtNP	Platinum nanoparticle
PXRD	Powder x-ray diffraction
Q	Swelling degree
Qv	Swelling degree by volume
RCM	Ring closing metathesis
ROMP	Ring opening metathesis polymerisation

rpm	Revolutions per minute
SBU	Secondary building unit
SEM	Scanning electron microscopy
SEM-EDS/EDX	Scanning electron microscopy-Energy Dispersive X-Ray Spectroscopy
SMO	Sorbitan monooleate
tdc	Thiophenedicarboxylic acid
TFA	Trifluoroacetic acid
TGA	Thermal gravimetric analysis
THF	Tetrahydrofuran
Ti	Titanium
UiO	Universitetet i Oslo
UV	Ultraviolet
VBC	Vinyl benzyl chloride
Zr	Zirconium

Contents

Chapter 1 – Introduction

1.1 Metal Organic Frameworks

Metal organic frameworks (MOFs) are a category of porous materials with large internal surface areas that have shown great promise for the applications as heterogeneous catalysis, and in gas storage, separation and chemical sensing.[1] The formation of a MOF structure involves the connection of metal cations or clusters to multitopic organic linkers/ligands to form an extended crystalline structure.[2] Due to the large assortment of metal cations and organic linkers that are accessible for the formation of MOFs, this results in lots of structural possibilities.
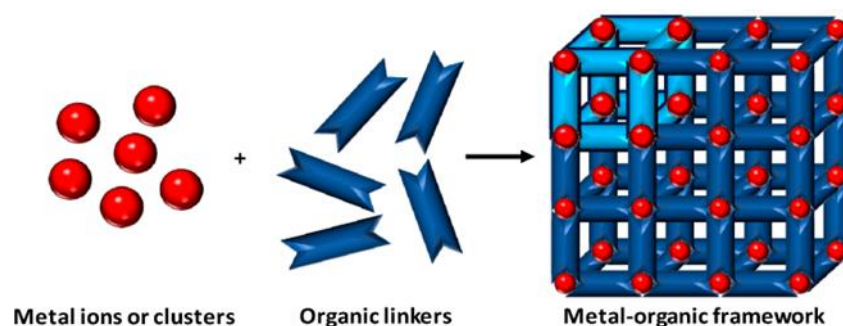
Figure 1.1 A schematic illustrating the formation of a metal organic framework. Reprinted with permission from Ref.[2]

1.1.1 Metal Clusters/Ions and Organic Linkers

Metal ions or clusters (also known as the secondary building unit or SBU), and organic linkers are connected via strong covalent bonds (shown in Figure 1.1).[3] As previously mentioned, there is a plethora of both of these two constituents that can be used. Some notable examples from literature are shown below:
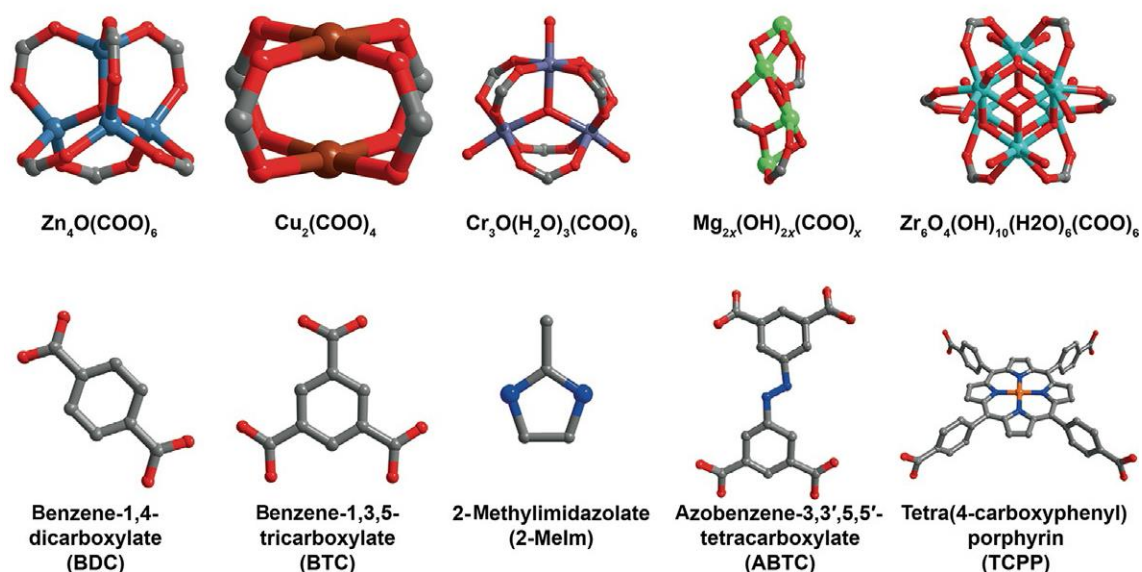
Figure 1.2 Examples of metal ions/clusters (top row) and organic linkers (bottom row). Colour code: Grey – carbon, red – oxygen, dark blue – nitrogen, light blue – zinc, brown – copper, purple – chromium, green – magnesium, turquoise – zirconium, orange – iron. Reprinted with permission from Ref.[4]

A variety of metals have been used (shown in Figure 1.2), all proving useful in a number of different applications. Zinc[5], copper[6] and aluminium[7] MOFs have been used in gas storage and delivery; this is due to their large surface areas. Iron[8], zinc[9] and zirconium[10] frameworks have been used for biomedical applications, more specifically there has been research into their uses in drug delivery as the properties of the structure can be modified and the pore size can be finely tuned.[11] There are a number of different metal centres used in MOF catalysis; cobalt[12], cadmium[13], silver[14], chromium[15] and palladium[16] have all been reported in catalytic procedures. MOFs have also been used in sensing due to their luminescence properties, the majority of luminescent MOFs are made up of metals from the lanthanide series.[17]

 A ligand is defined as an ion or molecule that is attached to a metal atom by coordination bonding. Ligands act as electron pair donors (Lewis bases) and the central metal atom acts as an electron pair acceptor (Lewis acid). Ligands have at least one atom with a donor pair of electrons which are used to form a covalent bond with metal atom.[18] The majority of organic linkers used are carboxylates such as benzene-1,4-dicarboxylate (bdc) and benzene-1,3,5-

3

tricarboxylate (btc), they are used to bridge to the SBU. Phosphonates[19], pyridines[20] and imidazoles[21] can be used as alternative linkers. The choice of ligand is vital for determining the pore size, ditopic and tritopic ligands will vary the pore shape of the MOF.[22,23] Having a longer linker will increase the diameter of the pores.[24]

During the past half century, porous materials such as zeolites, coordination polymers and metal organic frameworks have been extensively studied. The porosity of these materials was of major interest due to their ability to host guest molecules through diffusion into their structures. Porosity results from the presence of lengthy organic linkers which create large storage areas and a high volume of absorption. MOF-5 ($Zn_4O(bdc)_3$) and HKUST-1 ($Cu_3(btc)_2$) were the benchmarks in the early history of MOFs with extensive porosity. These were closely followed by MIL-101 ($Cr_3O(OH)(H_2O)_2(bdc)_3$) which showed high chemical stability, this provided an important breakthrough as early MOF synthesis showed a large amount of collapse in MOF structures.[25,26]
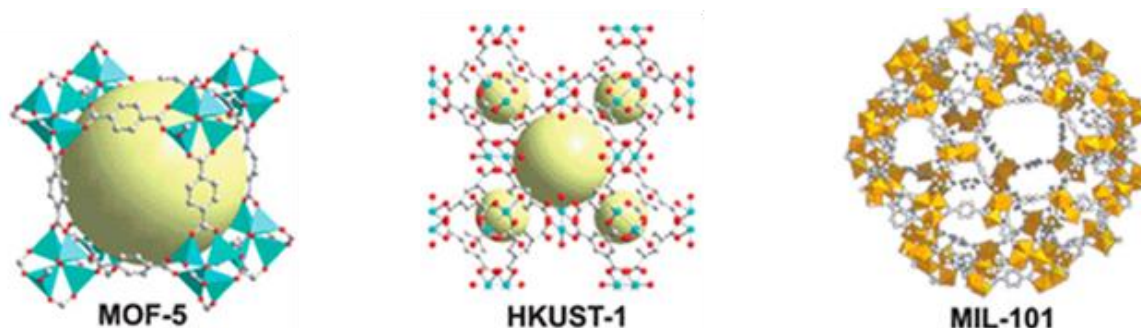
Figure 1.3 An illustration of MOF-5, HKUST-1 and MIL-101. Reprinted with permission from Ref.[27]

The discovery of these early MOFs (shown in Figure 1.3) which exhibited many desirable properties such as their high porosity, large surface areas and extensive tunability led to a wide range of research to further develop MOFs.

1.1.2 Synthetic Approaches

There are a number of different ways to synthesise a MOF, the 'conventional' way of synthesising a MOF was using conventional heating with either a solvothermal or non-

solvothermal temperature range. Solvothermal reactions consist of the metal cation and organic linker being dissolved in the chosen solvent, and being sealed in a closed reaction vessel which is heated above the chosen solvents boiling point. The majority of solvothermal reactions will take place at higher temperatures exceeding 100°C for an extended amount of time (> 12 hours). The most common solvent used in these reactions is DMF due to its high boiling point and its ability to dissolve most multitopic organic linkers. Other polar solvents such as methanol and acetonitrile can be used. Acetic acid is commonly used as a modulator in these reactions to inhibit the crystallisation of the metal complexes.[28] Once the complex has been heated solvothermally (shown in Figure 1.4), the material is commonly retrieved via filtration or centrifugation before being dried under vacuum to yield the crystalline product. In some cases activation may be required, this refers to the removal of any excess solvent or other chemical used during the synthesis. Activation can be done by heating under vacuum or via solvent exchange, solvent exchange is where the high boiling point solvent (i.e. DMF) is exchanged with a lower boiling point solvent (i.e. methanol) before being removed under milder vacuum conditions.[29]
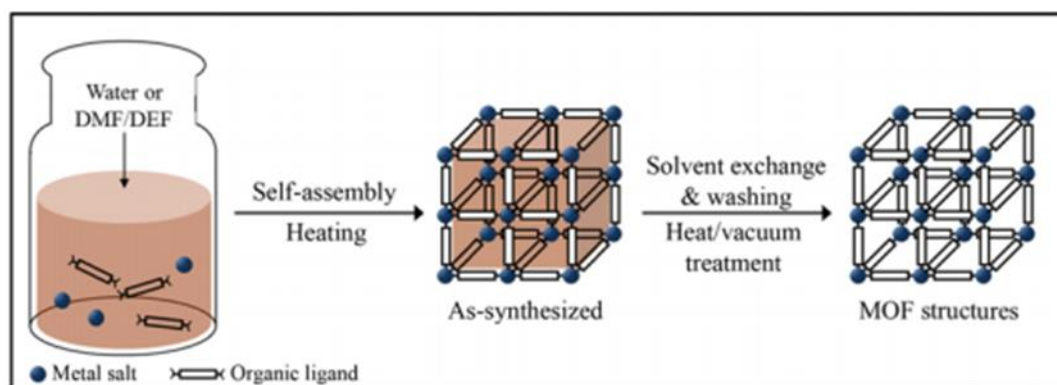
Figure 1.4 A schematic illustration showing the solvothermal synthesis of a MOF followed by activation. Reprinted with permission from Ref.[30]

Non-solvothermal refers to a reaction taking place at or below the boiling point of the solvent.[31] Non-solvothermal reactions are commonly defined as precipitation reactions followed by slow cooling of the system to recrystallize.[32]
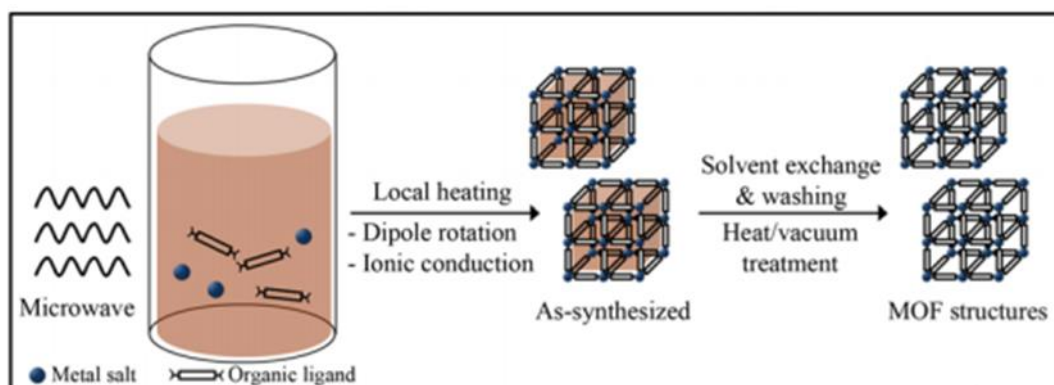
Figure 1.5 A schematic illustration showing the microwave assisted synthesis of a MOF. Reprinted with permission from Ref.[30]

Microwave-assisted synthesis (shown in Figure 1.5) refers to the interaction of electromagnetic waves with mobile electric charges. This can be either a solution with polar solvent molecules or solids electrons. This synthesis is normally carried out at temperatures exceeding 100°C and the reaction will rarely take more than 1 hour.[33]

There are many more ways of synthesising MOFs including mechanochemical, electrochemical and sonochemical. Using other synthetic methods will result in the formation of novel compounds with varying particle sizes, which can alter the catalytic abilities of the framework.

1.1.3 Metal Cluster and Organic Linker Assembly

The choice of metal cluster and organic linker in MOFs is vital when deciding the connected cluster desired, there are infinite different combinations of the two, which will inherently alter the capabilities of the MOF. The active sites on a MOF can initially come from the inorganic or organic component, or through the introduction of a host molecule which acts as an active site.[34] The node connections of the framework will have an effect on applications such as catalysis. A simple comparison can be made between 6, 8 and 12 connected nodes, the 6-connected node has the greatest catalytic activity due to having more vacant sites within the framework when compared to the 12-connected node. The 12-connected node relies on structural defects to work as catalytic sites, the 8-connected node shows catalytic activity lower than the 6-connected node but greater than the 12-connected.[35]

6
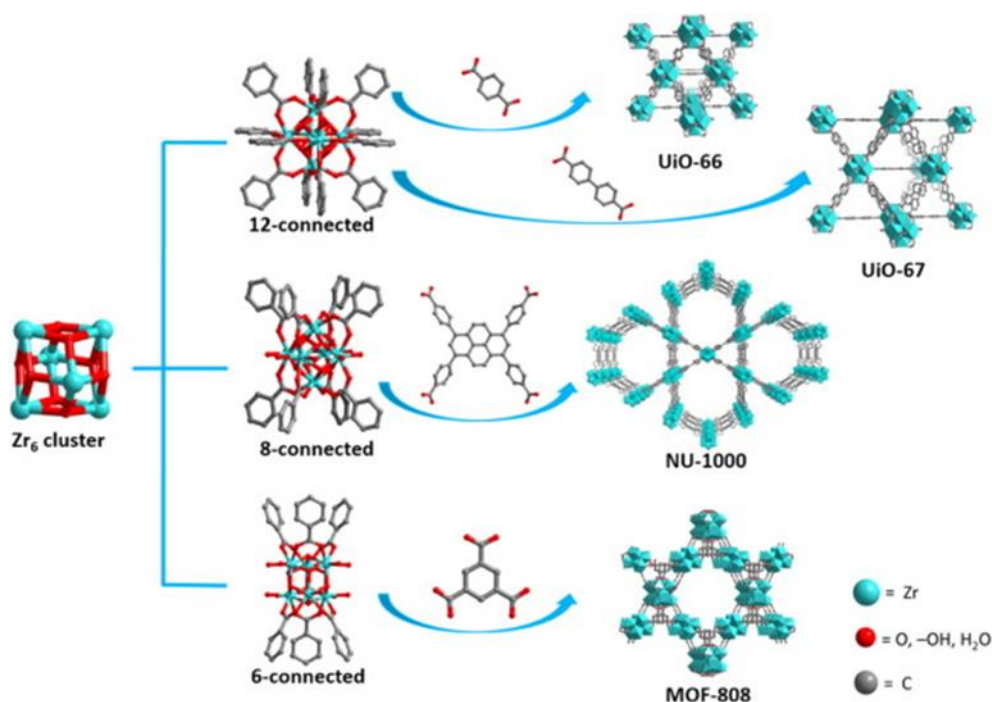
Figure 1.6 An illustration showing 6, 8 and 12-connected nodes and their resultant MOFs. Reprinted with permission from Ref.[36]

The organic linkers in each MOF are 1,4-benzenedicarboxylic acid (bdc) for UiO-66, biphenyl-4,4'-dicarboxylic acid (BPDC) for UiO-67, 1,3,6,8-tetrakis(*p*-benzoate)pyrene (TBAPy^{4-}) for NU-1000 and 1,3,5-benzenetricarboxylic acid (btc) for MOF-808 (shown in Figure 1.6). Studies to show catalytic activity and its relation to the connected nodes have been carried out by looking at titrations and degradation. A titration study looked at the missing linkers, which are caused by structural defects.[35] The cause of these defects occurs either during the synthetic procedure or through post modification. To control the formation of these structural defects during the synthesis of a MOF, a functionalised modulator can be used to subsidise defect formation and compensate for their absence.[37]

1.1.4 Types of Metal Organic Framework

Metal organic frameworks are made up of a single metal cluster or metal ion but in some MOFs there may be cases of two metal clusters/ions, these MOFs are known as bimetallic. For the purpose of this thesis, this section will focus on zirconium, titanium and bimetallic (zirconium-titanium) MOFs in more detail.

1.1.4.1 Zirconium MOFs

Zirconium MOFs are one of the most extensively studied metal centres, the first Zr-MOFs reported were synthesised by Lillerud et al. in 2008, this was the UiO series.[38] UiO-66 is constructed by linking 12-connected $[Zr_6(\mu_3\text{-}O)_4(\mu_3\text{-}OH)_4(COO)_{12}]$ clusters with linear benzene-dicarboxylic acid (bdc) linkers.[39] Zr-MOFs are said to have superior stability against moist atmosphere, aqueous solutions and basic or acidic media.[40] The kinetic inertness of the Zr-carboxylate bonds causes robustness which results in Zr-MOFs being used in innovative applications.[41] Conversely, one of the issues with Zr-MOFs is the harsher reaction conditions they undergo in the synthesis process, with high temperatures and larger concentrations of acids for uses as modulators.[42]

1.1.4.2 Titanium MOFs

According to Zou et al., Ti-MOFs have been overlooked when compared to Zr-MOFs when it comes to the amount of research into them.[43] The lack of studies using titanium is seen as a surprise due to its large abundance in the earths crust as well as having low toxicity and redox activity. The first reported Ti-MOF was MIL-125, which was synthesised in 2009, a year after the first Zr-MOF. MIL-125 is constructed by 12-connected $[Ti_8O_8(OH)_4(COO)_{12}]$ clusters with bdc linkers. MIL-125 forms the same topology as UiO-66 although the cluster is less symmetric.[39] In addition, titanium-oxo clusters can be seen as TiO_2 nanoparticles, which results in them having photocatalytic properties.[44] However, there are some challenges that Ti-MOFs face such as the poor reversibility of the metal-ligand bond which prevents the formation of crystalline products.[45]

1.1.4.3 Bimetallic Ti-Zr MOFs

Ti-Zr bimetallic MOFs have been studied to attempt to find a solution for the synthetic difficulties Ti-MOFs encounter, namely the highly sensitive nature to reaction conditions. On the other hand, Zr-MOFs are robust enough to form a wide catalogue of different MOFs, therefore by combining the two, Ti containing MOFs may be more readily synthesised.[46] PCN-

415 and PCN-416 were the first synthesised bimetallic Ti-Zr MOFs, [$Ti_8Zr_2O_{12-}$ ($MeCOO)_{16}$] clusters and linear linkers containing different lengths and functional groups were used and the synthesis route followed was similar to that of Zr-MOFs.[47] PCN-415 and PCN-416 once again shared the same topology as UiO-66 (shown in Figure 1.7), they displayed impressive chemical stability, tuneable photo response and good activity towards photocatalytic reactions.[39]
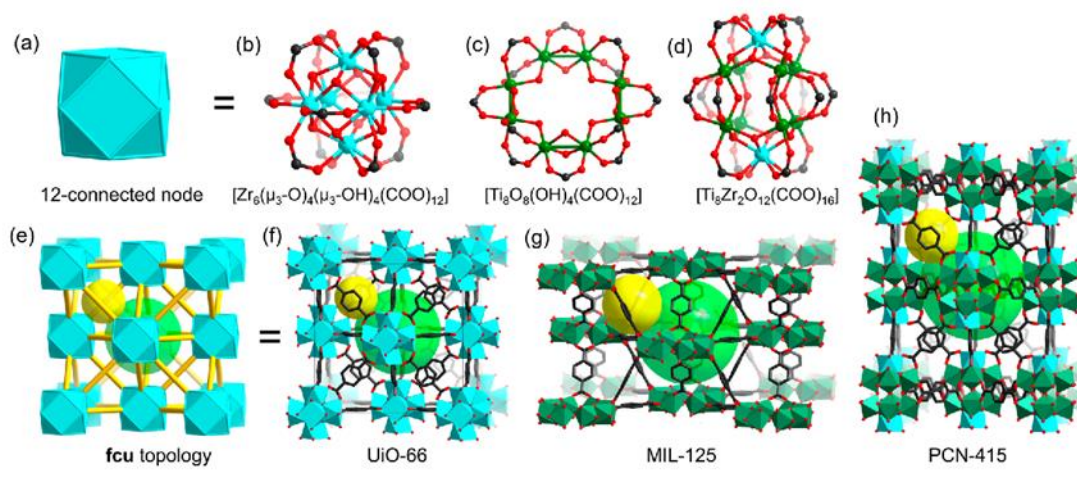
Figure 1.7 Illustration showing the structures and topology of UiO-66 (b, f), MIL-125 (c,g) and PCN-415 (d,h). Reprinted with permission from Ref.[39]

1.2 Poly High Internal Phase Emulsions

1.2.1 Emulsion Polymerisation

An emulsion polymerisation involves the heterogeneous free radical polymerisation of a reasonably hydrophobic monomer in water by a water-in-oil emulsifier.[48] This is followed by an initiation process using either a water insoluble initiator or oil insoluble initiator. Common monomers used in these polymerisations include styrene, acrylate and methacrylate esters and vinyl chloride. As the polymerisation progresses, particle nuclei form resulting in a large interfacial oil-water area. To counteract this a non-ionic surfactant is used to stabilise the emulsion and prevent coagulation.[49]
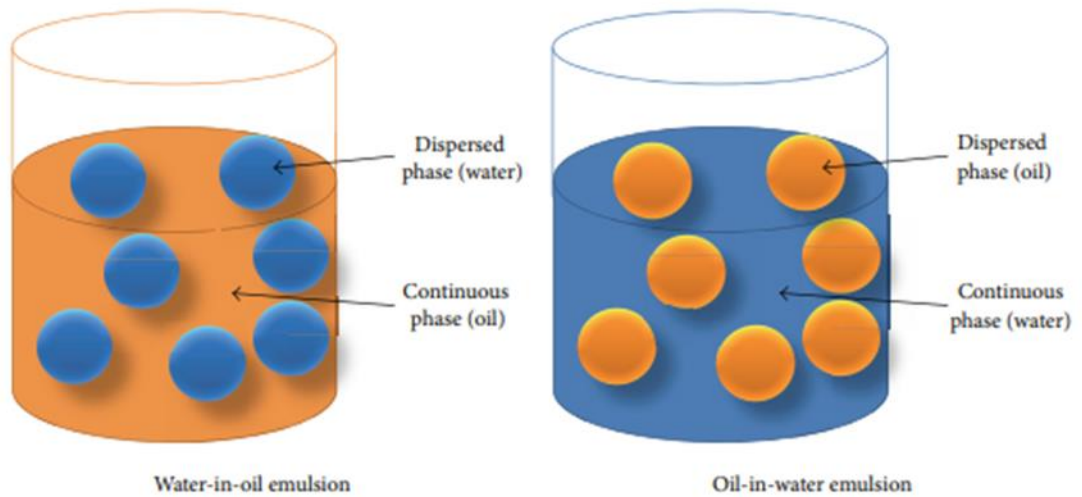
Figure 1.8 Illustration showing an oil-in-water and water-in-oil emulsion. Reprinted with permission from Ref.[50]

Oil-in-water emulsions (shown in Figure 1.8) are seen as being thermodynamically unstable, there are 5 mechanisms that cause this instability: creaming, flocculation, coalescence, Ostwald ripening and phase inversion.[51] Coalescence and phase inversion can be counteracted by using neutral pH conditions, creaming and flocculation is dependent on factors such as protein-oil ratio, temperature average droplet size and ionic strength, these conditions must be optimised to neutralise these instability factors.[52] Ostwald ripening (shown in Figure 1.9) can occur when the dispersed phase contains some solubility in the continuous phase. Ostwald ripening is the occurrence when larger droplets grow in place of smaller ones due to the diffusion of the material in the dispersed phase.[51]
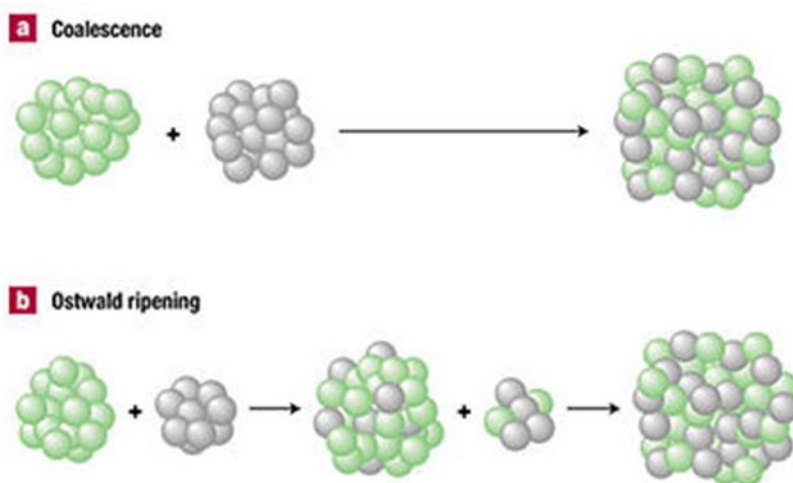
Figure 1.9 Schematic illustration displaying coalescence and Ostwald ripening. Reprinted with permission from Ref.[53]

The instability caused by these factors means that reaction conditions must be meticulously thought out and optimised to ensure the accurate synthesis of the emulsion.

1.2.2 High Internal Phase Emulsions

High internal phase emulsions (HIPE) are oil-in-water emulsions where the volume of the internal phase is higher than 74.05% of the total volume of emulsion.[54] In an oil-in-water emulsion, the oil is in the internal phase and the water is the continuous phase.[55] These emulsions have many applications which include the food, cosmetic, pharmaceutical and petroleum industries. However, they could also be used as a building block into synthesising highly porous polymers.[56] In the 1960's, reports of a polymer foam were published which would be named a Poly High Internal Phase Emulsion (PolyHIPE). PolyHIPEs were synthesised through polymerising the continuous phase of the HIPE.[54] The preparation involved polymerising water in oil (w/o) HIPEs where monomers and crosslinkers make up the organic continuous phase. This emulsion was subsequently stabilised by a non-ionic surfactant, before the addition of an aqueous solution to make the emulsion.[57] Upon curing the emulsion, a porous polymer composite forms. Figure 1.10 refers to the process of forming a polyHIPE. The initial organic phase is mixed before the addition dropwise of the aqueous phase, the two phases are then mixed to homogenise before being cured. Finally, the polymer is dried to form the porous composite.
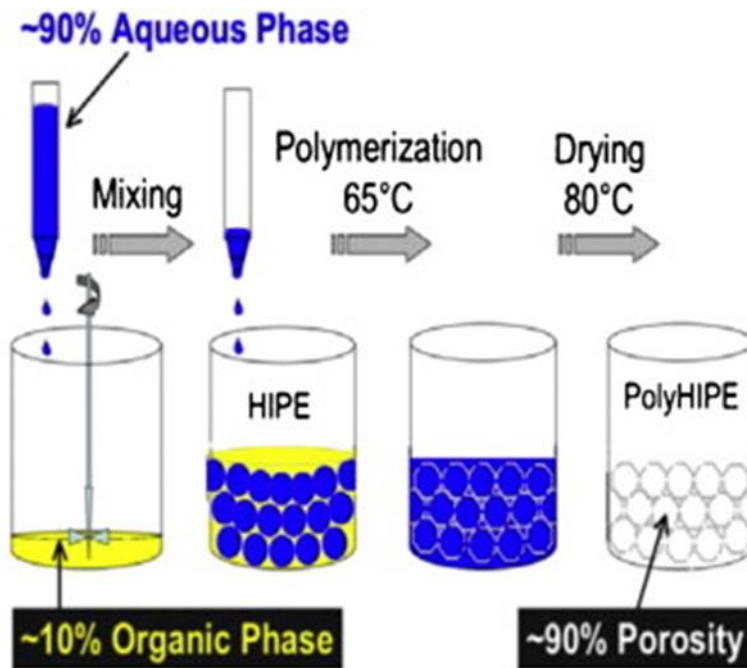
Figure 1.10 Schematic illustration showing the polymerisation to form a polyHIPE. Reprinted with permission from Ref.[58]

Within the polyHIPE there are three specific areas (shown in Figure 1.11), the first are known as 'voids' that present as spherical cavities. Next are 'windows' which are interconnecting pores between each void and its neighbours. Thirdly, the more miniscule pores that appear within the walls of the material are known as 'pores'.[59] The most common polyHIPEs are styrene-DVB (divinylbenzene) based, they can be visualised using SEM where distinct pores can be seen.
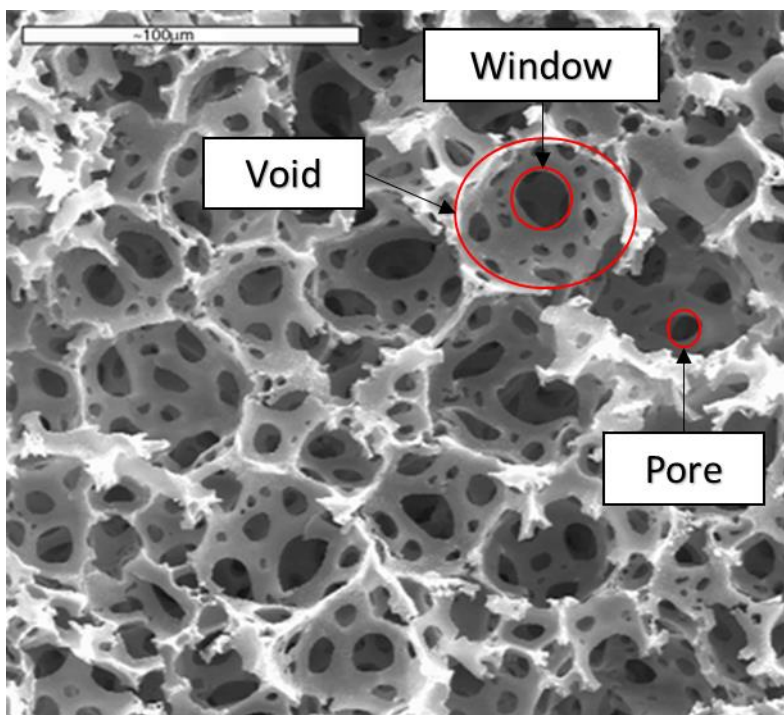
Figure 1.11 SEM image of a styrene-DVB based polyHIPE clearly showing the pores. Reprinted with permission from Ref.[60]

PolyHIPEs can also show impressive swelling degrees, this was shown in a study where the absorption degrees of water were up to 330.[61] The polyHIPE used in this study had an organic phase (toluene) of 86% with a crosslinking co-monomer (N,N'-methylenebisacrylamide) to form a hydrophilic polyHIPE. This could be attributed to the large surface areas possessed by these materials, with BET surface areas of up to 1210 $m^2\,g^{-1}$ having been recorded.[62] In this study the polyHIPE was made up of vinylbenzyl choride (VBC) (31.54 mmol), styrene (12.35 mmol) and divinylbenzene (DVB) (5 mmol). The polyHIPE was hypercrosslinked using an iron chloride catalyst. PolyHIPEs are also known for their ability to store active catalysts within their pores.[63]

1.2.3 PolyHIPE Porosity

PolyHIPEs are generally defined as highly porous materials; subsequently there are a number of ways in which the porosity of polyHIPEs can be altered. Factors such as changing the quantity of the crosslinking monomers, the level of one monomer increasing can result in decreased pore sizes.[64] The amount of surfactant used can effect the pore size (shown in

Figure 1.12), low surfactant concentrations cause a closed cell structure with smaller pore sizes, whereas a greater amount of surfactant resulted in unconnected polymers with higher pore sizes. Increased monomer concentrations meant styrene required less surfactant to produce open cell structures with larger pore sizes.[65]
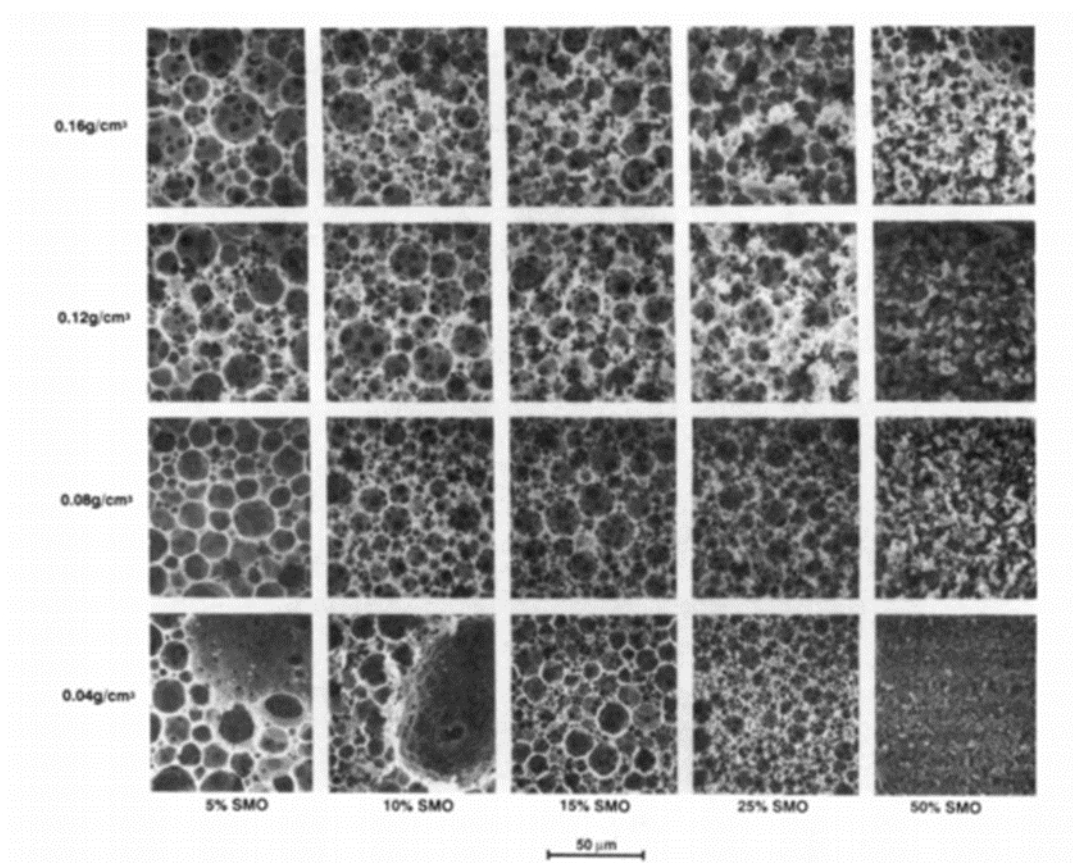
Figure 1.12 Illustration showing SEM images of a polyHIPE using different amounts of surfactant (SMO) and varying monomer (DVB) content (g/cm³). Reprinted with permission from Ref.[64]

The amount of aqueous electrolyte added also results in changes of pore size, an increased amount of K_2SO_4 resulted in smaller pore sizes. The aqueous electrolyte is used to increase the stability of the emulsion.[66] Subsequently, changes in pore size can occur due to swelling of the polymer composite, when the polymer is swollen it attains additional porosity that in the dried state is not arising. The swelling ability of the polyHIPE will be important in this study as when the polyHIPE incorporates the MOF into its matrix, the polymer will need to swell in order for the solvent to permeate into the matrix of the polymer. This will allow the MOF to show its catalytic activity in the hydrolysis studies that will be pertinent to the success of this study.

14

Further to this porogenic solvents can be used to increase the surface area of the polymer matrix, this results in a more porous material.[67] Effects on surface area and porosity will be important within this thesis to explain catalytic activity of different materials.

1.2.4 PolyHIPE Pores Storing Active Catalysts

PolyHIPEs have been reported as having pores which can store active catalysts, they can play host to different materials such as MOFs,[68] platinum nanoparticles (PtNPs)[69] and N-heterocyclic carbene ligands (NHCs).[70] One study looking at polyHIPE supported PtNPs showed they could be reused up to 1500 times as catalysts in reduction reactions. The catalyst was added into the aqueous phase and stirred in homogeneously.[69] Another study researched the propensity of a polyHIPE to support an NHC-bearing ruthenium alklydene complex for its use as a catalyst in ring opening metathesis polymerisation (ROMP). In this case, the polyHIPE was ground into a powder and stirred with the catalyst in a Schlenk tube before removal of the solvent and drying of the material. They found that the material synthesised was not reusable for ROMP but it could be recycled and used in ring closing metathesis (RCM).[70] For the purpose of this thesis, the addition of MOF catalysts into the polyHIPE pores will be looked into in more depth.

1.2.4.1 PolyHIPE-MOFs

Research into MOFs encapsulated within a polyHIPE has gained interest over the last 10 years due to their possible applications in separation and catalysis.[71,72,73,74,75] Studies have shown alternative ways of synthesising polyHIPE-MOF composites, one reports the addition of pieces of polyHIPE (made of 4-vinylbenzyl chloride and divinylbenzene) to the metal cluster $(Cu(NO_3)_2.3\ H_2O)$ and organic linker (btc) used in the MOF with the appropriate solvent using a hydrothermal formation.[68] The pieces of polyHIPE are added into a flask, after which the metal cluster and organic linker in a solution of ethanol and water (50/50) are added through a dropping funnel with the flask under reduced pressure. Once the MOF has fully permeated into the polyHIPE, the composite is dried to yield a blue monolith.[68] On the other hand,

15

another study prepares the polyHIPE-MOF using the standard emulsion polymerisation for a polyHIPE. Using this synthesis, the MOF was added into the aqueous phase and stirred in to create a homogenous mixture with the MOF fully dispersed throughout the polymer composite.[76] The concern behind combining these two materials was would they have an adverse effect on one another's chemical capabilities. The MOF integrated into the polymer matrix didn't pose an issue as the framework was still accessible for hosting molecules within its highly porous structure which is vital for its uses in catalysis and gas storage.[77] The polyHIPE having MOF particles embedded within its matrix somewhat interestingly increased the surface area of the polymer composite, this can be explained quite simply due to the fact MOFs have large surface areas themselves. Moreover, the addition of a MOF didn't affect the pore size (shown in Figure 1.13) of the polymer as the droplet size in the aqueous internal phase was unchanged.[78]
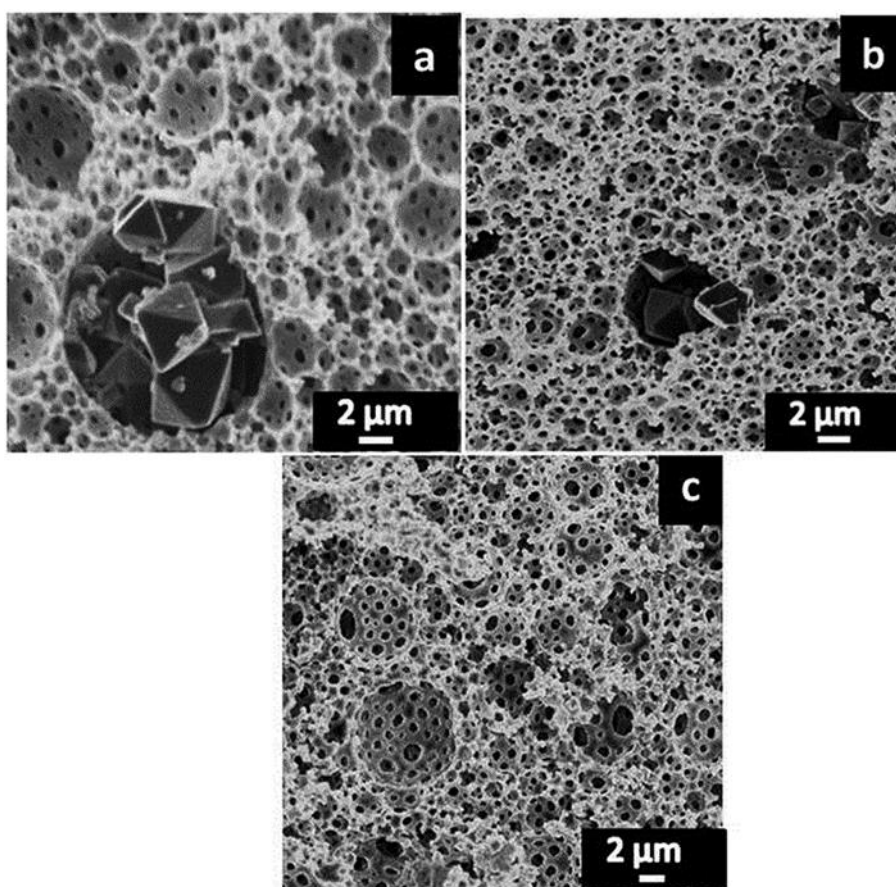
Figure 1.13 Illustration showing three SEM images; a & b show polyHIPE-MOFs and c shows a polyHIPE without MOF. Reprinted with permission from Ref.[78]

The inclusion of the MOF in the polyHIPE structure will be further studied throughout this thesis for its uses as a catalyst in a dipeptide hydrolysis. Swelling studies, pore sizes and surface area measurements will also be shown to further justify the combination of these two materials.

1.3 Catalysis

Catalysis is a concept that has been used since the early 1800s; a report published in 1836 by J. J. Berzelius quoted his findings of catalysis as a new force: *"It is, then, proved that several simple or compound bodies, soluble and insoluble, have the property of exercising on other bodies an action very different from chemical affinity. By means of this action they produce, in these bodies, decompositions of their elements and different recombinations of these same elements to which they remain indifferent."*[79] These early findings have led to a widespread use of catalysis in a number of different reactions. A modern day definition of catalysis is *"the science and technology of influencing the rate of chemical reactions".*[80] The two main types of catalysis are heterogeneous and homogeneous. Homogeneous catalysis is a system in which the reaction compounds and the catalyst are in the same phase, which is commonly the solution phase. Homogeneous catalysis can be used in many different chemical reactions, for example ester hydrolysis, Diels-Alder reactions, epoxidations, hydroxylations, enzymatic processes and polyester condensations.[81] Heterogeneous catalysis is a system in which the reaction compounds and the catalyst are in different phases.[80]

1.3.1 MOFs as Catalysts

MOFs are known to be robust, chemically stable materials with large internal surface areas, they also have a number of active sites (shown in Figure 1.14) within their structures. They have therefore been studied for their possible uses as heterogeneous catalysts. The importance of active sites within a MOF has been greatly reported, so much so that it is now customary to design specific active sites to enhance their use in catalytic applications.[82]

Designing a MOF to have specific properties is made easier by the fact they are extremely tuneable structures with what is described as infinite structural possibilities.
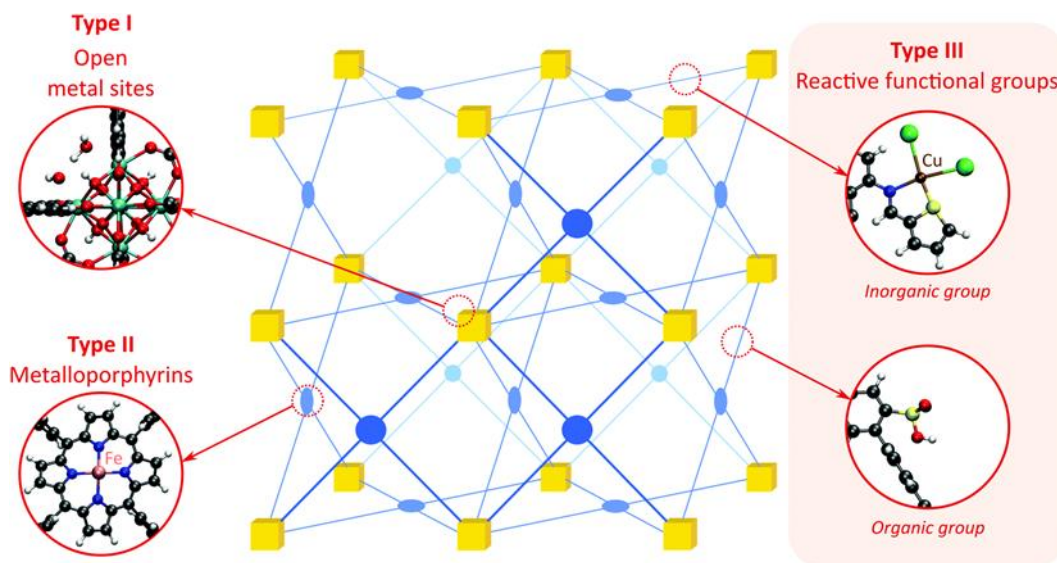
Figure 1.14 Illustration showing the different positions on a MOF structure where active sites are present. Reprinted with permission from Ref.[83]

Catalytically active MOFs normally consist of a metal centre with a functionalised organic linker.[84] The number of connections and structural defects in MOFs has a large effect on the catalytic activity of the material. A previous study looked at UiO-66 (12-connected), NU-1000 (8-connected) and MOF-808 (6-connected) and tested them for missing linkers, before using them as catalysts in the ring opening of styrene oxide.[35]

MOF catalyst	Number of missing linkers (per M_6 cluster)	Relative reaction rate	Conversion (%)
UiO-66	1.75	1	40
NU-1000	4	1.3	90
MOF-808	6	1.9	100

Table 1 MOF catalysts and their corresponding number of missing linkers which was deduced by and acid-base titration, the relative reaction rate and the conversion of styrene oxide. Adapted with permission from Ref.[35]

This study was able to use an acid-base titration to determine the number of missing linkers and correlate this to the reaction rate (shown in Table 1). Subsequently this highlighted the

18

MOF's ability as a catalyst in the ring opening of styrene oxide. All of the data from this study relates to the connected nodes of each MOF and their catalytic sites. The number of missing linkers correlates to site defects within the MOFs structure so therefore the greater number of missing linkers results in greater reactivity.

The degradation studies focused on the degradation of a chemical warfare agent (CWA), in these cases the CWA was DMNP. Once again UiO-66 (12-connected), NU-1000 (8-connected) and MOF-808 (6-connected) were used as the catalysts (shown in Table 2).[85,86,87]

MOF catalyst	Mmol	Time (min)	Conversion %
UiO-66	0.0015	60	65
NU-1000	0.0015	60	75
MOF-808	0.0003	8	100

Table 2 MOF catalysts and the amount of catalyst used in each degradation study and the time taken to reach the conversion %. Adapted with permission from Refs.[85,86,87]

This study provided further proof that 6-connected nodes had greater catalytic activity due to a higher number of active sites within their frameworks.

There are a number of reports of MOF catalysis, one such report looks at a Zr-MOF catalyst for the CO_2 reduction to formate. The MOF catalyst used in this study was an anthracene based MOF, NNU-28 (($[Zr_6O_4(OH)_4(L)_6]\cdot 6DMF$)) which was subsequently compared to UiO-66-NH$_2$ and PCN-222. This comparison provided evidence to show that NNU-28 was not only using the metal centre as an active site like the other two MOFs but it was also using its organic linker as a catalytically active site. The reduction study (shown in Figure 1.15) then compared the MOFs catalytic activity to its ligand and a standard without a catalyst. The results not only showed the MOFs capabilities as a catalyst but also indicated that the organic linker was in fact a catalytically active site.[88]
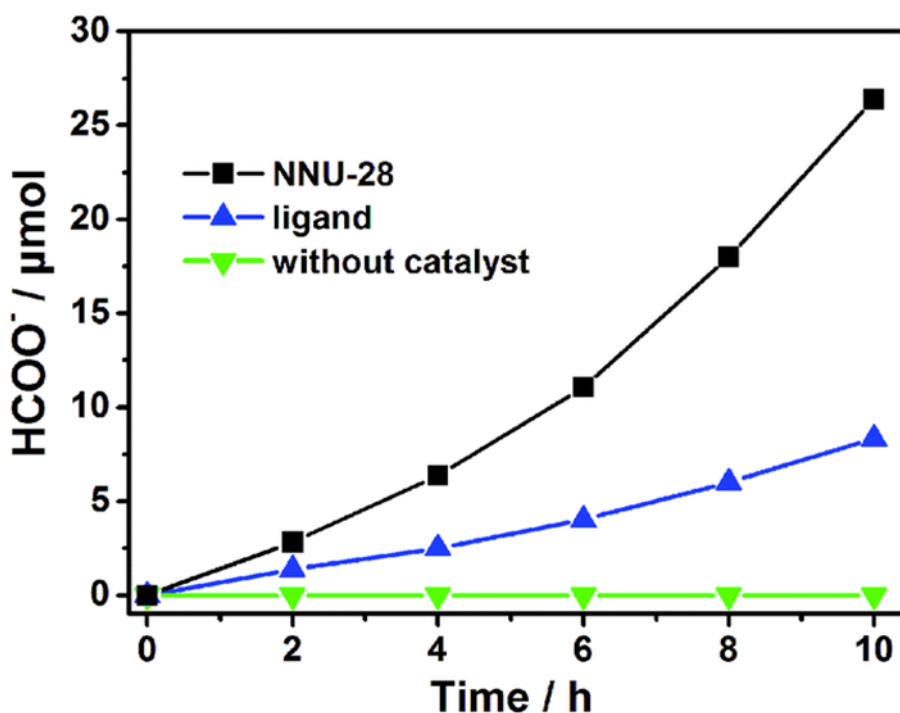
Figure 1.15 Reduction plots of NNU-28, its organic ligand and a standard without a catalyst in the reduction of CO_2 to formate. Reprinted with permission from Ref.[88]

As previously mentioned, the tunability of a MOF is one of its most desirable characteristics, this was exploited in another study where a Zr-MOF was modified with the addition of an amide group onto the MOF UiO-66. Modifications like this alter the chemical and thermal ability of the framework as well as drastically effecting the electronic properties of the catalytically active site.[89] The UiO-66-NH_2 MOF derivative is proposed to act as a Lewis acid at the Zr sites and a Bronsted-base at the -NH_2 sites making it a bifunctional catalyst, therein increasing its activity and selectivity.[90] This study focused on aldol condensations in UiO-66 and UiO-66-NH_2, looking at the propanal conversion % (shown in Figure 1.16). The conversion rate of propanal in the early stages of the reaction favours the UiO-66-NH_2 derivative which was expected due to the lower energy barrier and the stronger adsorption. After 40 minutes, the conversion of the non-amino modified MOF increases as the modified version starts to plateau. This is due to the selectivity of the product formed, the modified UiO-66 favours the cross-aldol condensation product which occurs earlier in the reaction whereas the non-

20

modified prefers the self-aldol product which occurs later in the reaction.[91] The blank shown in green shows no conversion so is represented by a green line along the x-axis.
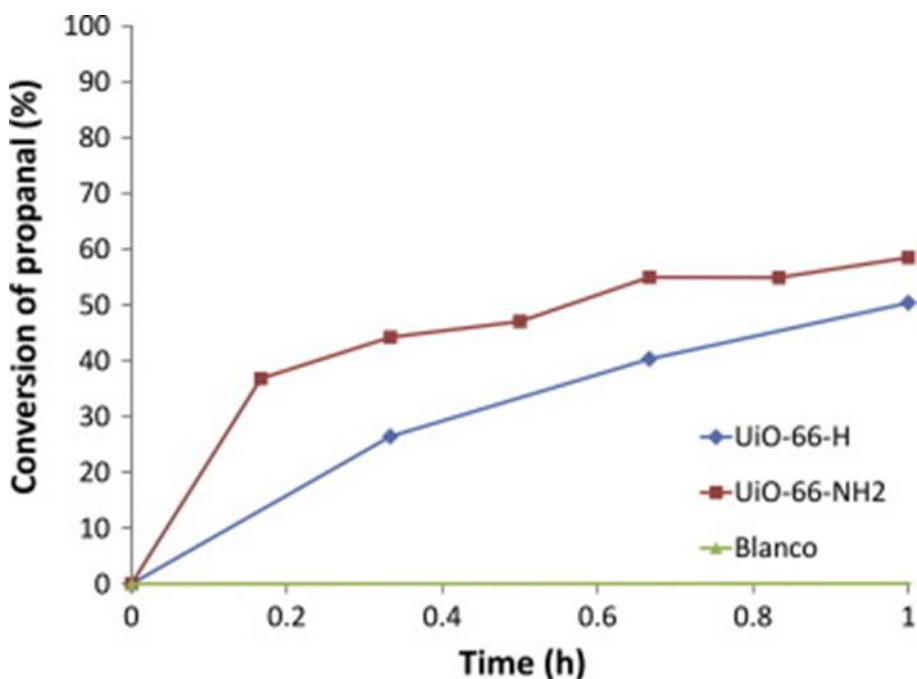
Figure 1.16 Conversion rate of propanal in Ui0-66, UiO-66-NH$_2$ and a blank standard. Reprinted with permission from Ref.[92]

As much as the importance of the catalytic ability, the reusability or recyclability of a catalyst is just as important as it can prove both cost effective and environmentally efficient. The recyclability of Zr-MOFs was studied in the hydrogenation of aromatics where they were able to use their MOF catalyst for up to 5 cycles. This was achieved by immobilizing iridium onto a functionalised Zr-MOF and subsequent characterisation showed that the MOF maintained its thermal stability and porosity. Furthermore, after each use in the hydrogenation reaction, the MOF catalyst was recovered through centrifugation and reused, the MOF didn't lose its initial catalytic activity after 5 cycles (shown in Figure 1.17) and its overall efficiency remained stable.[93]

21
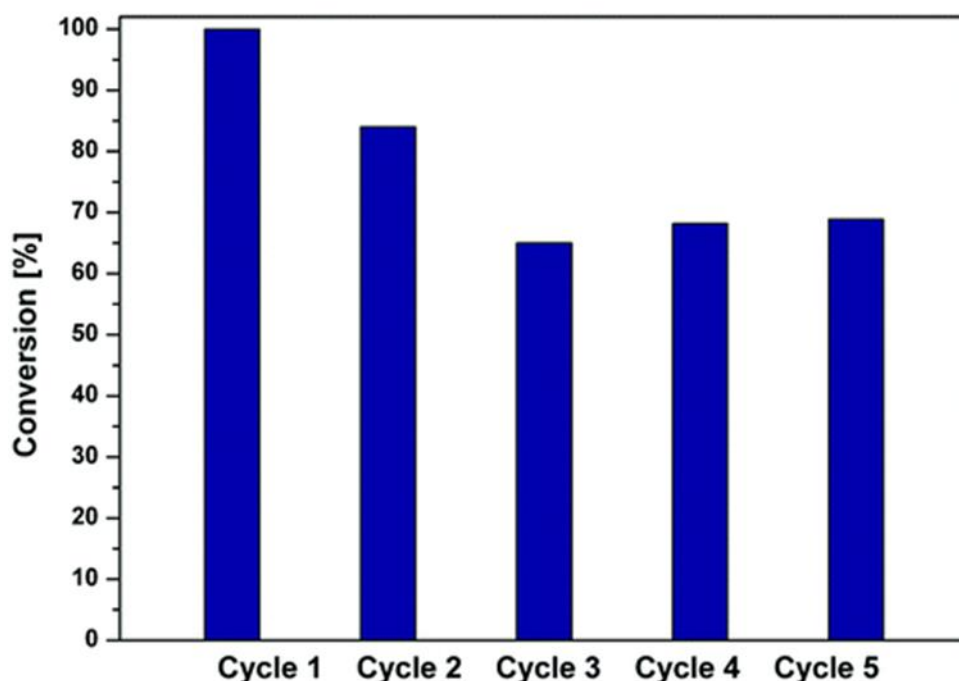
Figure 1.17 Conversion rate after 5 cycles of hydrogenation reactions using an Ir-Zr-MOF. Reprinted with permission from Ref.[93]

1.3.1.1 Titanium MOFs as Catalysts

Titanium metal organic frameworks as before mentioned have synthetic difficulties which has made the research into their catalytic activity limited. However, their photocatalytic activity has meant that attempts to overcome these difficulties were trialled to produce Ti-MOFs.[43] MIL-125 was subsequently synthesised and a study into CO_2 reduction with visible-light-induced activity. In this study MIL-125 was also functionalised with an amino group to provide a comparison to the standard MOF. The results of this study showed that under almost identical conditions for the reduction, MIL-125 was idle showing no photocatalytic activity. On the other hand, MIL-125-NH_2 showed impressive activity which suggests the amino functionality prompts the photoactivity within the framework. Further characterisation after the CO_2 reduction revealed that the amino functionalised material had a greater activity which was attributed to its higher uptake of CO_2.[94] The results of this study showed promising results for titanium MOFs but only when it was functionalised using an amino group, the next section will cover the other possible way of using titanium in MOFs to utilise their photoactivity.

1.3.1.2 Titanium-Zirconium Bimetallic MOFs as Catalysts

As aforementioned Ti-MOFs have difficulties with structural stability, so being able to combine these materials with another metal centre which has a more structurally robust framework is a potential solution. A metal that has been extensively studied for their uses in MOFs is zirconium, this research has showed that zirconium MOFs have high chemical stability and have extremely robust frameworks. Therefore, it is believed that the combination of these two metals in a MOF would result in a stable structure with potential used in photocatalysis.[95] This theory was put in to practice with a CO_2 reduction study which compared the bimetallic MOF to Zr-UiO-66, both MOFs were modified with a functionalised amino group, the modification was made due to its greater activity for CO_2 reduction. In this CO_2 reduction, the bimetallic MOF produced a greater amount of $HCOO^-$ over time when compared to the Zr-MOF (shown in Figure 1.18). The greater catalytic activity in the bimetallic material could not be simply attributed to the greater affinity of its CO_2 adsorption capacity, it is theorised that the Ti moiety within the framework must cause certain driving factors to improve the photocatalytic activity of the structure.[96]
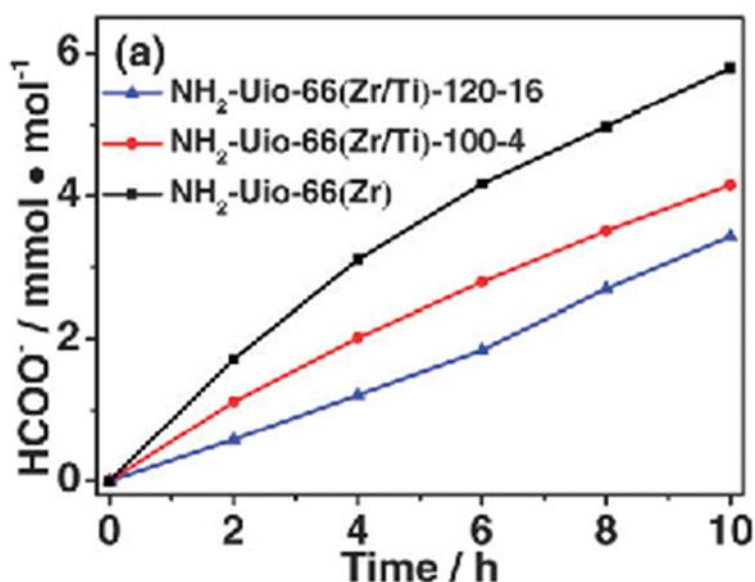
Figure 1.18 Conversion rate of HCOO⁻ over time using two functionalised bimetallic MOF derivatives and a functionalised Zr-MOF. Reprinted with permission from Ref.[96]

As aforementioned, there are other factors that occur within the bimetallic MOF that attribute to its enhanced photocatalytic activity. An explanation of these factors has been theorised where the ligand on the structure transfers electrons from its excited state to the Ti^{3+} moiety. Due to the overlap of electronic states between the Zr and Ti, there is a further transfer of electrons from Ti^{3+} to Zr^{4+} to form Zr^{3+}, which is photocatalytically active. Therefore, the Ti moiety is acting as a mediator in the transfer of electrons from the excited ligand to the Zr metal centre. The probability of electrons being transferred to Ti is greater than Zr, so $(Ti^{3+}/Zr^{4+})_6O_4(OH)_4$ is formed (shown in Figure 1.19).[97] In this form the Ti^{3+} can act as an electron donor and readily donate electrons to Zr^{4+} to form Ti^{4+}-O-Zr^{3+}.[98] The interfacial charge transfer from the excited ligand to Zr-O oxo clusters increases which is favourable for photocatalysis.[96]
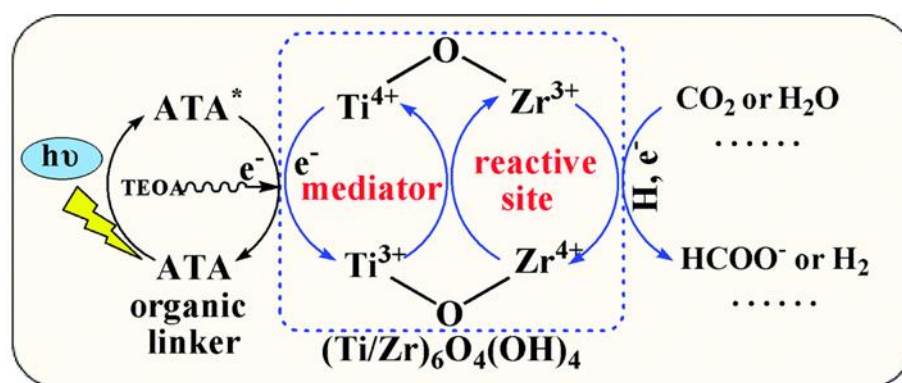
Figure 1.19 The proposed mechanism for photocatalytic reactions using the functionalised bimetallic MOF. Reprinted with permission from Ref.[96]

1.3.2 Dipeptide Hydrolysis

Hydrolysis is the chemical breakdown of a compound due to a reaction with water. Hydrolysis will in most cases need a catalyst to help the reaction reach completion. In the specific case of dipeptide hydrolysis, catalysts such as metal ions[99], biological catalysts[100] and acid-base catalysts.[101] The hydrolysis of a dipeptide results in two individual amino acid molecules forming. A recent study surfaced looking at MOFs as catalysts in dipeptide hydrolysis, they would act as a heterogeneous catalyst as in most cases MOFs are insoluble in water. Due to

their large internal surface areas and extensive porosity, MOFs have a high affinity for catalysis as has previously been shown in section 1.3.1.

1.3.3 MOF Catalysts for the Hydrolysis of Diglycine

A study that has looked into the hydrolysis of dipeptides with a MOF catalyst looked at the different elements that are required to optimise this type of reaction. Their research looked at the hydrolysis of GLY-GLY using zirconium based MOF-808 as a catalyst. In this study they performed the hydrolysis at 60°C and pH 7.4, they used these conditions after looking in more depth at the effects of pH and temperature. Values of pH from 4.6 to 9.8 were trialled, the hydrolysis rate was very low at pH 4.6 but increased at pH 7.4 before decreasing once more when the pH was increased further. PXRD patterns also suggested that the structure of the MOF started to breakdown under increasingly alkaline conditions. The value for pH suggests a more neutral value is preferred in dipeptide hydrolysis. The temperature of the system was also tested, a temperature range of 37 to 80°C was used. The results of this showed that there was an increase in reaction rate with temperature, but the thermal stability of the MOF decreased at higher temperatures. Analysis into the reaction conditions resulted in the above conditions being used, the hydrolysis took place over 3 hours and was monitored by ^{1}H NMR at intermittent times. After 3 hours the hydrolysis of GLY-GLY to glycine had almost reached completion. The results of this study showed that MOF-808 has specific activity towards the peptide bond, this activity was attributed to its ability to form active complexes via the amide oxygen and nitrogen atoms which create two adjacent Zr centres of the Zr_6O_8 core.[102] This particular study was the first to prove MOFs had an application in the hydrolysis of dipeptides. In this thesis, the hydrolysis of dipeptides using MOFs will be studied further, additional to this the MOF embedded into a polymer network will also be investigated as a potential catalyst in dipeptide hydrolysis.

1.4 Aims of this Thesis

The aims of this thesis were to synthesise a MOF with high catalytic activity for hydrolysis studies with a dipeptide. In addition, the MOF would then be encapsulated within a polymer network to form a swellable composite with a stable catalyst embedded within it. To calculate the polymers swelling ability, a number of solvent fronts containing THF and water would be used, therefore determining the solvent front used in the hydrolysis studies. The polymer would then be tested for its recyclability and reusability as a catalyst. A number of other well known MOFs with different metal centres and organic linkers will be studied alongside the originally selected MOF. A comparison of all of the MOFs catalytic abilities would be monitored through dipeptide hydrolysis.

1.5 References

1   L. E. Kreno, K. Leong, O. K. Farha, M. Allendorf, R. P. Van Duyne and J. T. Hupp, *Chem. Rev.*, 2012, **112**, 1105–1125.

2   S. Carrasco, *Biosensors*, 2018, **8**, 92.

3   M. J. Kalmutzki, N. Hanikel and O. M. Yaghi, *Sci. Adv.*, 2018, **4**, 10.

4   Y. R. Miao and K. S. Suslick, *Mechanochemical Reactions of Metal-Organic Frameworks*, Elsevier Inc., 1st edn., 2018, vol. 71.

5   S. S. Han, J. L. Mendoza-Cortés and W. A. Goddard, *Chem. Soc. Rev.*, 2009, **38**, 1460–1476.

6   S. D. Burd, S. Ma, J. A. Perman, B. J. Sikora, R. Q. Snurr, P. K. Thallapally, J. Tian, L. Wojtas and M. J. Zaworotko, *J. Am. Chem. Soc.*, 2012, **134**, 3663–3666.

7   D. Alezi, Y. Belmabkhout, M. Suyetin, P. M. Bhatt, L. J. Weseliński, V. Solovyeva, K. Adil, I. Spanopoulos, P. N. Trikalitis, A. H. Emwas and M. Eddaoudi, *J. Am. Chem. Soc.*, 2015, **137**, 13308–13318.

8   P. Horcajada, C. Serre, G. Maurin, N. A. Ramsahye, F. Balas, M. Vallet-Regí, M. Sebban, F. Taulelle and G. Férey, *J. Am. Chem. Soc.*, 2008, **130**, 6774–6780.

9   K. Koh, A. G. Wong-Foy and A. J. Matzger, *Angew. Chemie - Int. Ed.*, 2008, **47**, 677–680.

10   W. Morris, W. E. Briley, E. Auyeung, M. D. Cabezas and C. A. Mirkin, *J. Am. Chem. Soc.*, 2014, **136**, 7261–7264.

11   S. Keskin and S. Kizilel, *Ind. Eng. Chem. Res.*, 2011, **50**, 1799–1812.

12   M. Tonigold, Y. Lu, A. Mavrandonakis, A. Puls, R. Staudt, J. Möllmer, J. Sauer and D. Volkmer, *Chem. - A Eur. J.*, 2011, **17**, 8671–8695.

13   A. Pramanik, S. Abbina and G. Das, *Polyhedron*, 2007, **26**, 5225–5234.

14   X. Jing, C. He, D. Dong, L. Yang and C. Duan, *Angew. Chemie - Int. Ed.*, 2012, **51**, 10127–10131.

15   A. Henschel, K. Gedrich, R. Kraehnert and S. Kaskel, *Chem. Commun.*, 2008, 4192–4194.

16   A. H. Chughtai, N. Ahmad, H. A. Younus, A. Laypkov and F. Verpoort, *Chem. Soc. Rev.*, 2015, **44**, 6804–6849.

17   B. D. Chandler, D. T. Cramb and G. K. H. Shimizu, *J. Am. Chem. Soc.*, 2006, **128**, 10403–10412.

18   J. D. (2007). G. chemistry: P. and modern applications. U. S. R. P. P. H. Petrucci, R. H., Harwood, W. S., Herring, G. F., & Madura, .

19   Z. H. Fard, Y. Kalinovskyy, D. M. Spasyuk, B. A. Blight and G. K. H. Shimizu, *Chem. Commun.*, 2016, **52**, 12865–12868.

20   Y. Takashima, S. Furukawa and S. Kitagawa, *CrystEngComm*, 2011, **13**, 3360–3363.

21   B. Assfour, S. Leoni and G. Seifert, *J. Phys. Chem. C*, 2010, **114**, 13381–13384.

22   M. J. Katz, Z. J. Brown, Y. J. Colón, P. W. Siu, K. A. Scheidt, R. Q. Snurr, J. T. Hupp and O. K. Farha, *Chem. Commun.*, 2013, **49**, 9449–9451.

23   W. Liang, H. Chevreau, F. Ragon, P. D. Southon, V. K. Peterson and D. M. D'Alessandro, *CrystEngComm*, 2014, **16**, 6530–6533.

24   B. Kesanli, Y. Cui, M. R. Smith, E. W. Bittner, B. C. Bockrath and W. Lin, *Angew. Chemie - Int. Ed.*, 2004, **44**, 72–75.

25   M. Drahansky, M. Paridah, A. Moradbak, A. Mohamed, F. abdulwahab taiwo Owolabi, M. Asniza and S. H. Abdul Khalid, *Intech*, 2016, **i**, 13.

26   J. L. C. Rowsell and O. M. Yaghi, *Microporous Mesoporous Mater.*, 2004, **73**, 3–14.

27   Z. C. Kampouraki, D. A. Giannakoudakis, V. Nair, A. Hosseini-Bandegharaei, J. C.

Colmenares and E. A. Deliyanni, *Molecules*, 2019, **24**, 1–23.

28   A. K. P. Leite, B. S. Barros, J. Kulesza, J. F. S. Do Nascimento, D. M. De Araújo Melo and A. A. S. De Oliveira, *Mater. Res.*, 2017, **20**, 681–687.

29   J. E. Mondloch, O. Karagiaridi, O. K. Farha and J. T. Hupp, *CrystEngComm*, 2013, **15**, 9258–9264.

30   Y. R. Lee, J. Kim and W. S. Ahn, *Korean J. Chem. Eng.*, 2013, **30**, 1667–1680.

31   N. Stock and S. Biswas, *Chem. Rev.*, 2012, **112**, 933–969.

32   V. V Butova, M. A. Soldatov, A. A. Guda, K. A. Lomachenko and C. Lamberti, *Russ. Chem. Rev.*, 2016, **85**, 280–307.

33   J. Klinowski, F. A. Almeida Paz, P. Silva and J. Rocha, *Dalt. Trans.*, 2011, **40**, 321–330.

34   V. I. Isaeva and L. M. Kustov, *Pet. Chem.*, 2010, **50**, 167–180.

35   Y. Liu, R. C. Klet, J. T. Hupp and O. Farha, *Chem. Commun.*, 2016, **52**, 7806–7809.

36   Y. Liu, A. J. Howarth, N. A. Vermeulen, S. Y. Moon, J. T. Hupp and O. K. Farha, *Coord. Chem. Rev.*, 2017, **346**, 101–111.

37   J. Ren, M. Ledwaba, N. M. Musyoka, H. W. Langmi, M. Mathe, S. Liao and W. Pang, *Coord. Chem. Rev.*, 2017, **349**, 169–197.

38   H. R. Abid, G. H. Pham, H. M. Ang, M. O. Tade and S. Wang, *J. Colloid Interface Sci.*, 2012, **366**, 120–124.

39   S. Yuan, J. S. Qin, C. T. Lollar and H. C. Zhou, *ACS Cent. Sci.*, 2018, **4**, 440–450.

40   J. H. Cavka, S. Jakobsen, U. Olsbye, N. Guillou, C. Lamberti, S. Bordiga and K. P. Lillerud, *J. Am. Chem. Soc.*, 2008, **130**, 13850–13851.

41   S. Yuan, Y. P. Chen, J. S. Qin, W. Lu, L. Zou, Q. Zhang, X. Wang, X. Sun and H. C. Zhou, *J. Am. Chem. Soc.*, 2016, **138**, 8912–8919.

42   H. Furukawa, F. Gándara, Y. B. Zhang, J. Jiang, W. L. Queen, M. R. Hudson and O. M. Yaghi, *J. Am. Chem. Soc.*, 2014, **136**, 4369–4381.

43   L. Zou, D. Feng, T. F. Liu, Y. P. Chen, S. Yuan, K. Wang, X. Wang, S. Fordham and H. C. Zhou, *Chem. Sci.*, 2016, **7**, 1063–1069.

44   L. Zou, D. Feng, T. F. Liu, Y. P. Chen, S. Yuan, K. Wang, X. Wang, S. Fordham and H. C. Zhou, *Chem. Sci.*, 2016, **7**, 1063–1069.

45   D. Feng, K. Wang, Z. Wei, Y. P. Chen, C. M. Simon, R. K. Arvapally, R. L. Martin, M. Bosch, T. F. Liu, S. Fordham, D. Yuan, M. A. Omary, M. Haranczyk, B. Smit and H. C. Zhou, *Nat. Commun.*, 2014, **5**.

46   Y. Bai, Y. Dou, L. H. Xie, W. Rutledge, J. R. Li and H. C. Zhou, *Chem. Soc. Rev.*, 2016, **45**, 2327–2367.

47   S. Yuan, J. S. Qin, H. Q. Xu, J. Su, D. Rossi, Y. Chen, L. Zhang, C. Lollar, Q. Wang, H. L. Jiang, D. H. Son, H. Xu, Z. Huang, X. Zou and H. C. Zhou, *ACS Cent. Sci.*, 2018, **4**, 105–111.

48   C. S. Chern, *Prog. Polym. Sci.*, 2006, **31**, 443–486.

49   E. J. W. Verwey and J. T. G. Overbeek, *J. Colloid Sci.*, 1955, 10, 224–225.

50   M. Yahaya Khan, Z. A. Abdul Karim, F. Y. Hagos, A. R. A. Aziz and I. M. Tan, *Sci. World J.*, 2014.

51   E. Dickinson, C. Ritzoulis, Y. Yamamoto and H. Logan, *Colloids Surfaces B Biointerfaces*, 1999, **12**, 139–146.

52   D. G. Dalgleish, *Trends Food Sci. Technol.*, 1997, **8**, 1–6.

53   M. Bowker, *Nat. Mater. 1*, 2002, 205–206.

54   I. Pulko and P. Krajnc, *Macromol. Rapid Commun.*, 2012, **33**, 1731–1746.

55   P. Becher, *J. Dispers. Sci. Technol.*, 1985, **6**, 147–148.

56   V. O. Ikem, A. Menner and A. Bismarck, *Angew. Chemie - Int. Ed.*, 2008, **47**, 8277–8279.

57   A. Menner, V. Ikem, M. Salgueiro, M. S. P. Shaffer and A. Bismarck, *Chem. Commun.*, 2007, **41**, 4274–4276.

58   M. S. Silverstein, *Prog. Polym. Sci.*, 2014, **39**, 199–234.

59   N. R. Cameron, *Polymer (Guildf).*, 2005, **46**, 1439–1449.

60   A. Barbetta, N. R. Cameron and S. J. Cooper, *Chem. Commun.*, 2000, 221–222.

61   S. Kovačič and M. S. Silverstein, *Macromol. Rapid Commun.*, 2016, **37**, 1814–1819.

62   M. G. Schwab, I. Senkovska, M. Rose, N. Klein, M. Koch, J. Pahnke, G. Jonschker, B. Schmitz, M. Hirscher and S. Kaskel, *Soft Matter*, 2009, **5**, 1055–1059.

63   S. D. Kimmins and N. R. Cameron, *Adv. Funct. Mater.*, 2011, **21**, 211–225.

64   J. M. Williams, A. J. Gray and M. H. Wilkerson, *Langmuir*, 1990, **6**, 437–444.

65   J. M. Williams and D. A. Wrobleski, *Langmuir*, 1988, **4**, 656–662.

66   C. Zhao, E. Danish, N. R. Cameron and R. Kataky, *J. Mater. Chem.*, 2007, **17**, 2446–2453.

67   K. Jeřábek, I. Pulko, K. Soukupova, D. Štefanec and P. Krajnc, *Macromolecules*, 2008, **41**, 3543–3546.

68   M. G. Schwab, I. Senkovska, M. Rose, M. Koch, J. Pahnke, G. Jonschker and S. Kaskel, *Adv. Eng. Mater.*, 2008, **10**, 1151–1155.

69   Y. Wan, Y. Feng, D. Wan and M. Jin, *RSC Adv.*, 2016, **6**, 109253–109258.

70   V. Ş. Ünnü and S. Çetinkaya, *Catal. Letters*, 2018, **148**, 2432–2445.

71   S. Kovac, M. Jes, D. Pahovnik and C. Slugovc, **100**, 1605–1611.

72   H. B. T. Jeazet, C. Staudt and C. Janiak, *Chem. Commun.*, 2012, **48**, 2140–2142.

73   M. Rose, B. Böhringer, M. Jolly, R. Fischer and S. Kaskel, *Adv. Eng. Mater.*, 2011, **13**,

356–360.

74   L. D. O'Neill, H. Zhang and D. Bradshaw, *J. Mater. Chem.*, 2010, **20**, 5720–5726.

75   M. L. Pinto, S. Dias and J. Pires, *ACS Appl. Mater. Interfaces*, 2013, **5**, 2360–2363.

76   F. Du, L. Sun, W. Tan, Z. Wei, H. Nie, Z. Huang, G. Ruan and J. Li, *Anal. Bioanal. Chem.*, 2019, **411**, 2239–2248.

77   M. Mazaj, N. Z. Logar, E. Žagar and S. Kovačič, *J. Mater. Chem. A*, 2017, **5**, 1967–1971.

78   C. Le Calvez, M. Zouboulaki, C. Petit, L. Peeva and N. Shirshova, *RSC Adv.*, 2016, **6**, 17314–17317.

79   J. Blum, *J. Econ. Hist.*, 1951, **11**, 153–158.

80   R. Schlögl, *Angew. Chemie - Int. Ed.*, 2015, **54**, 3465–3520.

81   C. A. Tolman and J. P. Jesson, *Science.*, 1973, 181, 501–505.

82   M. Ranocchiari and J. A. Van Bokhoven, *Phys. Chem. Chem. Phys.*, 2011, **13**, 6388–6396.

83   S. M. J. Rogge, A. Bavykina, J. Hajek, H. Garcia, A. I. Olivos-Suarez, A. Sepúlveda-Escribano, A. Vimont, G. Clet, P. Bazin, F. Kapteijn, M. Daturi, E. V. Ramos-Fernandez, F. X. I. Llabrés Xamena, V. Van Speybroeck and J. Gascon, *Chem. Soc. Rev.*, 2017, **46**, 3134–3184.

84   S. A. Burgess, A. Kassie, S. A. Baranowski, K. J. Fritzsching, K. Schmidt-Rohr, C. M. Brown and C. R. Wade, *J. Am. Chem. Soc.*, 2016, **138**, 1780–1783.

85   M. J. Katz, S. Y. Moon, J. E. Mondloch, M. H. Beyzavi, C. J. Stephenson, J. T. Hupp and O. K. Farha, *Chem. Sci.*, 2015, **6**, 2286–2291.

86   J. E. Mondloch, M. J. Katz, W. C. Isley, P. Ghosh, P. Liao, W. Bury, G. W. Wagner, M. G. Hall, J. B. Decoste, G. W. Peterson, R. Q. Snurr, C. J. Cramer, J. T. Hupp and O. K. Farha, *Nat. Mater.*, 2015, **14**, 512–516.

87   S. Y. Moon, Y. Liu, J. T. Hupp and O. K. Farha, *Angew. Chemie - Int. Ed.*, 2015, **54**, 6795–6799.

88   D. Chen, H. Xing, C. Wang and Z. Su, *J. Mater. Chem. A*, 2016, **4**, 2657–2662.

89   T. Lescouet, C. Chizallet and D. Farrusseng, *ChemCatChem*, 2012, **4**, 1725–1728.

90   F. Vermoortele, A. Vimont, C. Serre and D. De Vos, *Chem. Commun.*, 2011, **47**, 1521–1523.

91   J. Hajek, M. Vandichel, B. Van De Voorde, B. Bueken, D. De Vos, M. Waroquier and V. Van Speybroeck, *J. Catal.*, 2015, **331**, 1–12.

92   J. Hajek, M. Vandichel, B. Van De Voorde, B. Bueken, D. De Vos, M. Waroquier and V. Van Speybroeck, *J. Catal.*, 2015, **331**, 1–12.

93   A. M. Rasero-Almansa, A. Corma, M. Iglesias and F. Sánchez, *Green Chem.*, 2014, **16**, 3522–3527.

94   Y. Fu, D. Sun, Y. Chen, R. Huang, Z. Ding, X. Fu and Z. Li, *Angew. Chemie - Int. Ed.*, 2012, **51**, 3364–3367.

95   D. Sun and Z. Li, *Chinese J. Chem.*, 2017, **35**, 135–147.

96   D. Sun, W. Liu, M. Qiu, Y. Zhang and Z. Li, *Chem. Commun.*, 2015, **51**, 2056–2059.

97   T. H. Xie, X. Sun and J. Lin, *J. Phys. Chem. C*, 2008, **112**, 9753–9759.

98   W. Lin and H. Frei, *J. Am. Chem. Soc.*, 2005, **127**, 1610–1611.

99   M. Yashiro, Y. Sonobe, A. Yamamura, T. Takarada, M. Komiyama and Y. Fujii, *Org. Biomol. Chem.*, 2003, **1**, 629–632.

100   J. K. Bashkin, *Curr. Opin. Chem. Biol.*, 1999, **3**, 752–758.

101   L. Lawrence and W. J. Moore, *J. Am. Chem. Soc.*, 1951, **73**, 3973–3977.

102   H. G. T. Ly, G. Fu, A. Kondinski, B. Bueken, D. De Vos and T. N. Parac-Vogt, *J. Am. Chem. Soc.*, 2018, **140**, 6325–6335.

Chapter 2 – A PolyHIPE-MOF for the Catalytic Hydrolysis of Diglycine

2.1 Introduction

The aims of the research described in this chapter were to synthesise both a highly catalytically active metal organic framework (MOF) and then incorporate this MOF inside a poly high internal phase emulsion (PolyHIPE). The synthesised MOF would then be used in a hydrolysis reaction with diglycine using a number of different conditions. The polyHIPE-MOF formed would then be subjected to the same testing to see if the catalytically active MOF was still as effective inside a polymer network. MOF-808 was chosen as the MOF for these studies due to its previously reported success as a catalyst.[1] Recent work using MOF-808, of which there are a significant number of studies, have shown its effectiveness as a catalyst in multiple different reactions.[2,3,4,5] One such study indicates its use as a catalyst in the reduction of a challenging carbonyl compound where it showed a yield two times greater than that of UiO-66 after 2 hours.[3] The polyHIPE has previously shown that it is capable of storing active catalysts within its pores.[6] Therefore, MOF-808 was stored as an active catalyst within the pores of the polyHIPE. Furthermore, it has been reported that polyHIPEs have impressive absorption capabilities which will prove essential in catalysis studies.[7] The choice of polyHIPE was styrene crosslinked with divinylbenzene (DVB).

2.1.1 Hydrolysis

Hydrolysis is one of the many reaction pathways for which MOFs can be utilised as catalysts. In the hydrolysis of dipeptides, the procedure works by the addition of water splitting the bond between O=C and N-H to form two separate peptide bonds (shown in Figure 2.1).
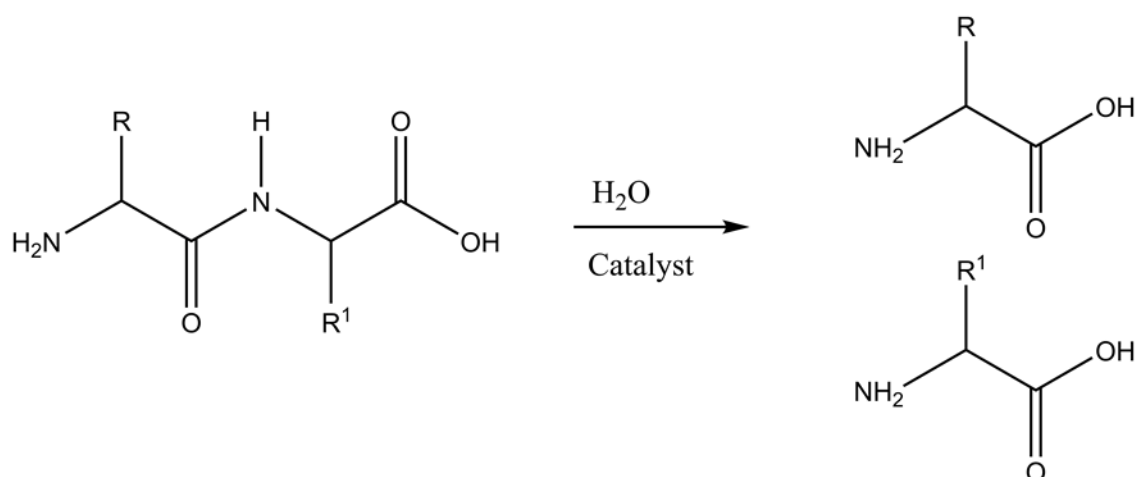
Figure 2.1 Schematic outlining the hydrolysis of a dipeptide.

The use of a MOF as the catalyst in a hydrolysis reaction is attributed in part to its extensive porosity.[8] The proposed mechanism for the hydrolysis of diglycine (gly-gly) using a Zr-MOF catalyst is the gly-gly binds to two Zr (IV) metal centres in the Zr_6O_8 core via the oxygen atom of the amide group and the N-terminus. Furthermore, the amine nitrogen and oxygen atoms coordinate to Zr (IV), polarising the peptide bond, making it more vulnerable for nucleophilic attack by water, although the actual reaction mechanism is not confirmed and work into it is ongoing.[9] There are many reports of its ability to act as a catalyst in phosphoester hydrolysis.[10,11] The main study on dipeptide hydrolysis using a MOF catalyst outlined an impressive selectivity for diglycine over its cyclisation product.[9] The Lewis-acidic Zr^{IV} ionic sites within the Zr_6 node on the MOF are a major factor for their catalytically efficacy.[12] The catalytic activity of Zirconium-MOFs differs depending on the number of connected sites, any MOFs with a connectivity lower than 12 or with site defects are said to have a greater number of active sites due to a greater number of uncoordinated Zr^{IV} sites.[13] Therefore, MOF-808 with a 6-connected framework was synthesised as the choice of MOF for the hydrolysis studies outlined in this chapter. PolyHIPE-MOFs are relatively unrecognised materials for hydrolysis. However, due to the polyHIPEs absorption capabilities it is believed that by swelling the polymer with the active catalyst stored within its network it can be just as effective in catalysis and the polyHIPE as a solid support makes recyclability easy.

2.2 Experimental

2.2.1 Materials

Zirconium(IV) chloride, reactor grade (99.5+%, Alfa Aesar), 1,4-benzenedicarboxylic acid (98%, Sigma), 1,3,5-benzenetricarboxylic acid (95%, Sigma), 2,6-naphthalenedicarboxylic acid (Fluorochem), 2,5-thiophenedicarboxylic acid (99%, Sigma), pivalic acid (99%, Sigma), trifluoroacetic acid (99%, Fluorochem), dimethylformamide (99%, Fisher), acetic acid glacial (99.98%, Fisher), acetone (99+%, Fisher), acetonitrile (99.9%, Fisher), methanol (99.9%, Fisher), ethanol absolute (99.8+%, Fisher, certified AR for analysis), GLY-GLY (99%, Sigma), deuterium oxide (99.9%, Goss), tetrahydrofuran-d8 (Cambridge isotope laboratories) were all used as received.

2.2.2 Equipment

Infra-red spectroscopy was carried out at room temperature on a Shimadzu IRAffinity-1S, with an ATR gate, a sweep of 500 - 4000 cm^{-1} , a resolution of 2 cm^{-1} and 64 scans.

Electron micrographs were obtained using a Hitachi S-3400 scanning electron microscope. The pHIPE samples were prepared for SEM by cutting into thin square slices with a completely flat surface. The chamber was set to full vacuum, with an electron beam voltage of 20 kV and an emission current of 80 mA. SEM images were taken using the backscatter electron detector. SEM-EDX was carried out using the backscatter electron detector in the analysis mode, the spectrum range for the analysis was 0-20 keV, with 10 frames processed over a livetime of 10 seconds.

^{1}H NMR spectra were acquired on a Bruker Avance Neo NMR, running a proton frequency of 400 MHz at room temperature (22 °C), with 16 scans and D_2O and *d*-THF used as solvents.

PXRD analysis was conducted by placing the powdered sample of MOF onto a zero-background sample holder and analysed in a Rigaku Miniflex 600 desktop diffractometer. The polyHIPE was cut into flat thin slices and placed into the centre of a zero-background sample holder.

Thermal analyses of samples were performed using a Netzsch STA 409 PC25 instrument and an aluminium crucible was used for all thermogravimetric analyses at a heating rate of 10 °C min^{-1} under nitrogen, from 25 °C to 500 °C.

Raman spectroscopy was carried out at room temperature on a Metrohm Mira M-3 Raman spectrometer, a sweep of 400-2300 cm^{-1} and a resolution of 14 cm^{-1}.

Surface area and porosity measurements were carried out on a Surfer gas adsorption porosimeter. MOF and polyHIPE samples were prepared as powders, the degassing process was at 60 °C for 10 hours at 1x10^{-3} torr. The analysis process was carried out at 77 K under nitrogen atmosphere, the analysis time varied for each sample.

2.2.3 Synthesis of MOF-808

MOF-808 was synthesised using a previously reported method.[14] $ZrCl_4$ (1.281 g, 5.50 mmol) and 1,3,5-benzenetricarboxylic acid (0.3883 g, 1.85 mmol) were added to DMF (110 ml) and acetic acid (61.6 ml, 964.91 mmol). The reaction mixture was then sonicated for 20 minutes. The solution was then sealed in a Duran flask and placed into a preheated oven at 135°C for 24 hours. The flask was removed from the oven and allowed to cool to room temperature at which point a white precipitate was visible at the bottom of the flask. Once cooled, the solution was vacuum filtered using a Buchner funnel before being washed with DMF (3 x 20 ml), methanol (3 x 20 ml) and acetone (3 x 20 ml). The solid was then dried under vacuum for 48 hours to yield a white microcrystalline powder. The synthesised MOF-808 was characterised using PXRD and IR by comparison to a literature pattern and spectrum.

Yield 1.028 g (61.6 %) **FT-IR**: 645.1 cm^{-1}, 1657.5 cm^{-1}.

2.2.3.1 Alternative Synthesis of MOF-808

MOF-808 was synthesised through a different method.[15] Zirconyl chloride octahydrate (0.97 g, 2.99 mmol) and 1,3,5-benzenetricarboxylic acid (0.21 g, 0.99 mmol) were added to DMF (45 ml) and acetic acid (45 ml, 780 mmol). The solution was then sealed in a Duran flask and

placed into a preheated oven at 120°C for 48 hours. The flask was removed from the oven and allowed to cool to room temperature at which point a white precipitate was visible at the bottom of the flask. Once cooled, the solution was vacuum filtered using a Buchner funnel before being washed with DMF (3 x 20 ml) and methanol (3 x 20 ml). The solid was then dried under vacuum for 48 hours to yield a white microcrystalline powder. The synthesised MOF-808 was characterised using PXRD and IR by comparison to a literature pattern and spectrum.

Yield 0.750 g (63.6 %) **FT-IR**: 648.4 cm^{-1}, 1657.4 cm^{-1}.

2.2.4 Synthesis of a PolyHIPE

The polyHIPE was synthesised using a previously reported method.[16] AIBN (0.0075 g, 0.05 mmol), sorbitan monooleate (0.8 g, 1.87 mmol), divinylbenzene (0.0494 g, 0.38 mmol), and styrene (3.95 g, 37.93 mmol) were added into a conical flask. This solution was stirred for 5 minutes at 200 rpm using a 4 cm hemispherical PTFE overhead stirrer to homogenise the oil phase. Potassium sulfate (0.25 g, 1.43 mmol) was dissolved in water (76 ml) and added into a dropping funnel. This aqueous phase was then added slowly dropwise over a period of 20 minutes, during this time the stirring rate was gradually increased to 500 and eventually 800 rpm. Once all of the aqueous phase had been added, the solution was stirred at 1000 rpm for 5 minutes to homogenise. The resulting white foam like mixture was transferred into a plastic cylinder and sealed before being placed into a preheated oven at 65°C for 24 hours to cure. Once the polyHIPE had cured it was removed from the cylinder and cut into smaller segments before being placed into a vacuum oven at 50°C for 48 hours to dry. The dryness of the sample was determined by repeated weighing until no mass change was detected and the final recorded mass matched that expected.

2.2.5 Synthesis of a PolyHIPE-MOF

The polyHIPE-MOF was synthesised using a previously reported method.[17] AIBN (0.012 g, 0.07 mmol), sorbitan monooleate (0.68 g, 1.59 mmol), divinylbenzene (0.04 g, 0.31 mmol), and

styrene (3.168 g, 30.42 mmol) were added into a conical flask. This solution was stirred for 5 minutes at 200 rpm using a 4 cm hemispherical PTFE overhead stirrer to homogenise the oil phase. Potassium sulfate (0.2 g, 1.15 mmol) was dissolved in water (65 ml) and MOF-808 (0.802 g, 25 % [monomers]) was added, this solution was stirred continuously to incorporate the MOF. This aqueous solution was then pipetted in slowly dropwise over a period of 20 minutes, during this time the stirring rate was gradually increased to 500 and eventually 800 rpm. Once all of the aqueous solution had been added, the solution was stirred at 1000 rpm for 5 minutes to homogenise. The resulting white foam like mixture was transferred into a plastic cylinder and sealed before being placed into a preheated oven at 65°C for 24 hours to cure. Once the polyHIPE had cured it was removed from the cylinder and cut into smaller segments before being placed into a vacuum oven at 50°C for 48 hours to dry.

2.2.6 Hydrolysis Studies of Diglycine using MOF-808

D_2O (10 ml) was added to a volumetric flask with diglycine (0.106 g, 0.80 mmol, 80 mM) as a stock solution for the hydrolysis. D_2O/diglycine stock solution (0.75 ml, 80 mM gly-gly) was added to a sample vial with D_2O (0.75 ml). D_2O (0.75 ml, 40mM gly-gly) was added to an NMR tube with MOF-808 (0.0013 g, 9.18×10^{-4} mmol). The NMR tube was inverted multiple times to evenly disperse the MOF, and the NMR tube was heated at 65°C. At different time increments, an NMR spectrum was recorded of the sample to monitor the progress of the hydrolysis.

2.2.7 Hydrolysis Studies of Diglycine using the PolyHIPE

D_2O (10 ml) was added to a volumetric flask with diglycine (0.106 g, 0.80 mmol, 80 mM) as a stock solution for the hydrolysis. D_2O/diglycine stock solution (0.75 ml, 80 mM gly-gly) was added to a sample vial containing d-THF (0.75 ml). D_2O (0.75 ml, 40mM gly-gly) was added to an NMR tube with polyHIPE (0.0050 g, 0.018 mmol). The NMR tube was inverted multiple times to fully immerse the polyHIPE, and subsequently heated at 65°C. At different time increments, an NMR was taken of the sample to monitor the progress of the hydrolysis.

2.2.8 Hydrolysis Studies of Diglycine using the PolyHIPE-MOF

D_2O (10 ml) was added to a volumetric flask with diglycine (0.106 g, 0.80 mmol, 80 mM) as a stock solution for the hydrolysis. D_2O/diglycine stock solution (0.75 ml, 80 mM gly-gly) was added to a sample vial containing d-THF (0.75 ml). D_2O (0.75 ml, 40mM gly-gly) was added to an NMR tube with polyHIPE-MOF (0.0465 g, 0.028 mmol). The NMR tube was inverted multiple times to fully immerse the polyHIPE, and subsequently heated at 65°C. At different time increments, an NMR was taken of the sample to monitor the progress of the hydrolysis.

2.2.9 Swelling Studies

A 14 ml glass vial was tared on a 100 g x 0.0001 g balance and a small piece of the polyHIPE/polyHIPE-MOF was added (usually 0.010 g) and the mass for each one was recorded. The polymer was then immersed in around 5 ml of THF, water and mixtures of the two. The sample vial was sealed and left for 72 hours. After 72 hours, the piece of polymer was removed and dabbed on a piece of parchment paper to remove excess solvent. Each piece was then weighed on a tared balance, this study was repeated with new polymer/solvent a further 2 times to provide an average value.

2.2.10 Ball Milling of MOF-808

Some samples of MOF-808 were ball milled after preparation using a planetary ball mill (ball diameter of 15 mm) at 600 rpm for 5, 10, 15 and 30 minutes respectively.
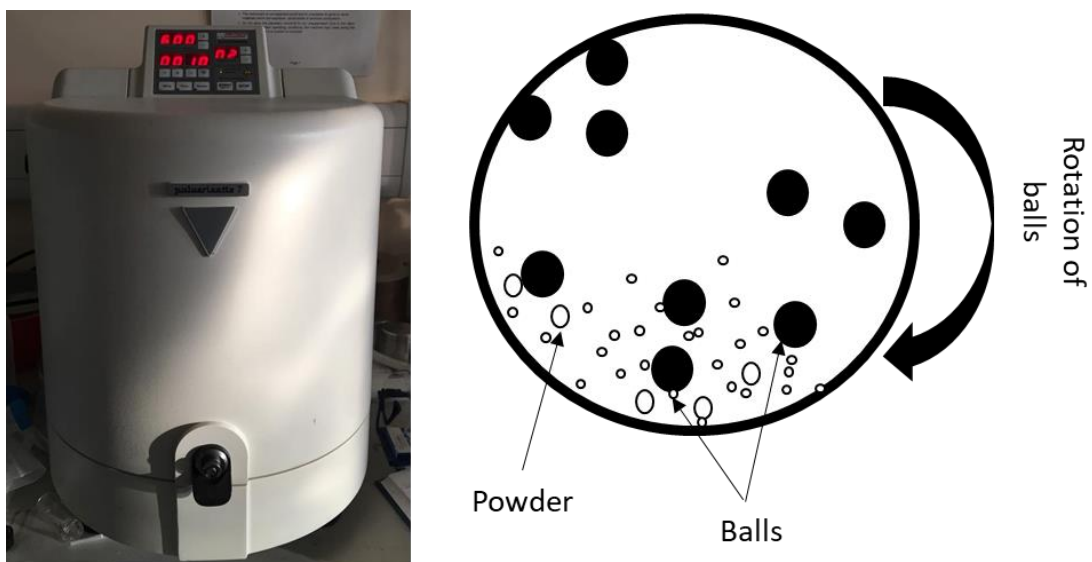
Figure 2.2 Image of the planetary ball mill (left) and the ball milling process (right).

2.2.11 Procedure for pH Measurement

A pH meter was calibrated using 3 different buffer solutions (pH 4,7 and 10).

H_2O (10 ml) was added into a volumetric flask with diglycine (0.106 g, 0.80 mmol) as a stock solution. H_2O/diglycine stock solution (2.5 ml) was added to a sample vial with H_2O (2.5 ml). A pH meter was placed into the solution and the pH was measured. The same procedure was used with tetrahydrofuran (2.5 ml) replacing water.

This procedure was used to calculate the pH of MOF-808 (0.290 g, 0.21 mmol) on its own as well as in tandem with diglycine. Further to this polyHIPE-MOFs (0.005 g, 3.04x10^{-3} mmol) pH was measured in addition to the polyHIPE-MOF with diglycine.

2.3 Results and Discussion

2.3.1 Characterisation

2.3.1.1 MOF-808

MOF-808 was synthesised following two published procedures.[14,15] The as-synthesised infrared

spectra and PXRD for both MOF-808s were compared to literature spectra and patterns
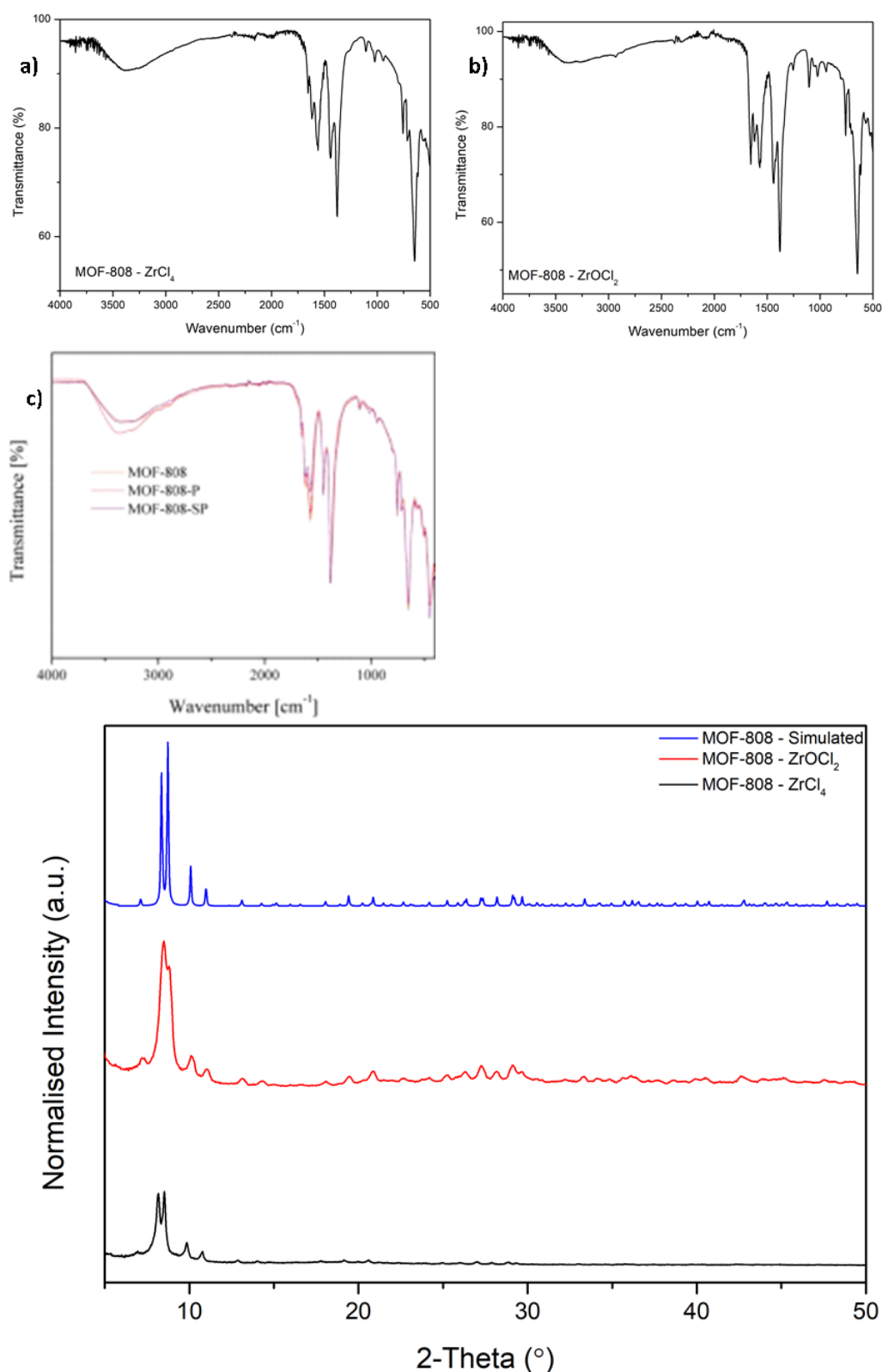
(shown in Figure 2.3).

Figure 2.3 Infrared spectra of MOF-808 – ZrCl$_4$ (a), ZrOCl$_2$ (b) and literature (c). Adapted with permission from Ref.[18] PXRD of MOF-808 – ZrCl$_4$ (black), ZrOCl$_2$ (red) and literature (blue). Adapted with permission from Ref.[19]

Both synthesised MOFs infrared spectra had the characteristic C=O peak at around 1600-1700

cm^{-1} indicative of the carboxylic acid group and the peak at around 1400 cm^{-1} indicative of the

aromatic group on the MOF. The PXRD for MOF-808 synthesised using ZrCl$_4$ has two peaks at

around 8-9° which is comparable to the simulated pattern. However, The PXRD for MOF-808 synthesised using $ZrOCl_2$ suggests that the powder is not completely crystalline, as the peaks are slightly broader suggesting that the product is slightly amorphous.[20] The simulated PXRD shows two peaks at around 8-9°, when compared to the as-synthesised PXRD, the peaks are slightly broader and there is 1 large peak at 8-9° with a smaller shoulder peak as opposed to the two sharp peaks. The above infrared spectrum and PXRD were compared to literature spectra and patterns to confirm MOF-808 had been synthesised.[14]
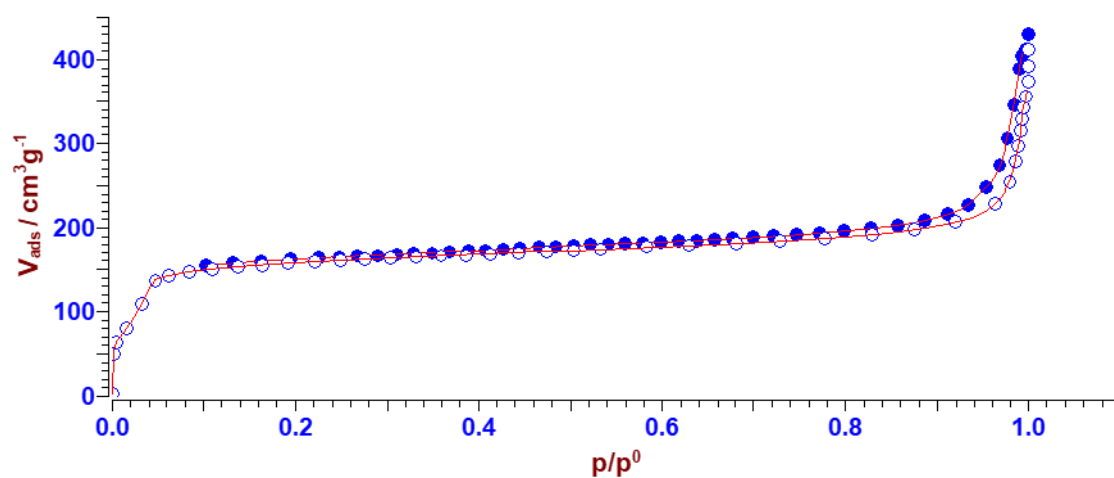

Figure 2.4 BET isotherm of MOF-808.

The porosity for MOF-808 was recorded on a Surfer gas adsorption porosimeter; the resulting isotherm is shown in Figure 2.4. The isotherm confirms that MOF-808 is mesoporous (pore widths between 2-50 nm) as it shows capillary condensation accompanied by hysteresis.[21] MOF-808 – $ZrOCl_2$ was not used in subsequent catalysis so no surface area or porosity measurements were taken.
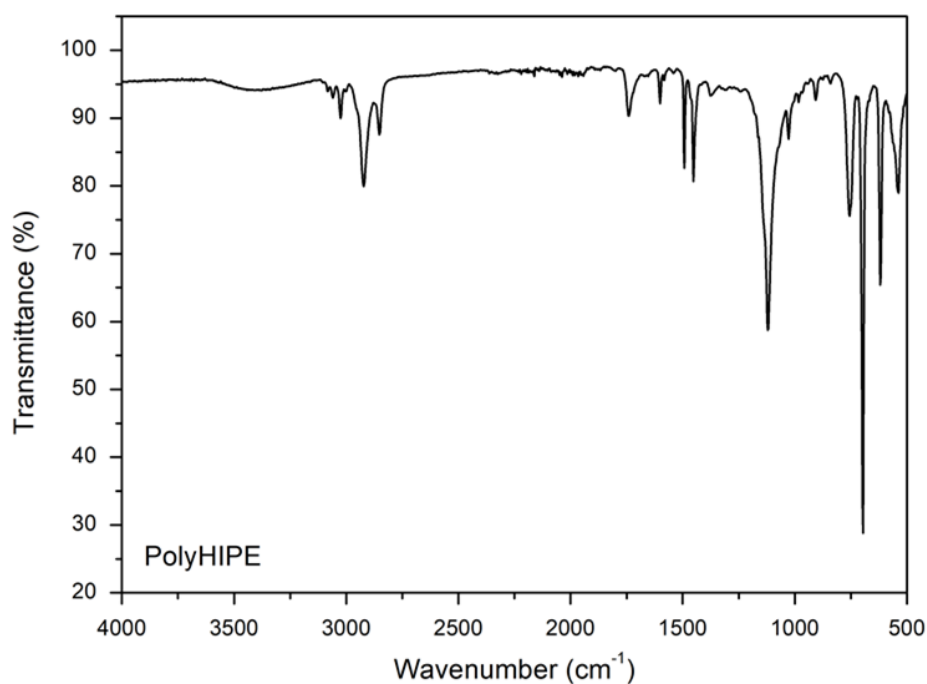
2.3.1.2 PolyHIPE

Figure 2.5 Infrared spectrum of the synthesised polyHIPE.

The polyHIPE was synthesised using a previously reported procedure.[16] The infrared spectrum

shown in Figure 2.5 was compared to literature spectra to confirm the formation of the

polyHIPE made up of styrene and divinylbenzene. The two characteristic peaks are at around

3000 cm^{-1} which indicates an aromatic C=C bond and at around 1750 cm^{-1} which indicates an
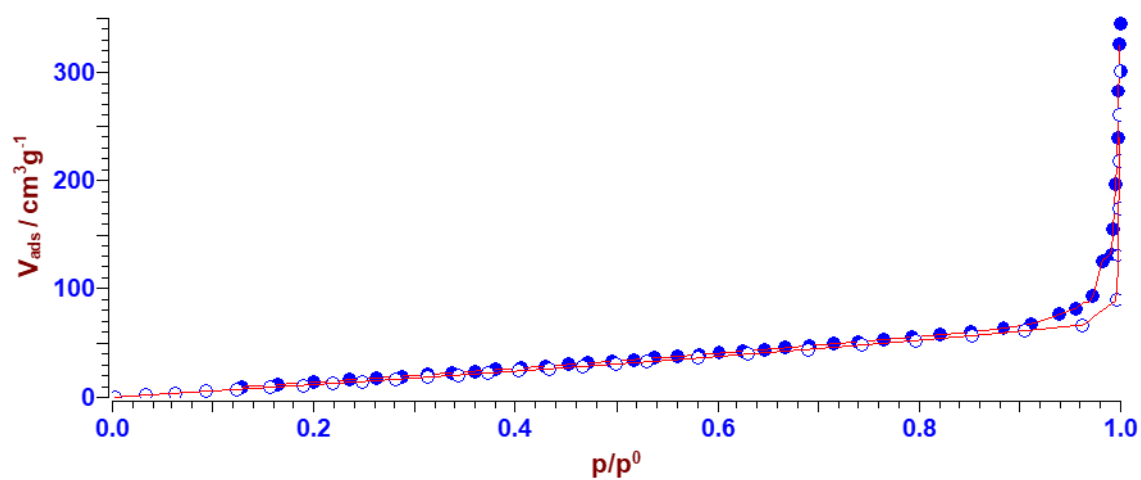
aromatic C-H bend.

Figure 2.6 BET isotherm of the polyHIPE.

The porosity for the polyHIPE was recorded on a Surfer gas adsorption porosimeter; the resulting isotherm is shown in Figure 2.6. The isotherm confirms the polyHIPE is microporous (pore widths <2 nm) as it shows monolayer adsorption.[21]

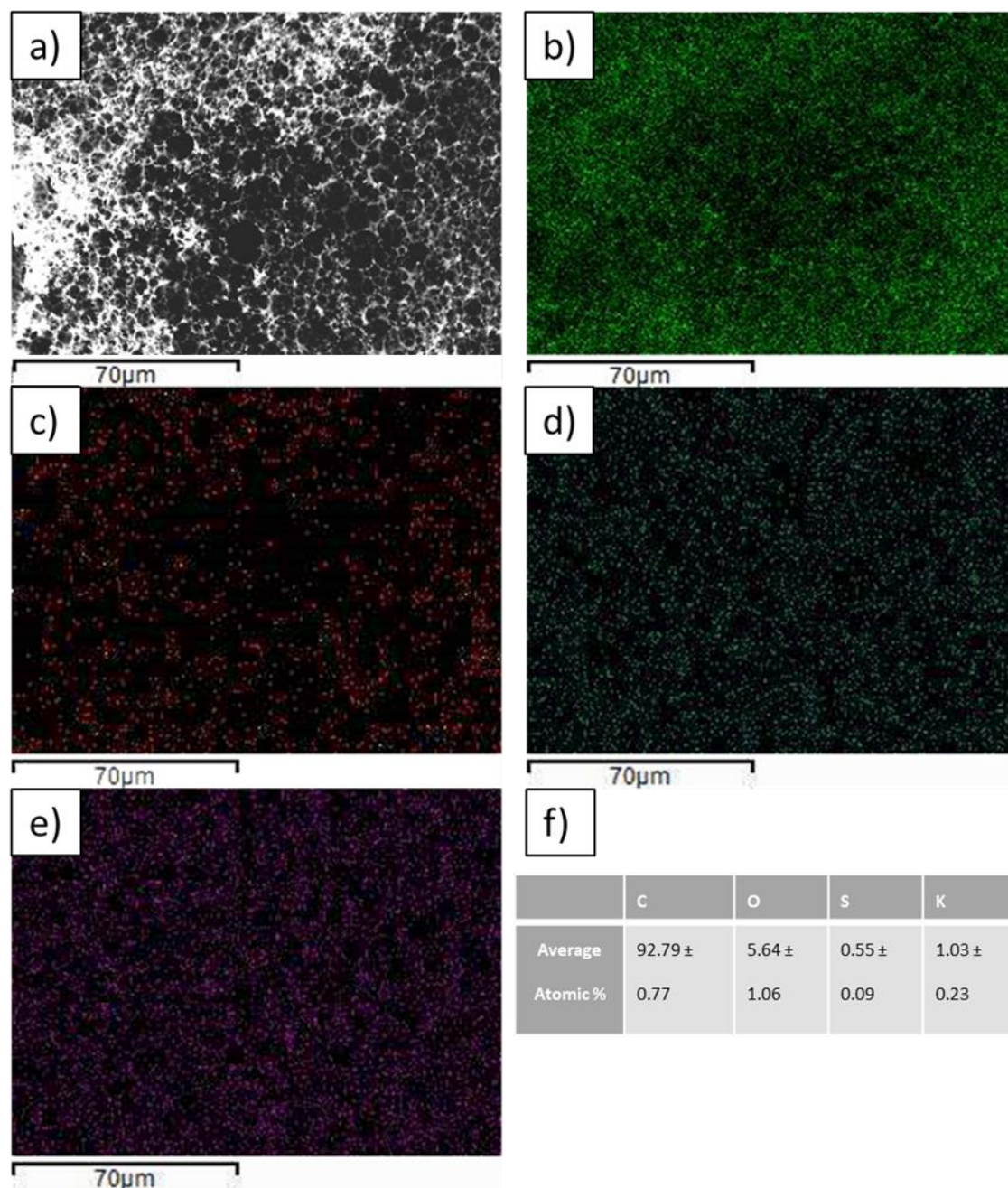|	C	O	S	K
Average	92.79 ±	5.64 ±	0.55 ±	1.03 ±
Atomic %	0.77	1.06	0.09	0.23

Figure 2.7 SEM image of the polyHIPE (a); the resultant elemental mapping (b,c,d and e) of carbon, oxygen, sulphur and potassium. A table showing the EDS analysis of the polyHIPE (f).

SEM images shown in Figure 2.7 were taken on samples of the polyHIPE after it has been cut into 3 different sections, three SEM images were taken of each section. The images show the

porous templated network with the SEM-EDS confirming the expected elements of the
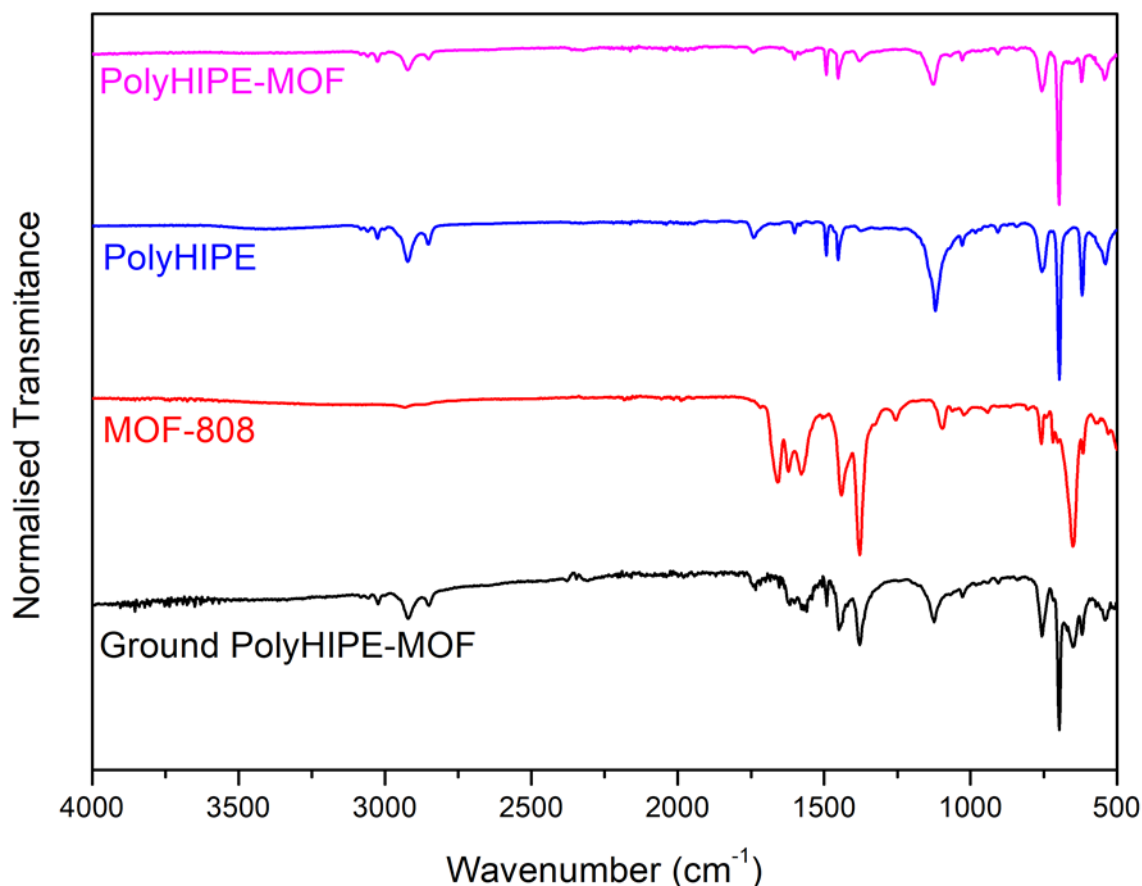
polymer.

2.3.1.3 PolyHIPE-MOF

Figure 2.8 Infrared spectra overlay of the polyHIPE, MOF-808 and polyHIPE-MOF.

The infrared spectra shown in Figure 2.8 shows the polyHIPE, MOF-808 and the polyHIPE-MOF

composite, in its original morphology and after it has been ground in order to show the

presence of the MOF as it is embedded within the polymer matrix. The piece of polyHIPE-MOF

shows very little presence of the MOF as it is not found on the surface of the polymer. The IR

spectra of the ground sample clearly shows the presence of the MOF peaks in the polyHIPE-

MOF at around 1600-1700 cm^{-1} which is indicative of the carboxylic acid group on the MOF.

When the polyHIPE-MOF is not ground into a powder, there are no peaks indicative of MOF-
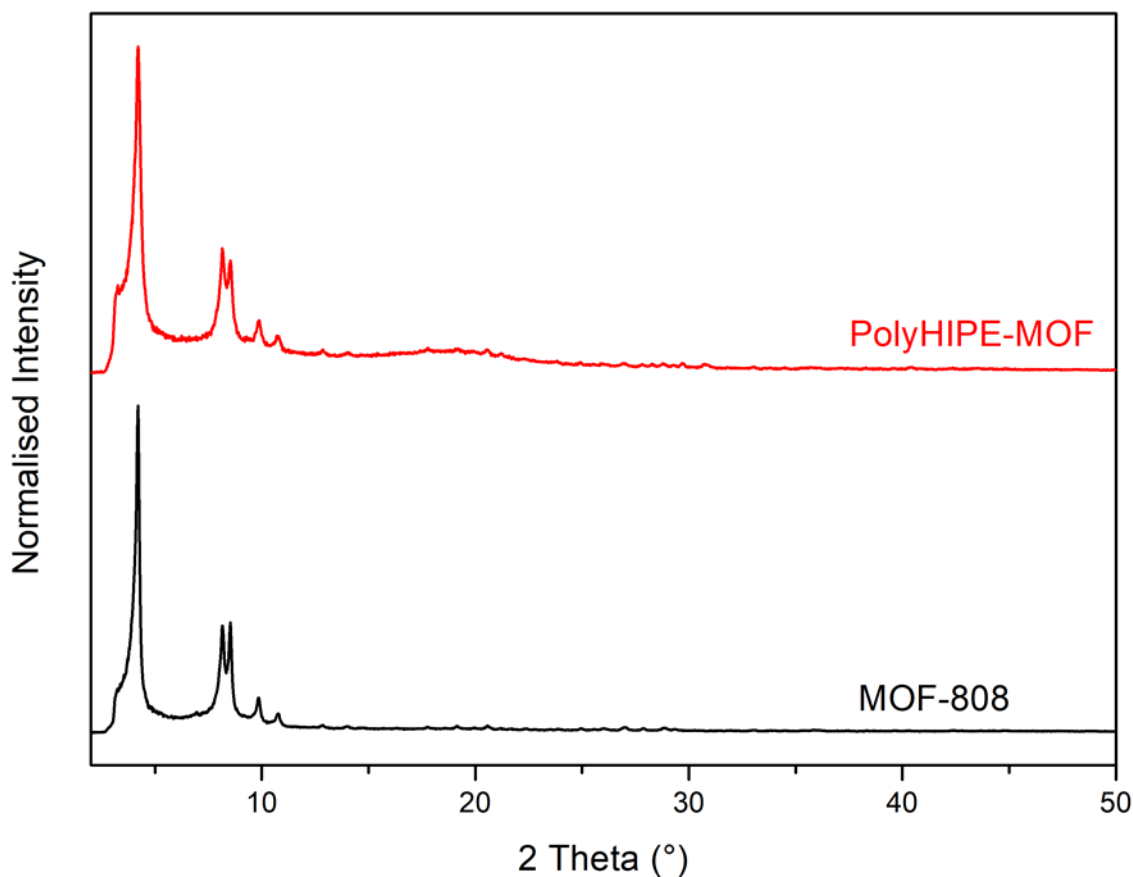
808 on the spectrum.

Figure 2.9 PXRD overlay of the polyHIPE-MOF and MOF-808.

The PXRDs shown in Figure 2.9 suggests the polyHIPE-MOF clearly shows a similar pattern to the MOF with the two peaks at around 8-9°. This shows that the MOF has been incorporated into the polymer matrix.
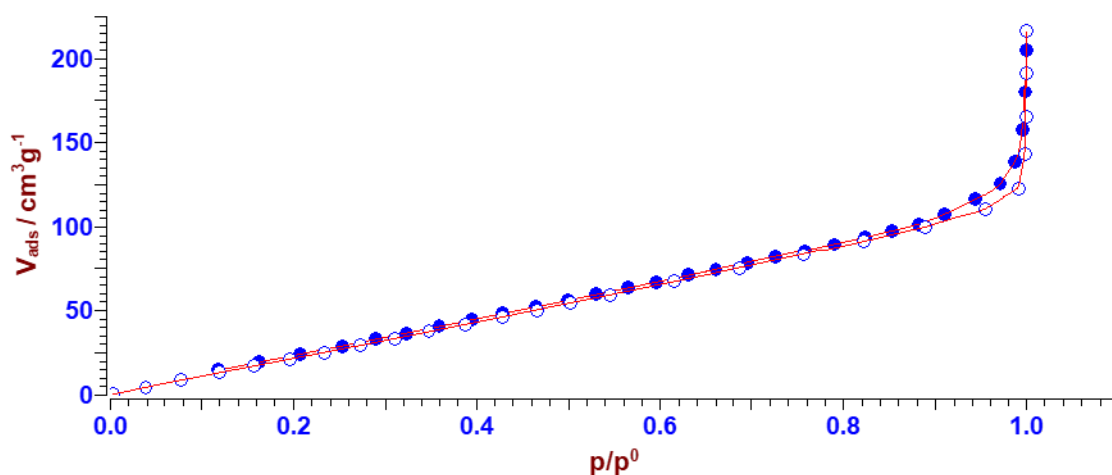

Figure 2.10 BET isotherm of the polyHIPE-MOF.

The porosity for the polyHIPE-MOF was recorded on a Surfer gas adsorption porosimeter; the resulting isotherm is shown in Figure 2.10. The isotherm confirms the polyHIPE is microporous as it shows monolayer adsorption.[21]

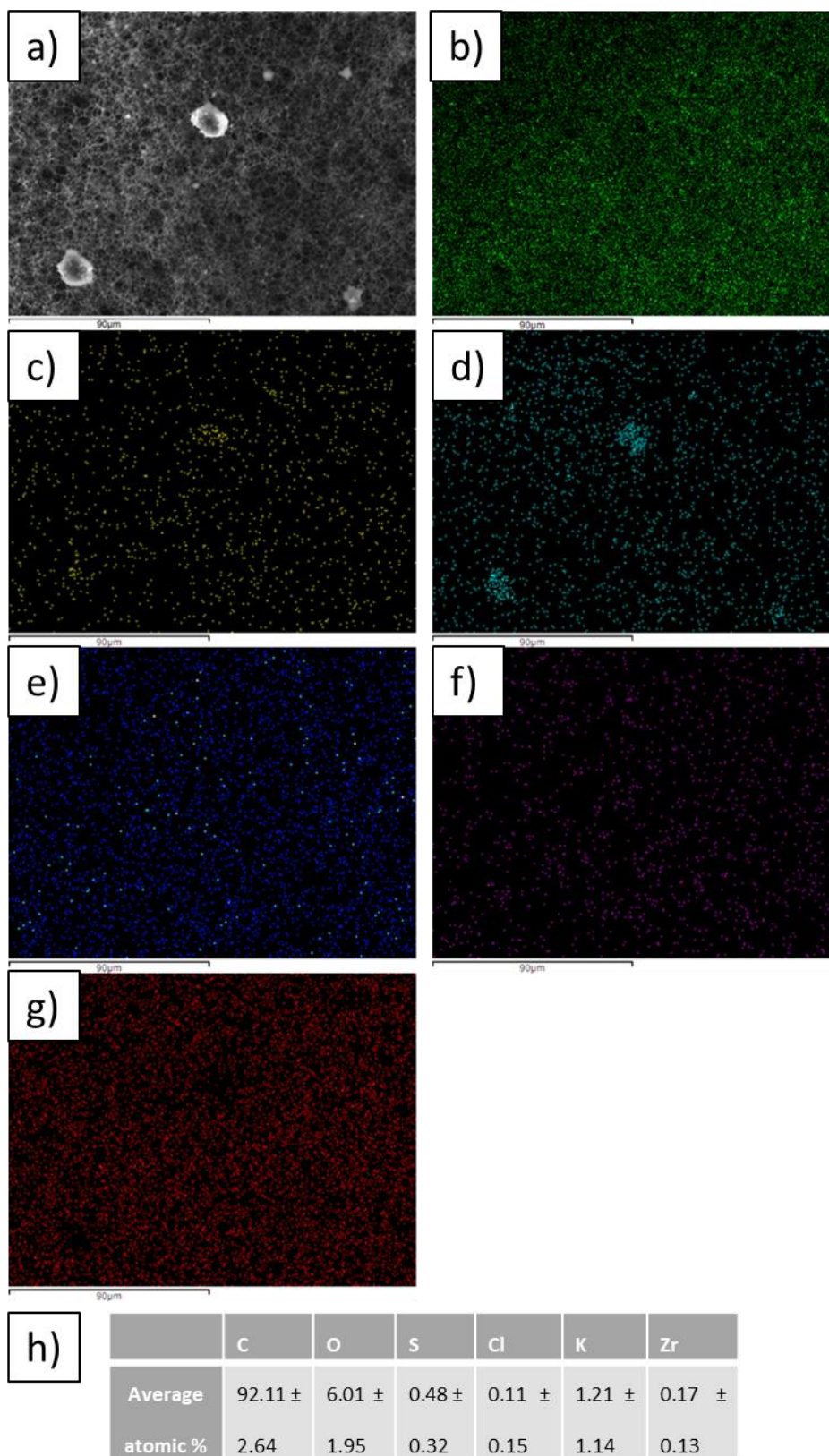|	C	O	S	Cl	K	Zr
Average	92.11 ±	6.01 ±	0.48 ±	0.11 ±	1.21 ±	0.17 ±
atomic %	2.64	1.95	0.32	0.15	1.14	0.13

Figure 2.11 SEM image of the polyHIPE-MOF (a): the resultant elemental mapping (b, c, d, e, f and g) of carbon, oxygen, zirconium, sulphur, chlorine and potassium. A table showing the EDS analysis of the polyHIPE-MOF (h)

The SEM-EDS analysis of the polyHIPE-MOF confirms the presence of the Zr-MOF within the polymer network. For the SEM-EDS, the polymer was cut into 5 sections, these 5 sections were then cut into 4. Each of the 20 pieces were then analysed by SEM, for each piece 3 measurements of its elemental analysis were taken. The reason for this extensive study was to show that the MOF was fully dispersed throughout the polymer. It indicated a good distribution of MOF throughout the polyHIPE, this was analysed by the SEM-EDS analysis of each of the 60 small pieces. Figure 2.12 shows the quantity of zirconium present in each small piece varies, this is shown in graph (f), the amount varies form 0.05-0.40 %.
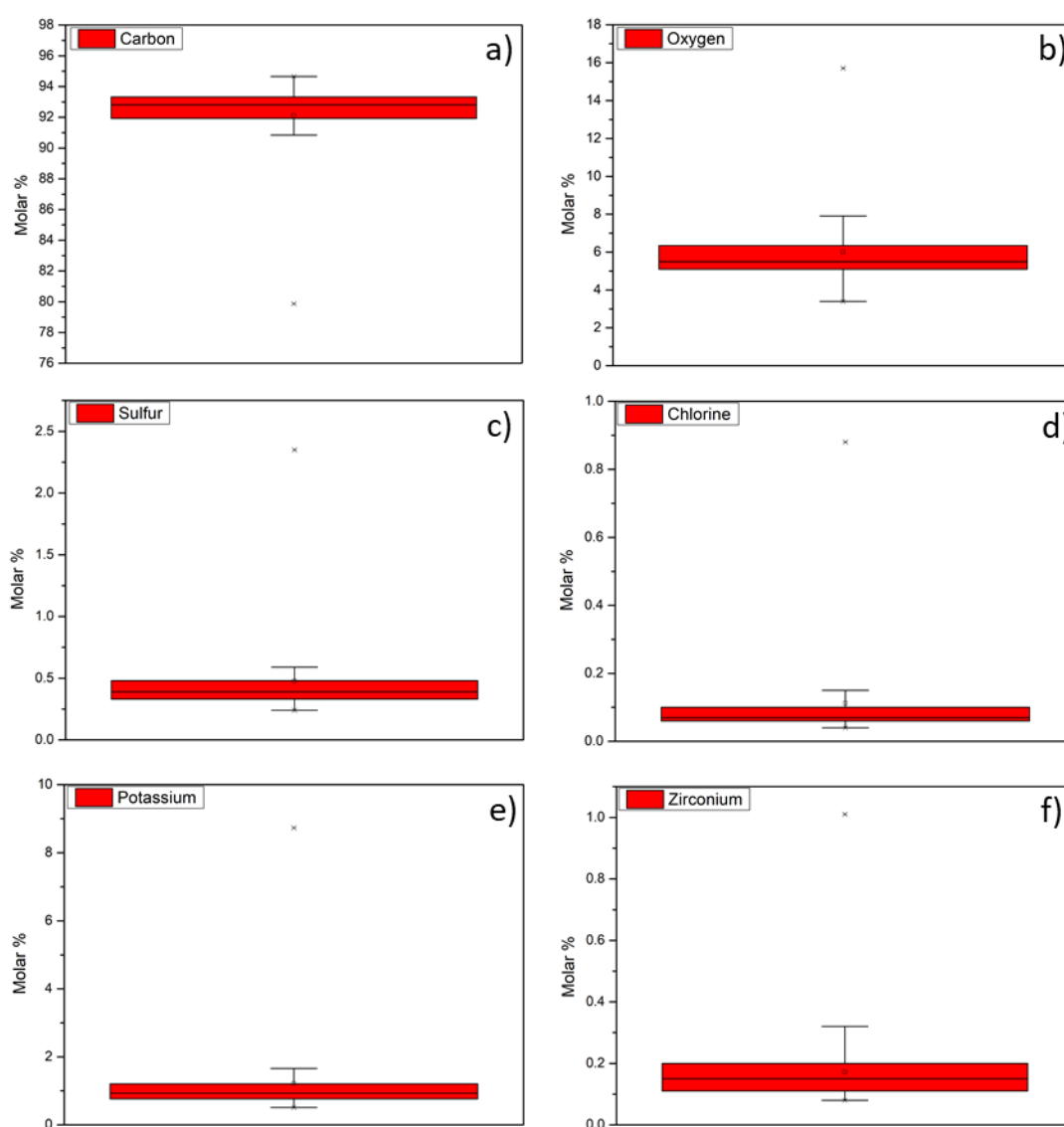

Figure 2.12 Box charts showing the elemental composition data for carbon, oxygen, sulfur, chlorine, potassium and zirconium (a-f). Error bars calculated from standard deviation, this was taken from analysing 60 pieces of the polyHIPE-MOF.

2.3.1.4 Curing of the PolyHIPE

An initial theory with the formation of the polyHIPE-MOF was the MOF not dispersing throughout the polymer. The polyHIPE was prepared as in 2.2.4 up until it was placed into a preheated oven at 65°C, the polyHIPE composite was placed into 10 separate sample vials which were sealed. After each hour a sample vial was removed from the oven for 10 hours. A sample of the emulsion and the polyHIPE after completion at 24 hours were also collected. The samples were all placed into the freezer until all samples had been collected. The samples were all removed from the freezer before being analysed with a handheld Raman spectrometer.

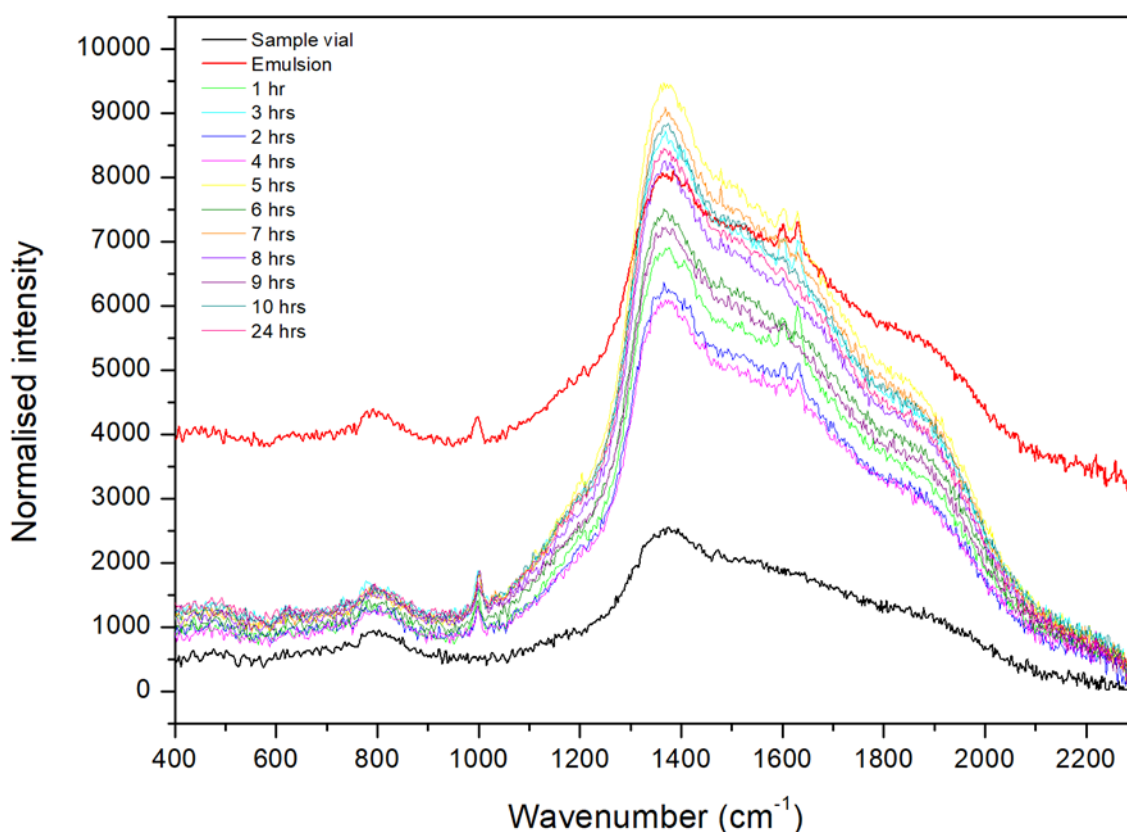*Figure 2.13 Raman spectra showing the curing of the polyHIPE.*

Raman was used and the two peaks at around 1600-1650 cm^{-1} which signifies a C=C bond[22] was determined to be the important peak in the curing of the polymer. Once this peak disappears from the spectrum it would indicate that the polymer had cured. Figure 2.13 shows clearly the points at which the peaks are visible and when it has disappeared from the

spectrum. The original curing process was carried out over 24 hours, however contrary to this, the Raman spectra suggested that the polymer had cured after 8 hours. After the analysis of the sections of polyHIPE-MOF it was confirmed that MOF did disperse throughout the polymer, so the polyHIPE-MOF was subsequently cured for 24 hours.
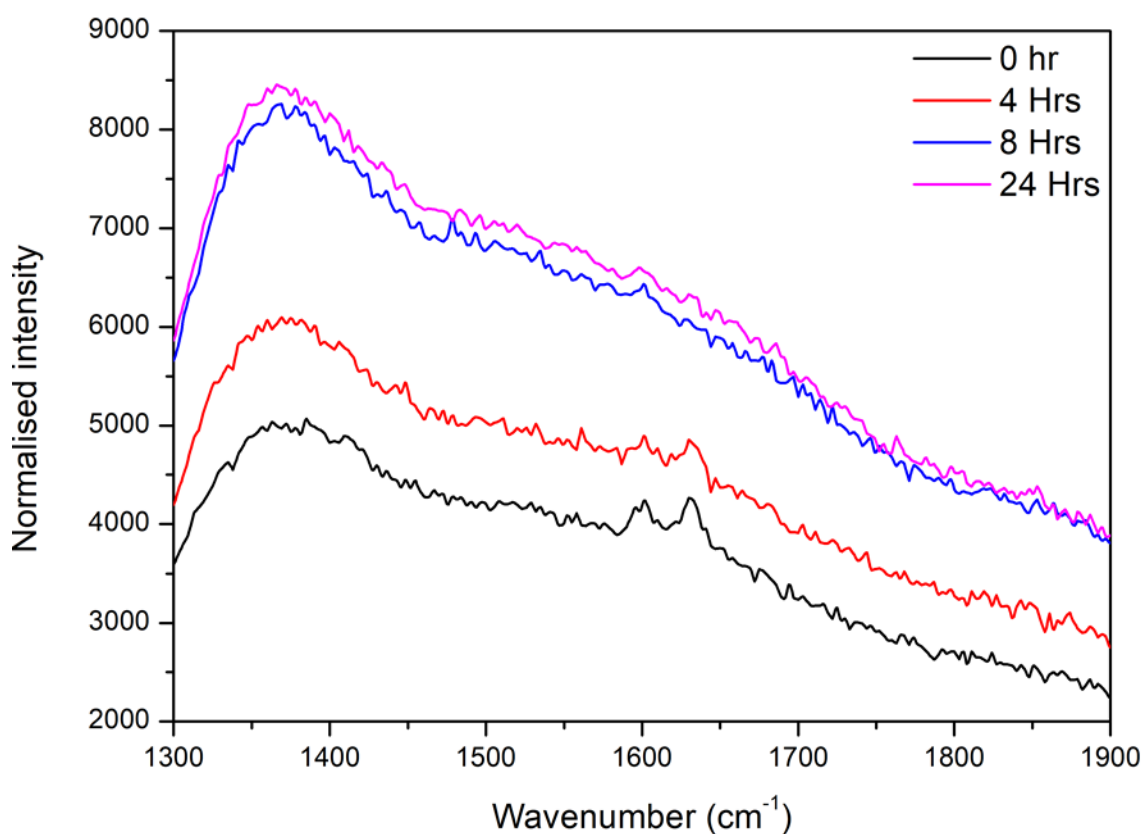
Figure 2.14 Raman spectra showing the progression of the polyHIPE as it cures.

2.3.2 Swelling Studies

The swelling of the polyHIPE and the polyHIPE-MOF were measured as it was clear from the infrared spectra for the polyHIPE-MOF that the MOF was embedded within the polymer. Therefore, it was important that the polymer swells in order to absorb into the polymer where the MOF is situated for subsequent catalysis. From the measured values a swelling degree by mass (Q) could be calculated using the following equation (2.1):

$$Q = \frac{mass\ of\ swollen\ polymer - mass\ of\ dry\ polymer}{mass\ of\ dry\ polymer}$$

(Equation 2.1)

The initial swelling studies of the polyHIPE had solvent mixes containing 0, 25, 50, 75 and 100% THF by volume in water.

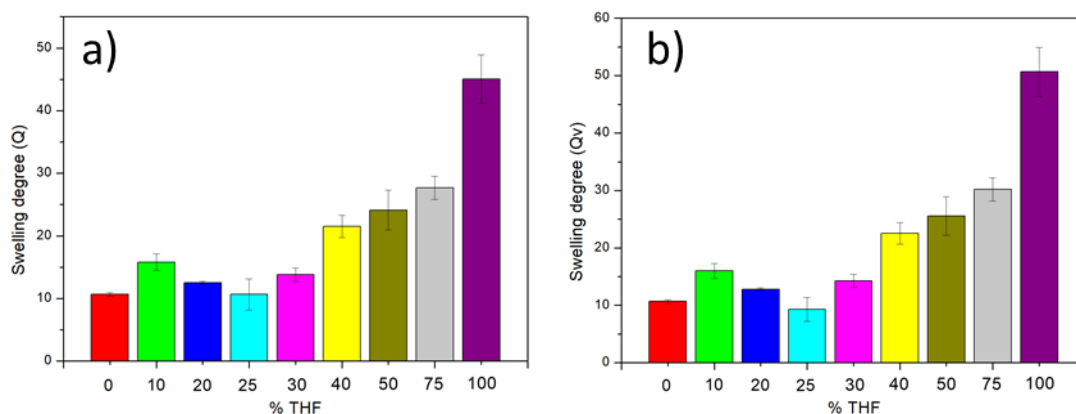Figure 2.15 Comparison of the swelling degrees of the polyHIPE in varying THF:H$_2$O solvent mixes. a) 0-100 % THF content (mass) and b) 0-100 % THF content (volume). Error bars calculated from standard deviation, this was taken from analysing the swelling of 5 pieces of polyHIPE.

In Figure 2.15 (a) the general trend for the swelling of the polyHIPE shows with increased THF content, there is an increase in swelling degree. However, at 0% THF content there is a higher Q value than at 25% THF content. At 0% THF content the polymer isn't swelling, its absorbing the water like a sponge. Furthermore, this anomaly can be attributed to thermodynamic effects, where the THF has a higher propensity to mix with the water instead of swelling into the polyHIPE. Alternatively, it could due to the polyHIPE acting as a sponge and absorbing the water. A more accurate way of calculating Q for studies with solvents is to calculate the value from volume. Calculating the swelling degree by volume results in the amount of solvent absorbed/swelled by the polymer being calculated.

$$Q_v = Q \frac{1}{\rho}$$

(Equation 2.2)

In Figure 2.15 (b) when the swelling degree is calculated by volume, this anomaly isn't so prominent and the error values suggest that there is a slight increase when there is 25% THF content. To look into this anomalous result further, swelling studies with 10, 20, 30 and 40% THF contents were carried out. There is an initial increase in Q from 0 to 10% THF content,

before the value decreases to 25% THF, before a final increase. This further supports the suggestion that it is a thermodynamic effect although there is no confirmation of this theory as of yet.

The polyHIPE-MOF was also studied for its swelling values with solvent mixes containing 0, 25, 50, 75 and 100% THF contents in water.
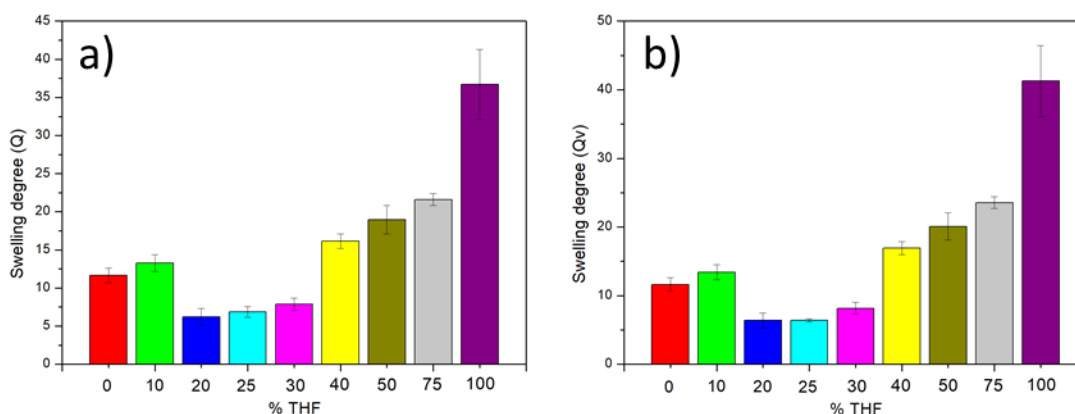

Figure 2.16 Comparison of the swelling degrees of the polyHIPE-MOF in varying THF:H$_2$O solvent mixes. a) 0-100 % THF content (mass) and b) 0-100 % THF content (volume). Error bars calculated from standard deviation, this was taken from analysing the swelling of 5 pieces of polyHIPE-MOF.

In Figure 2.16 (a & b) the polyHIPE-MOF shows a similar trend to the polyHIPE, however the initial decrease in Q from 0 to 25% THF content is greater. This suggests the thermodynamic effect theorised previously is more prominent when the MOF is embedded within the polymer matrix. The overall effect of the MOFs inclusion in the polymer didn't have a huge impact on the swelling capabilities of the polymer as shown in Figure 2.17 as the swelling degrees are very similar to that of the polyHIPE without the MOF. This is imperative when considering its use as a catalyst and the need for a solvent that swells the polymer to achieve its full catalytic potential.
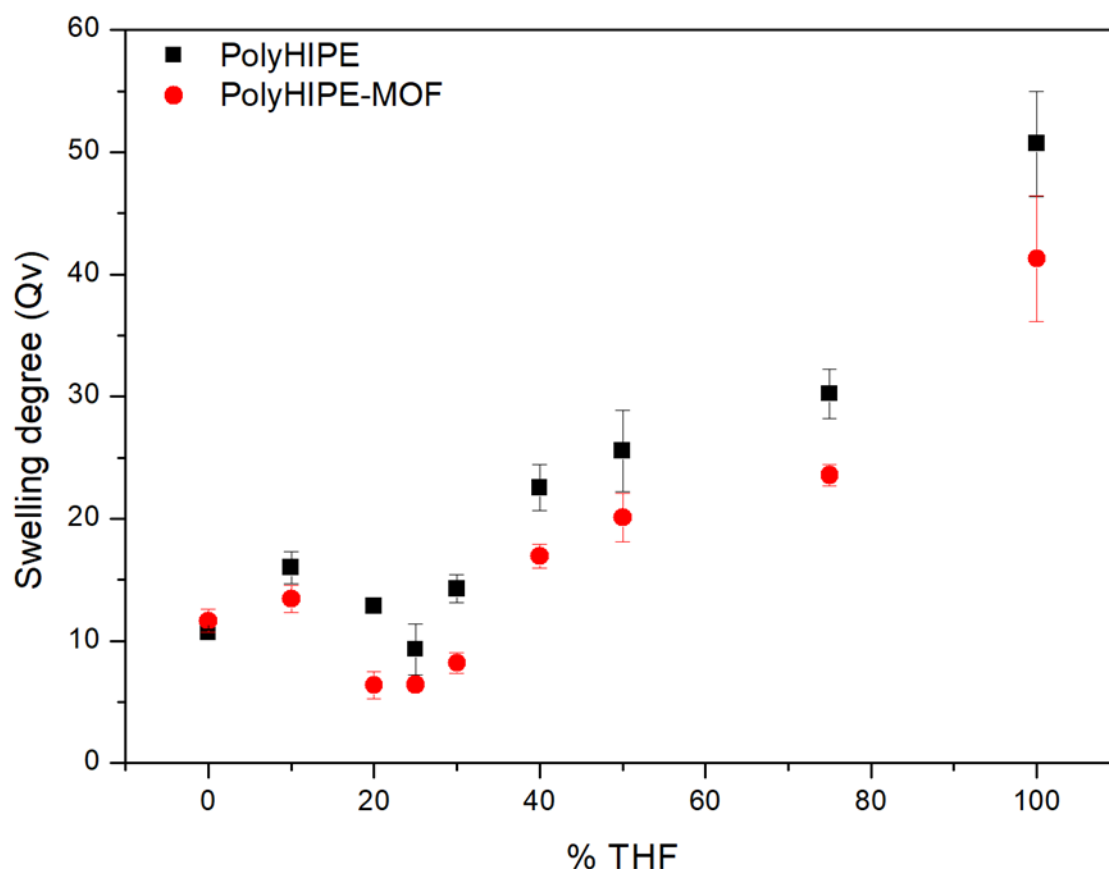
Figure 2.17 Comparison of the swelling studies for the polyHIPE and polyHIPE-MOF. Error bars calculated from standard deviation, this was taken from analysing the swelling of 5 pieces of polyHIPE.

The anomalous result from 0-25% THF content was once again looked into in more depth to see if a similar trend to the polyHIPE was observed. A similar trend was observed with the initial increase followed by a decrease, all of this data correlates to an unknown effect within the solvent mix that can only be theorised until further studies are performed such as thermodynamic properties.

2.3.3 Hydrolysis

	MOF-808 (g)	Diglycine (g)	D_2O (ml)	THF (ml)	Concentration (mM)	Molar ratio (MOF:gly-gly)
Reaction A	0.029	0.0080	0.75	0	40	1:2
Reaction B	0.029	0.0080	0.375	0.375	40	1:2
Reaction C	0.0013	0.0080	0.375	0.375	40	1:50

Table 3 A table showing the reaction parameters for this section.

Table 3 outlines the reaction parameters for this section which will look at the effects of altering conditions in this hydrolysis reaction on the catalytic activity of MOF-808. Firstly,

altering the molar ratio between the MOF-808 and diglycine in the reaction and the combination of two solvents.

2.3.3.1 MOF-808

The hydrolysis of diglycine was carried out following a previously reported procedure. The reaction was followed using NMR. The use of MOF-808 as a catalyst in the hydrolysis of diglycine has been previously studied, with nearly 100 % hydrolysis after 3 hours.[9] In the previously reported study, D_2O is used as the solvent at 60°C and the hydrolysis took place over 3 hours. The pH used in the study was optimised in order to achieve the ideal reaction conditions, to optimise the pH an aqueous buffer was used, to give a neutral pH. Diglycine and MOF-808 were in a 1:1 molar ratio in the previous study with a diglycine concentration of 40 mM. After 3 hours, the hydrolysis to glycine reached near completion. The reaction does not achieve 100 % conversion to glycine as the cyclisation form of glycine is formed as a by-product in this reaction, cyclisation will be mentioned further in 2.3.5. The reaction conditions for the results displayed in Figure 2.19 are identical for the temperature and concentrations used as shown by reaction C in Table 3 but the pH and the molar ratio between catalyst and diglycine differ. The pH used in literature was 7.4, which had been altered with the use of an aqueous buffer, however for reaction C the pH was 3.64. The molar ratio in literature was 1:1, compared to 1:50 in reaction C. The hydrolysis in literature took place over 3 hours whereas all reactions shown in this thesis were over 7 days.
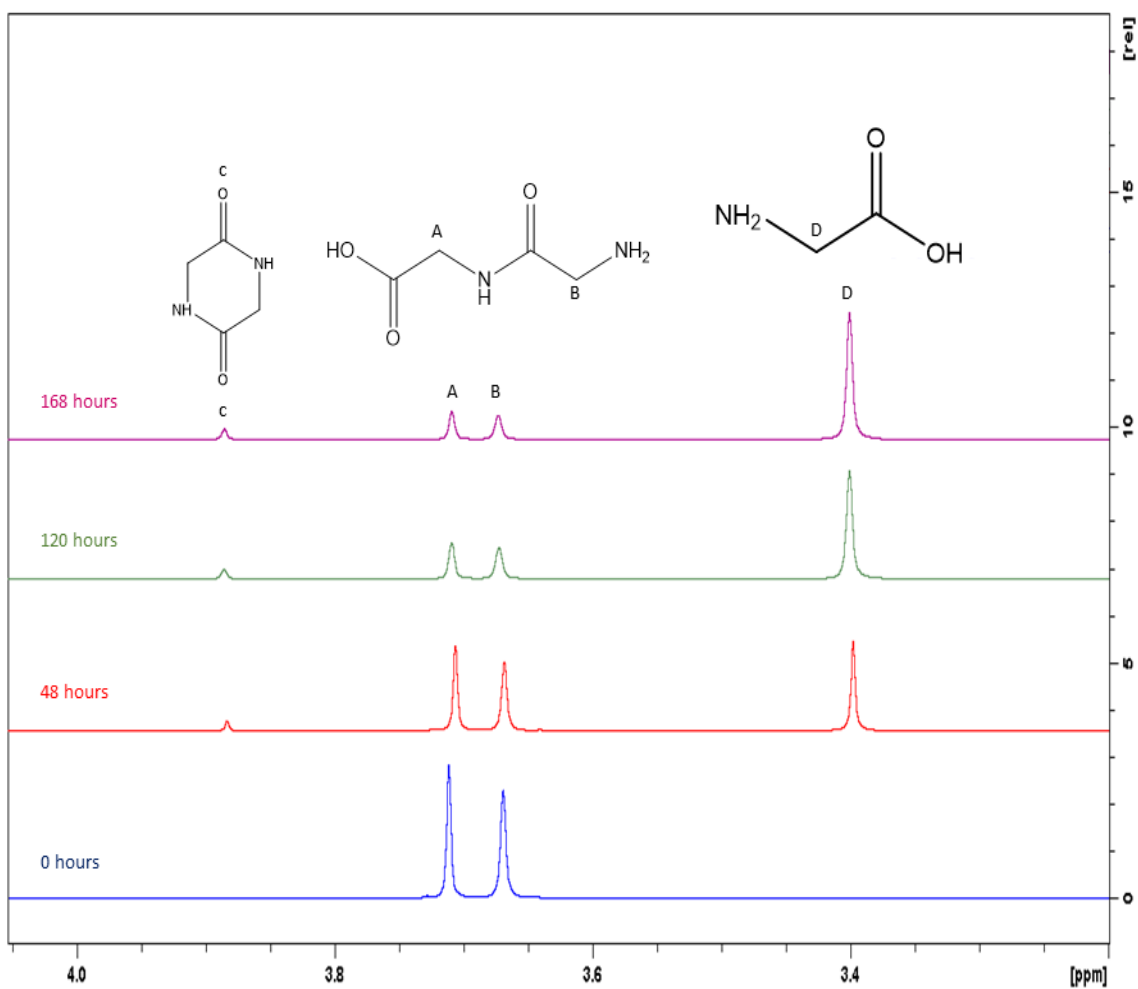
Figure 2.18 NMR spectra overlay showing the hydrolysis of diglycine after 0, 48, 120 and 168 hours.

The peak at around 3.4 ppm is due to glycine, the peaks at around 3.65-3.75 ppm are due to

the two diglycine peaks and the peak at around 3.9 ppm is due to the cyclisation form of
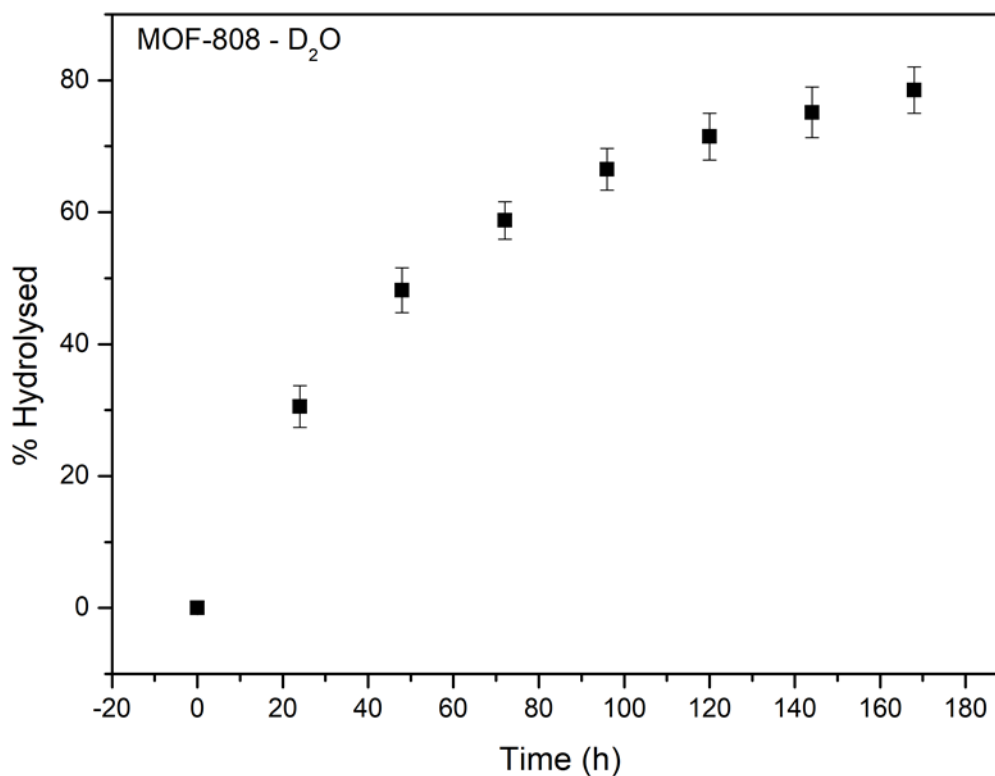
glycine.

Figure 2.19 Hydrolysis plot of diglycine in D₂O using MOF-808 as a catalyst. Error bars calculated from standard deviation, this was taken from 3 repeats of the hydrolysis experiment.

The hydrolysis reached around 80% completion after 7 days (shown in Figure 2.19). MOF-808 still shows catalytic activity in a 1:50 molar ratio with diglycine showing its propensity for catalysis.

The procedure outlined in 2.2.6 was repeated with d-THF (0.75 ml) replacing D_2O when being added to the stock solution. THF was important for reactions with the polyHIPE as it requires an organic solvent, which it can subsequently swell in as shown in 2.3.2. Therefore, THF was used in the hydrolysis studies with MOF-808 to show a comparison of the effect of THF with the polyHIPE and the MOF. MOF-808 (0.029 g, 0.4 mmol) was used in these hydrolysis studies.
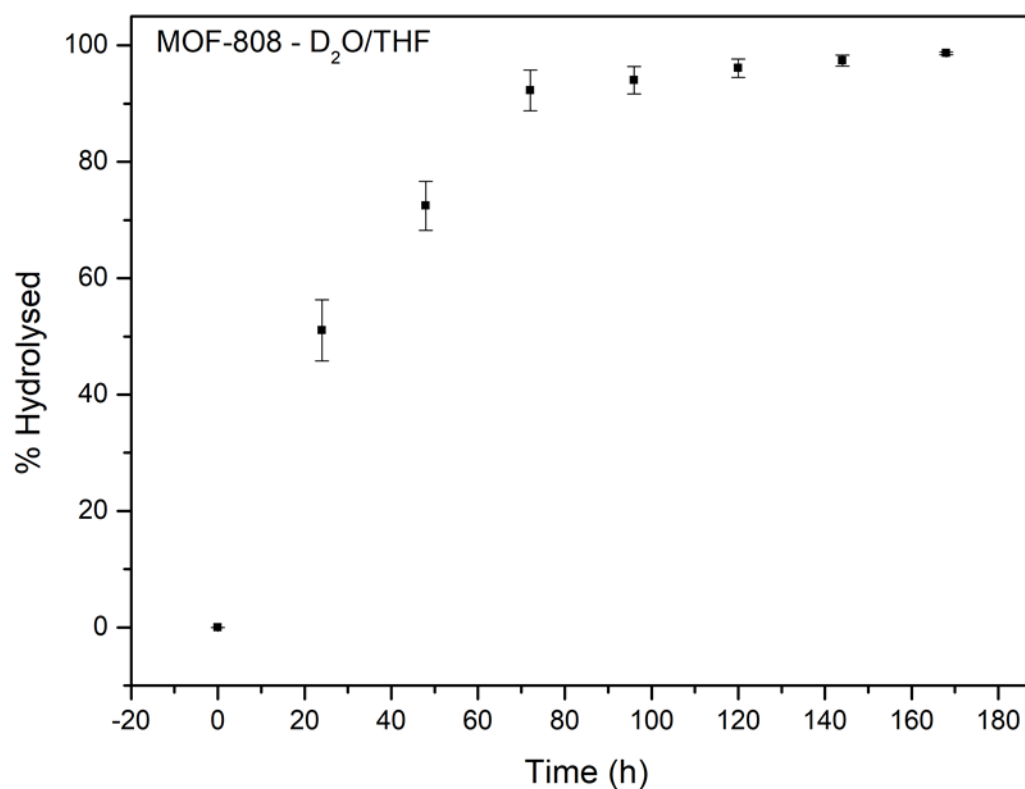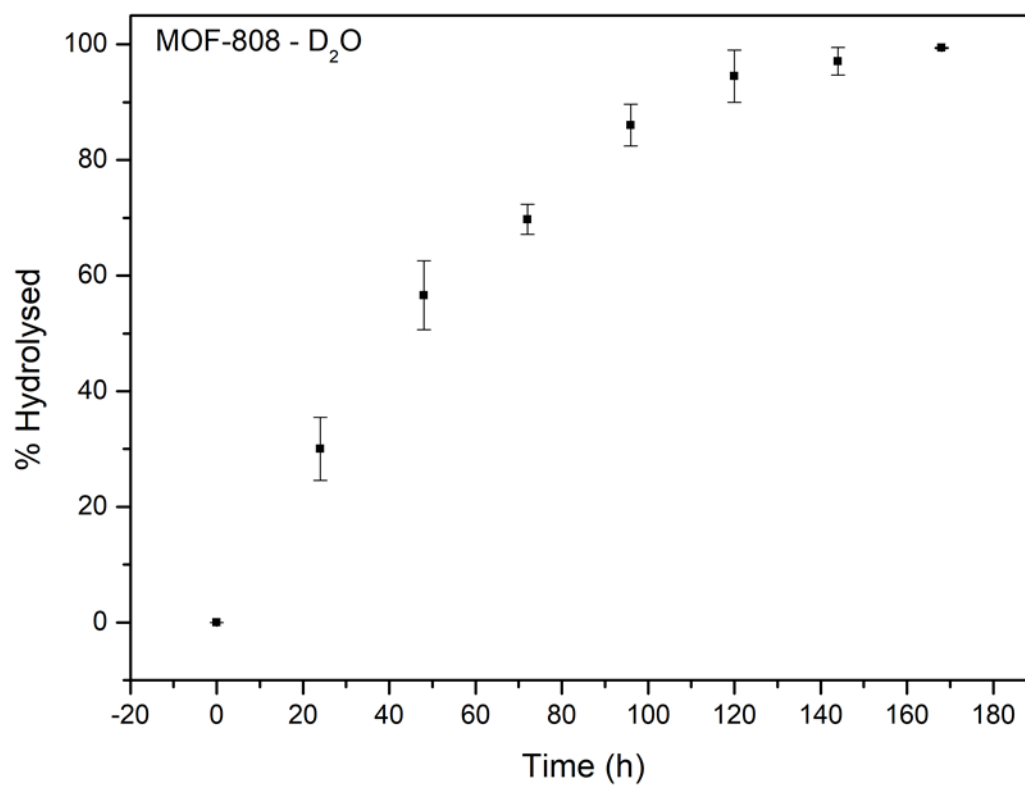
Figure 2.20 Hydrolysis plots of diglycine in D₂O/THF (bottom) and D₂O (top) using MOF-808 as a catalyst. Error bars calculated from standard deviation, this was taken from 3 repeats of the hydrolysis experiment.

In the previous section, the molar ratio between MOF-808 and diglycine was 1:50, for the

reaction in D₂O in this section the molar ratio is 1:2 as shown in reaction A from Table 3. Figure

2.20 shows that the difference in molar ratio results in improved catalytic activity and

62

therefore a greater hydrolysis percentage in a shorter time frame. After 4 days in this reaction the % hydrolysis had already surpassed the amount of glycine formed previously. This result is rather unsurprising as the molar ratio between catalyst and diglycine was 1:2, so it would be expected to improve reaction rate. The result of real interest is the difference between the hydrolysis in D_2O and D_2O/THF 50:50 mix results.
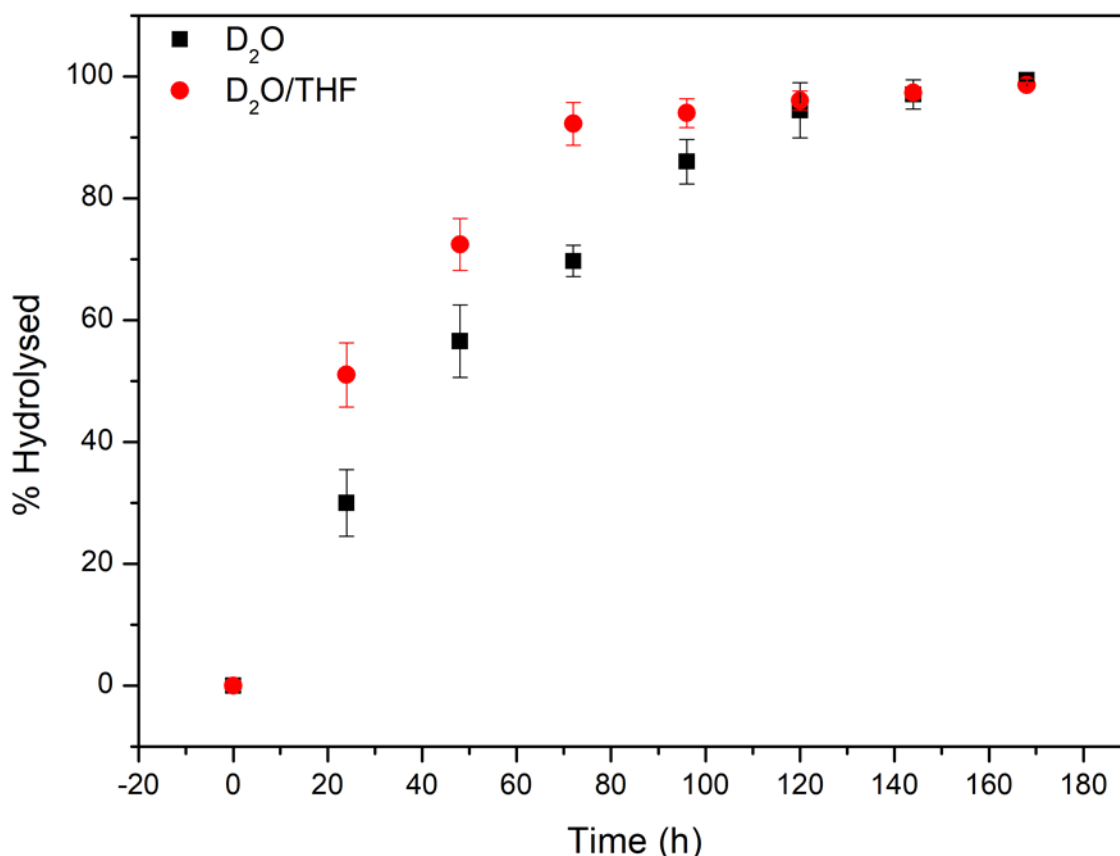
Figure 2.21 Hydrolysis plots of diglycine showing the comparison of MOF-808 in D_2O and D_2O/THF solvent mixes. Error bars calculated from standard deviation, this was taken from 3 repeats of the hydrolysis experiment.

The reaction rate in the D_2O/THF mix (shown in Figure 2.21) is greater than in just D_2O, this can be explained through its traits as a co-solvent in a binary mixture with water. Firstly, THF's impressive solvent properties are a result of its polar oxygen in its ring and the dispersive nature of the four methylene groups. In a mixture with water, THFs dispersive character increases as the THF content in the aqueous phase increases. This has been indicated in a previous study where it was shown that THF had a catalytic effect on the hydrolysis of cellulose to glucose.[23] This correlates with the addition of a co-solvent in this reaction increasing the catalytic activity.

Initial testing of MOF-808 as a catalyst in the hydrolysis of diglycine focused on the temperature variable, so using the procedure outlined in 2.2.6 the temperature was changed from 40°C to 60°C. In these studies MOF-808 (0.001 g, 7.34×10^{-4} mmol) was used and the hydrolysis was studied over a 3 hour period.

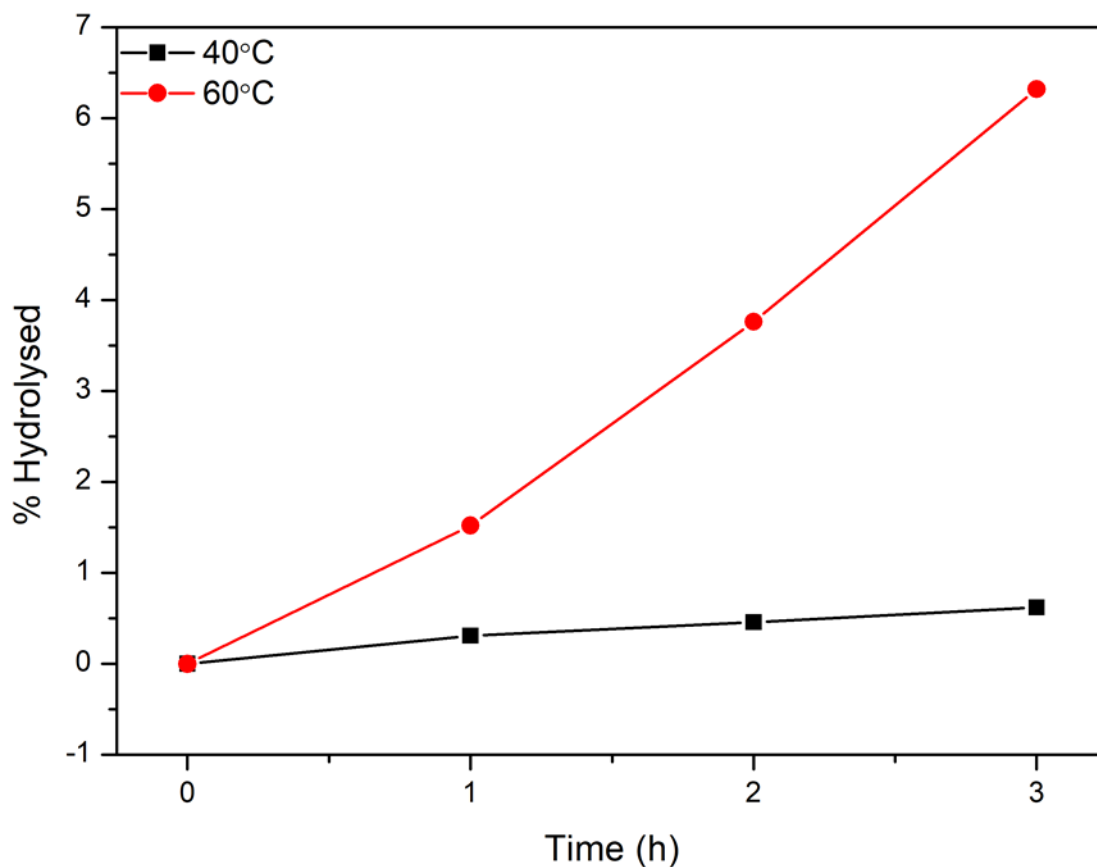*Figure 2.22 Hydrolysis plot of diglycine using MOF-808 as a catalyst at 40°C (black) and 60°C (red).*

This varied temperature hydrolysis study (shown in Figure 2.22) was only studied over a 3 hour period, a higher temperature showed a clear increase in reaction rate. The optimisation and combination of all of the dependent variables in this hydrolysis reaction would continue to increase the reaction rate.
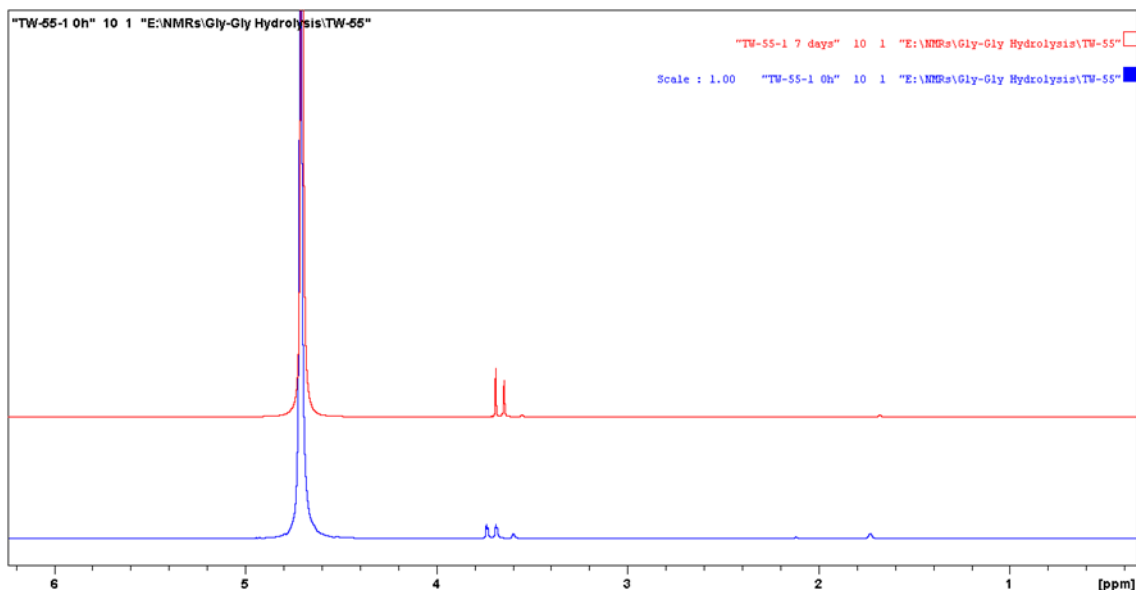
2.3.3.2 PolyHIPE

Figure 2.23 NMR spectra showing the hydrolysis of diglycine after 0 and 168 hours with the polyHIPE as the catalyst.

The hydrolysis studies with the polyHIPE without catalyst (shown in Figure 2.23) resulted in no conversion of diglycine, which was unsurprising as the reaction is dependent on the MOF catalyst being present.

2.3.3.3 PolyHIPE-MOF

	PolyHIPE-MOF (g)	Diglycine (g)	D_2O (ml)	THF (ml)	Concentration (mM)	Molar ratio (MOF:gly-gly)	Molar ratio (MOF content)
Reaction A	0.0465	0.0080	0.75	0	40	1:9	1:10
Reaction B	0.0465	0.0080	0.375	0.375	40	1:9	1:10
Reaction C	0.0050	0.0080	0.375	0.375	40	1:15	1:50
Reaction D	0.930	0.2915	27.5	27.5	40	1:1	1:4

Table 4 A table showing the reaction parameters for this section.

Table 4 outlines the reaction parameters for this section which will look at the effects of altering conditions in this hydrolysis reaction on the activity of the polyHIPE-MOF. Firstly, altering the molar ratio between the polyHIPE-MOF and diglycine in the reaction and the combination of two solvents. The hydrolysis of diglycine was carried out following a previously reported procedure. The reaction was followed using ^{1}H NMR. The hydrolysis of diglycine using polyHIPE-MOF as a catalyst is a relatively novel reaction, therefore the only comparison to be made is to the previously mentioned conditions in 2.2.6. Therefore, the initial reaction conditions were at 60°C as this was determined to be the most effective temperature, 40mM

gly-gly was used. The amount of polyHIPE-MOF used was determined by the 25% MOF content within the polymer matrix, so MOF-808 (0.0116 g, 8.5×10^{-3} mmol).

The procedure outlined in 2.2.8 was also used with D_2O (0.75 ml) replacing d-THF when added to the stock solution.
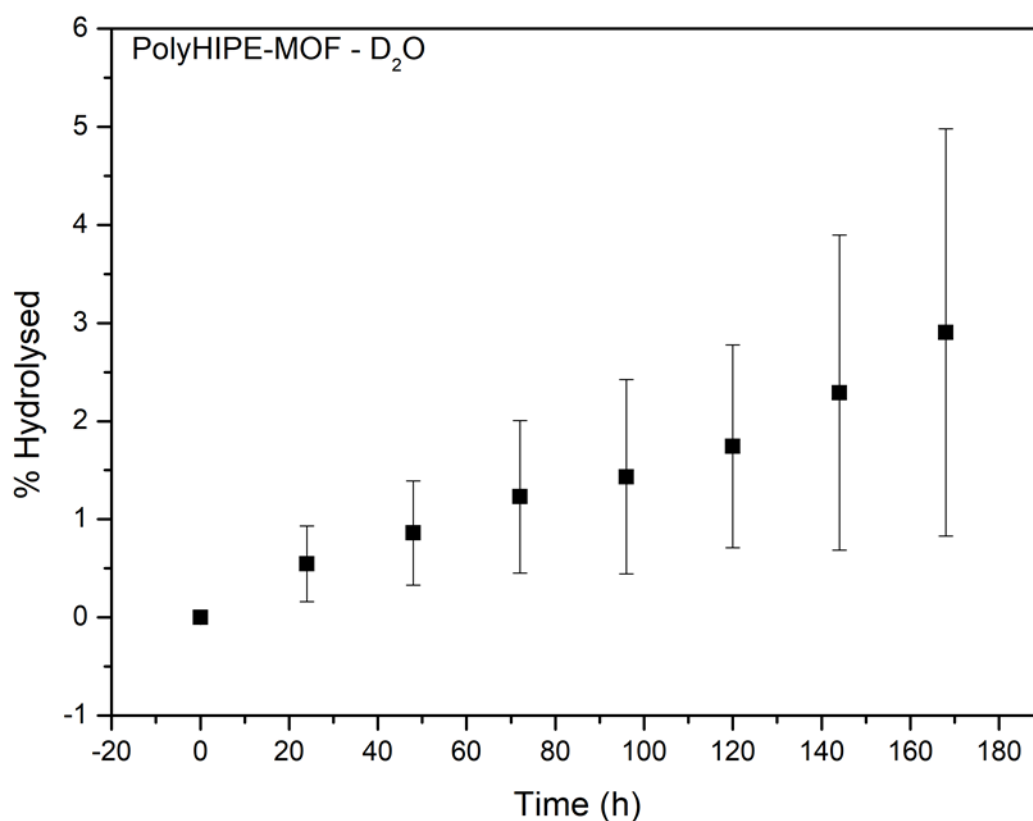
Figure 2.24 Hydrolysis plot of diglycine in D_2O using polyHIPE-MOF as a catalyst. Error bars calculated from standard deviation, this was taken from 3 repeats of the hydrolysis experiment.

The hydrolysis of diglycine with the polyHIPE-MOF as a catalyst in D_2O (shown in Figure 2.24) shows a very low conversion. This low hydrolysis percentage can be explained through the ability of the solvent used to swell the polymer as shown in 2.3.2.
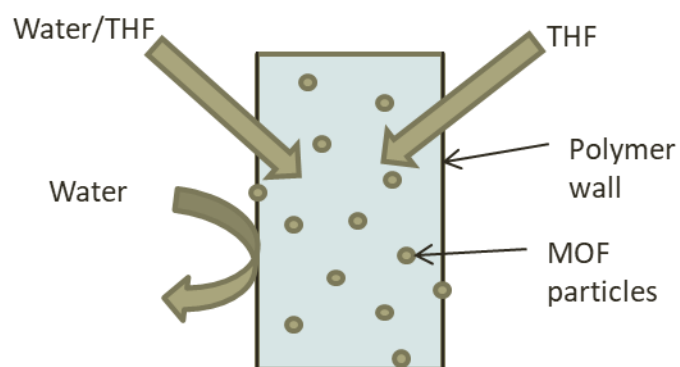
Figure 2.25 Illustration showing the ability of a solvent to permeate into the polymer matrix.

The diagram illustrated in Figure 2.25 shows the ability of water, water/THF and THF solvent mixes to permeate into the polymer matrix. THF is able to swell the polymer and therefore break through the polymer wall and access the MOF particles embedded within. This also applies to the solvent mix involving a 50:50 mix of water and THF, having the THF in this solvent mix results in the polymer once again swelling. However, a solvent mix made up of just water is unable to permeate through the walls of the polymer and is absorbed onto the walls of the polymer, therefore it is only able to access the small number of MOF particles based on that fragment of the polyHIPE. This explains the major discrepancy between the two hydrolysis studies.

The initial result for the hydrolysis of diglycine in D_2O/THF using polyHIPE-MOF as the catalyst produced an anomalous result.
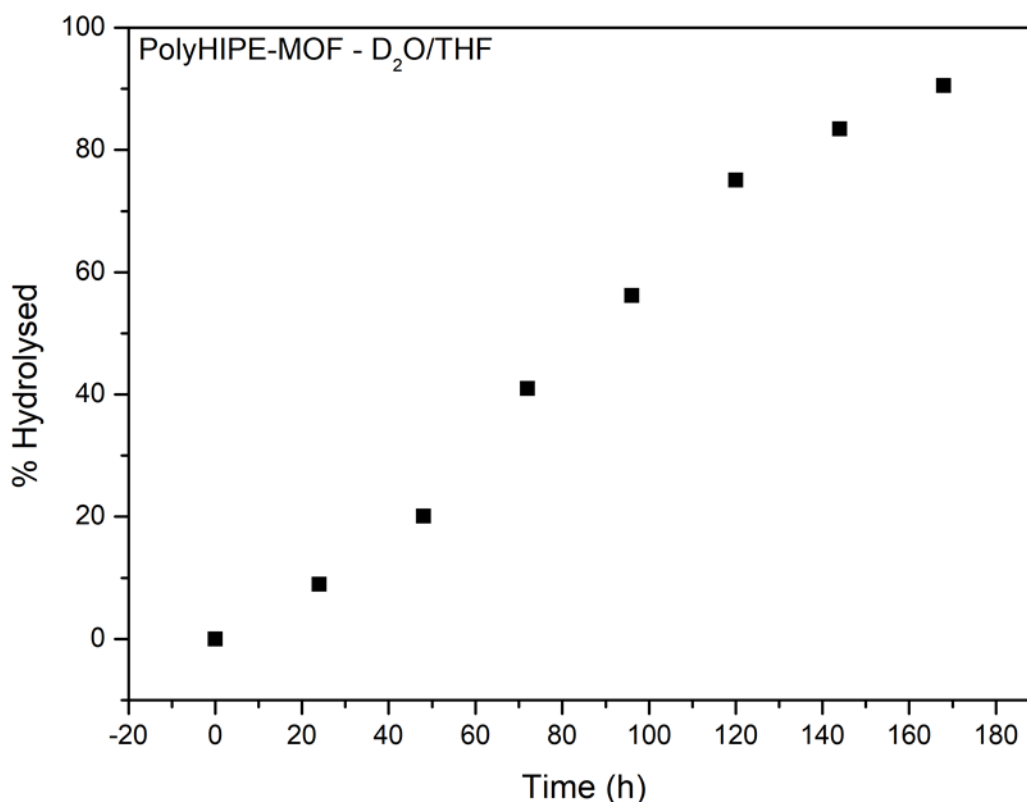
Figure 2.26 Hydrolysis plot of diglycine in D₂O/THF using polyHIPE-MOF (0.0465 g) as the catalyst.

As outlined in Figure 2.27 a 45% conversion of diglycine to glycine was achieved, however in another study using the same conditions around 90% conversion was achieved (shown in Figure 2.26). In this reaction, the polyHIPE-MOF swells within the NMR tube, the limitations to this are therefore heightened. Once the polymer swells to its full capacity, in some cases the polymer will no longer be immersed in the solvent containing the dipeptide. This was the case in the results shown in Figure 2.27 whereas in this study it is clear that the polyHIPE remained immersed in the solvent throughout the study to achieve a much higher hydrolysis rate. Another possibility for these differences could be attributed to the dispersion of the MOF, the SEM-EDS clearly indicates the MOF disperses throughout the whole polymer matrix. However, the amount of MOF may differ slightly from section to section which could cause such discrepancies in hydrolysis results.
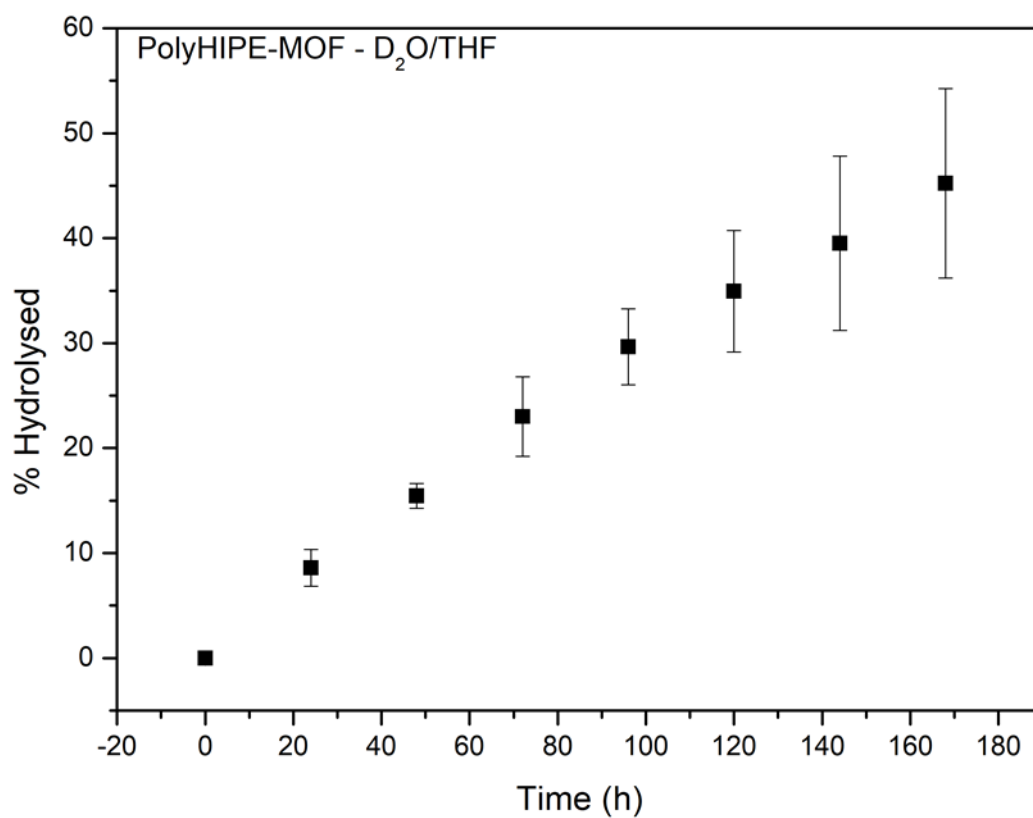
Figure 2.27 Hydrolysis plot of diglycine in D₂O/THF using polyHIPE-MOF (0.0465 g) as a catalyst. Error bars calculated from standard deviation, this was taken from 3 repeats of the hydrolysis experiment.

The procedure outlined in 2.2.8 was repeated with polyHIPE-MOF (0.0050 g, 3.04×10^{-3} mmol).

One of the possible limitations of the use of a large piece of polymer in an NMR tube was

counteracted by using a smaller piece. This meant a decrease in the amount of MOF-808

(0.0013 g, 9.18×10^{-4} mmol) used.
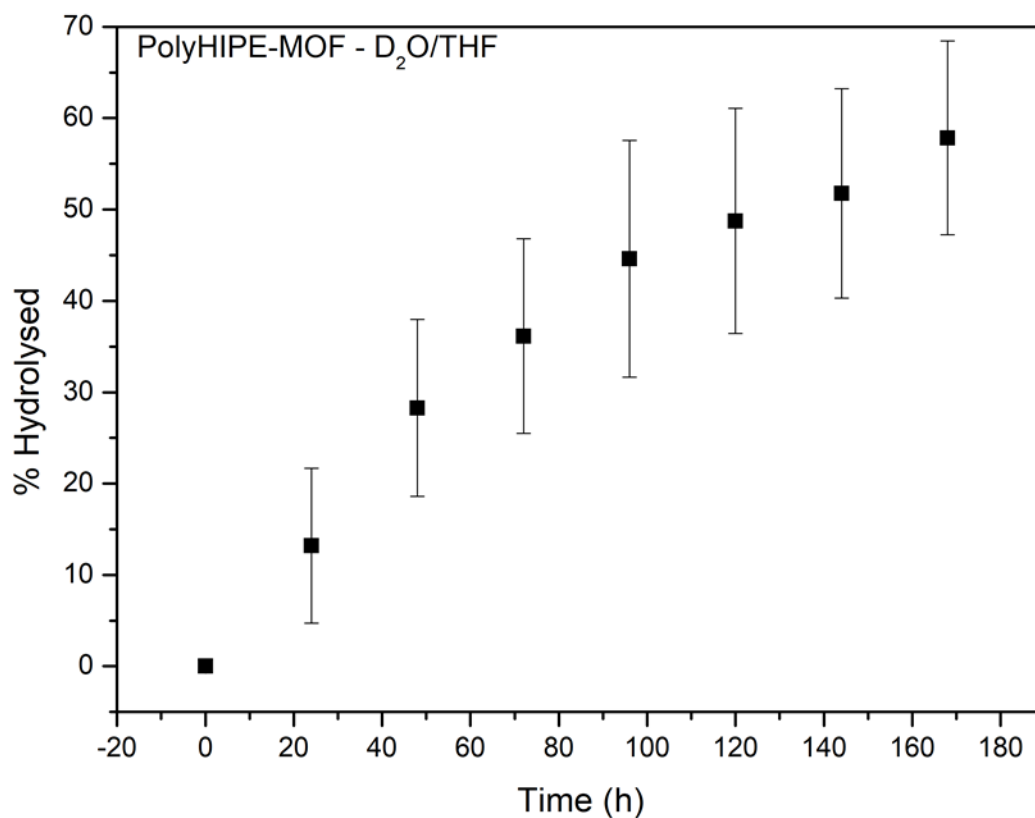
Figure 2.28 Hydrolysis plot of diglycine in D$_2$O/THF using polyHIPE-MOF (0.0050 g) as a catalyst. Error bars calculated from standard deviation, this was taken from 3 repeats of the hydrolysis experiment.

Figure 2.28 shows the hydrolysis conversion increased when using a smaller piece of the polyHIPE-MOF thus suggesting that the polymer was able to remain immersed within the solvent containing the dipeptide and therefore had a greater catalytic activity.

As shown in the characterisation of the polyHIPE-MOF, the MOF is embedded within the polymer matrix so when it is ground into a powder it could be theorised that the catalytic MOF will be more efficient in the reaction. Therefore, a powdered version of the polyHIPE-MOF was also used in the hydrolysis of diglycine.
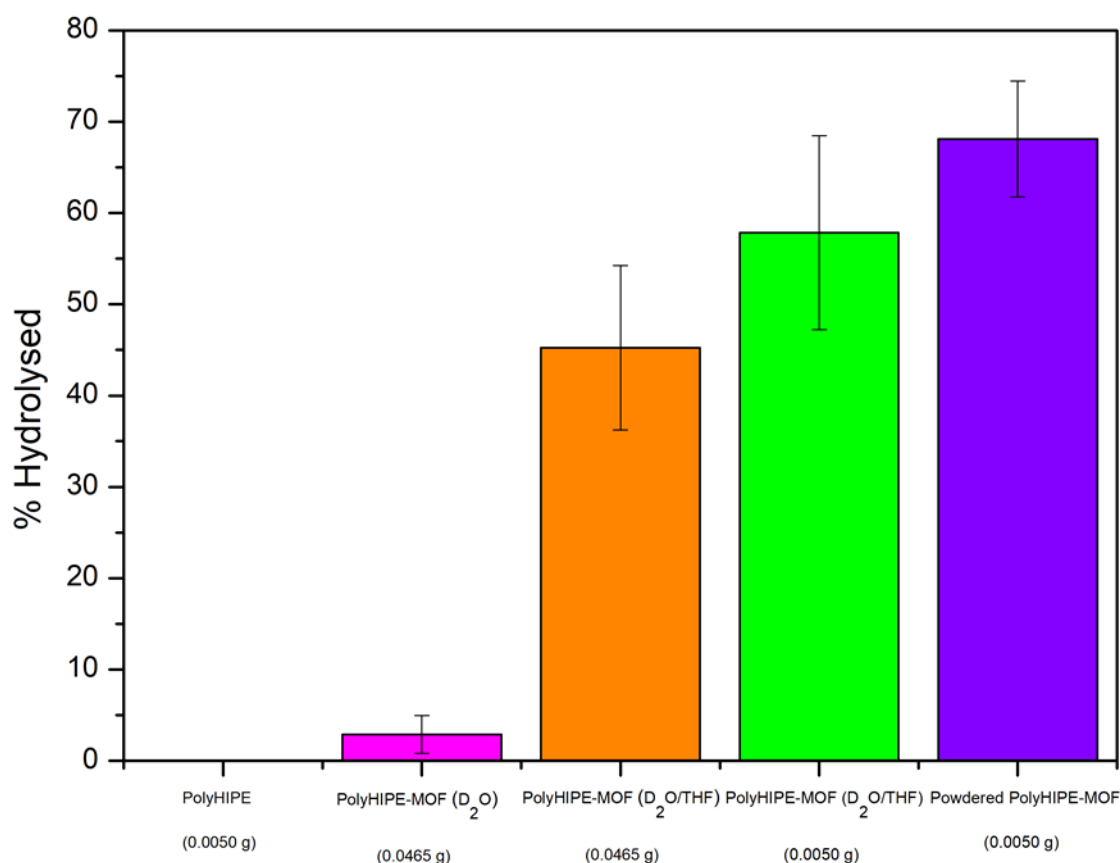
Figure 2.29 Comparison of the degree of hydrolysis of diglycine for the polyHIPE-MOF (in un-powdered and powdered morphologies) in D_2O and D_2O/THF and the polyHIPE after 7 days. Error bars calculated from standard deviation, this was taken from 3 repeats of the hydrolysis experiment.

The powdered form of the polyHIPE-MOF showed a further increase for the conversion to glycine (shown in Figure 2.29), as shown before in the infrared spectra, MOF-808 can be visualised when the polymer is ground into a powder. Therefore, the MOF catalyst is accessible to the solvent containing the dipeptide. Furthermore, the versatile nature of the polymer is indicated as it effective in both powdered and un-powdered forms, the powdered form is much more effective in a small environment like an NMR tube but in a scaled up reaction in a larger vessel the un-powdered piece of polymer may be more effective.

2.3.3.4 Scale Up Hydrolysis of Diglycine Using the PolyHIPE-MOF

D_2O (27.5 ml) was added to a round bottomed flask with diglycine (0.2915 g, 2.21 mmol, 80 mM). To this, THF (27.5 ml) was added to make a solution of D_2O/THF (55 ml, 40 mM gly-gly). PolyHIPE-MOF (0.930 g, 0.565 mmol) was added to this solution and subsequently heated at

65°C. At different time increments, 0.75 ml aliquots of the solution were extracted and an

NMR was taken of the sample to monitor the progress of the hydrolysis.
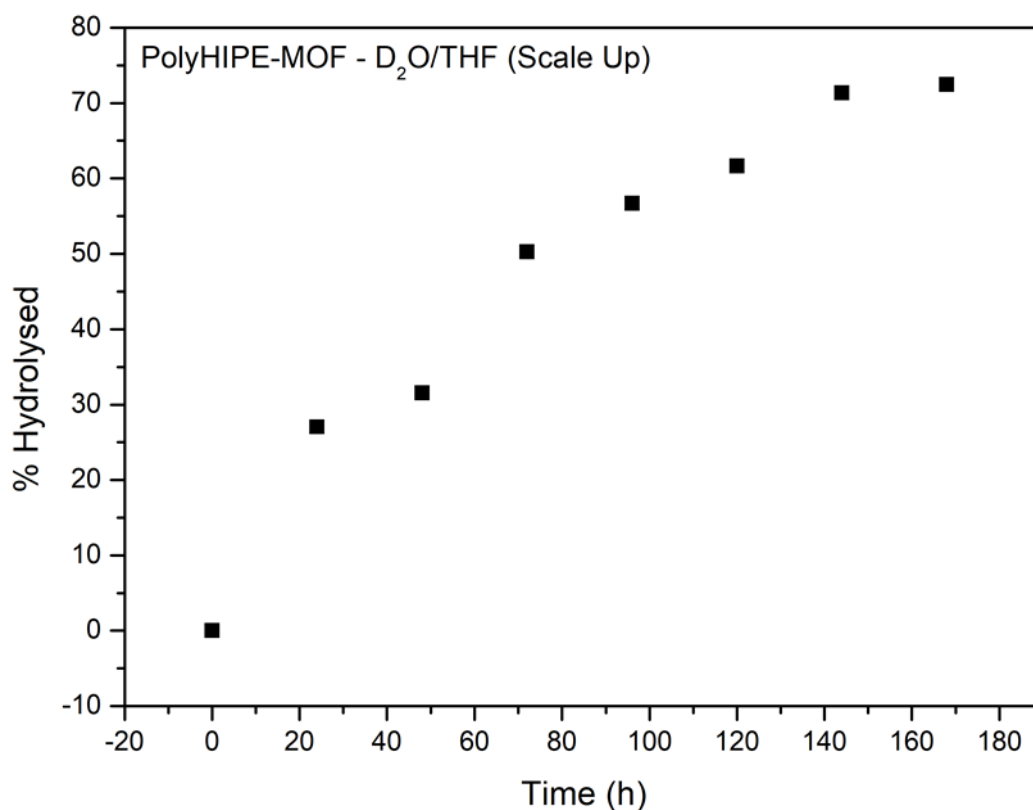
Figure 2.30 Hydrolysis plot of diglycine in D₂O/THF using the polyHIPE-MOF as a catalyst in a scaled up reaction.

Another factor of the polyHIPE-MOF that was in need of testing was its scalability, thus the

hydrolysis reaction was repeated on a much larger scale in a large excess of solvent. The excess

of solvent was required as the amount of solvent used originally, following the procedure

outlined in 2.2.8 was insufficient as the polymer swelled, absorbing all of the solvent into its

matrix. The results of this study implied that the hydrolysis reaction is scalable and the

catalytic activity of the polyHIPE is just as prominent (shown in Figure 2.30).

2.3.3.5 PolyHIPE-MOF Recyclability Studies

Using the procedure outlined in 2.2.8, with polyHIPE-MOF (0.0050 g, 3.04×10^{-3} mmol), the

polyHIPE-MOF was used as a catalyst in the hydrolysis of diglycine over 3 days. Once the 3 days

had past, the contents of the NMR tube were vacuum filtered using a Buchner funnel to

retrieve the hydrolysed product and the polyHIPE-MOF used. This piece of polyHIPE-MOF was then used in a repeat hydrolysis with the procedure being repeated 2 times.
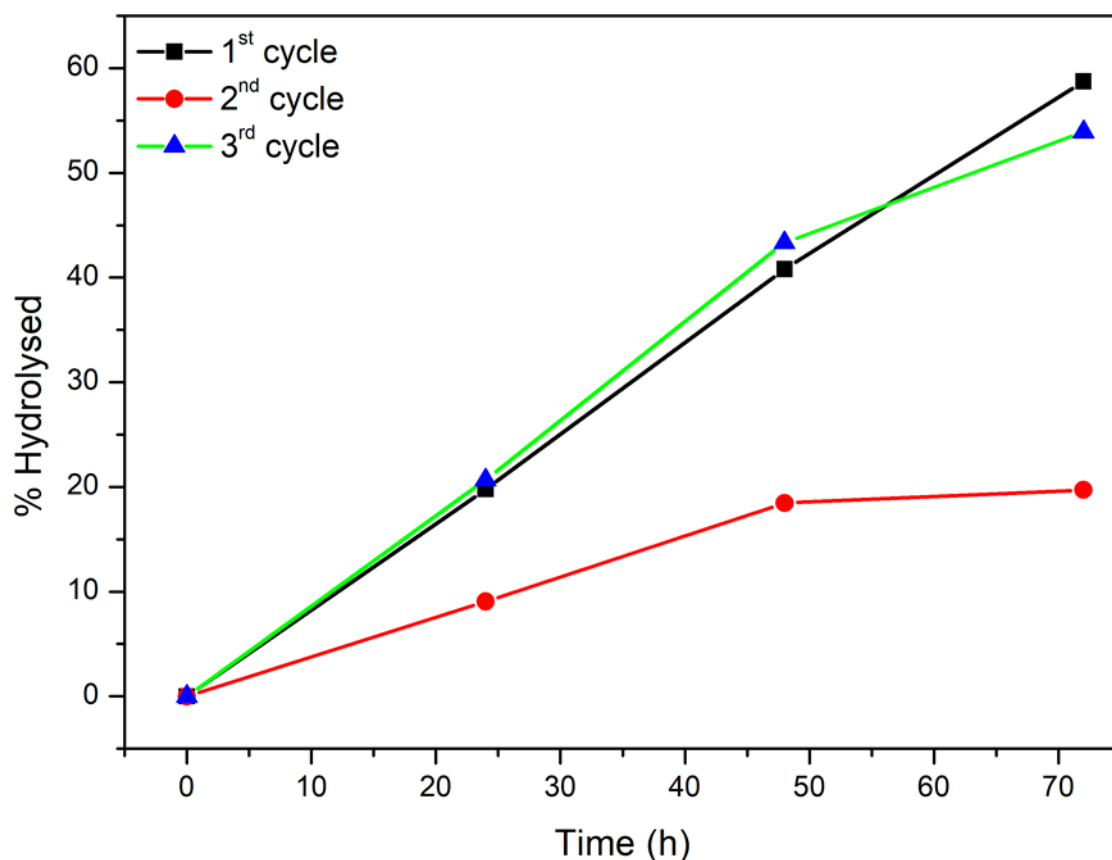
Figure 2.31 Hydrolysis plots of diglycine in D$_2$O/THF using polyHIPE-MOF as a catalyst showing 3 cycles of a recycled piece of polymer.

The recyclability studies of the polyHIPE-MOF (shown in Figure 2.31) have shown that the polymer can be used, extracted and used once again with the same effect as in the initial study. The second cycle in this study produced a lower percentage hydrolysis than in the first and third cycles, this may have been due to one of the aforementioned reasons of the polymer not being fully immersed. However, the final cycle had a conversion very similar to the first cycle suggesting that the catalytic activity was just as prominent after two extraction processes. This data indicates that not only is the polyHIPE-MOF easily recycled from a reaction using a simple vacuum filtration, but also that it can be reused at least twice with the catalytic effects of the material being just as effective.

2.3.4 pH Studies

The pH of each system was measured (shown in Table 5) to compare to the optimal value stated in literature of 7.4.[9] The difference in solvent mixes and the use of catalyst was expected to alter the pH and therefore the overall reaction rate of the system.

	Water	Water/THF
Diglycine	5.90	6.39
MOF-808	3.62	4.78
MOF-808/Diglycine	3.64	4.95

Table 5 pH values for MOF-808 and diglycine in water and water/THF 50:50 mix.

As mentioned in 2.3.3.1, in a previous study they determined that the pH needed to be altered in order to achieve optimal conditions for the hydrolysis reaction.[9] In order to achieve the desired pH a buffer was used and 7.4, a neutral pH was determined to be the ideal pH for this reaction. Therefore, to compare to the literature values, the pH of each reaction was measured. The results of which for the MOF catalyst were that the conditions were much more acidic than the ones used in the literature study. According this study, pH values that are more acidic decrease the rate of reaction. This goes a way to explaining the extended duration required to achieve almost 100% hydrolysis.

	Water	Water/THF
Diglycine	5.90	6.39
PolyHIPE-MOF	6.17	6.76
PolyHIPE- MOF/Diglycine	6.06	6.21

Table 6 pH values for the polyHIPE-MOF and diglycine in water and water/THF 50:50 mix.

The pH used in this reaction (shown in Table 6) was also lower when compared to the literature value, but was significantly higher than that used in the MOF-808 studies. The rate of reaction using a pH in the region of 6 is slightly decreased, on the other hand the change isn't great enough to cause a significant decrease in hydrolysis rate. Therefore suggesting there are more important factors effecting the reaction rate in the hydrolysis studies, when using the polyHIPE-MOF as a catalyst.

2.3.5 Comparison of MOF-808 and PolyHIPE-MOF Hydrolysis Studies
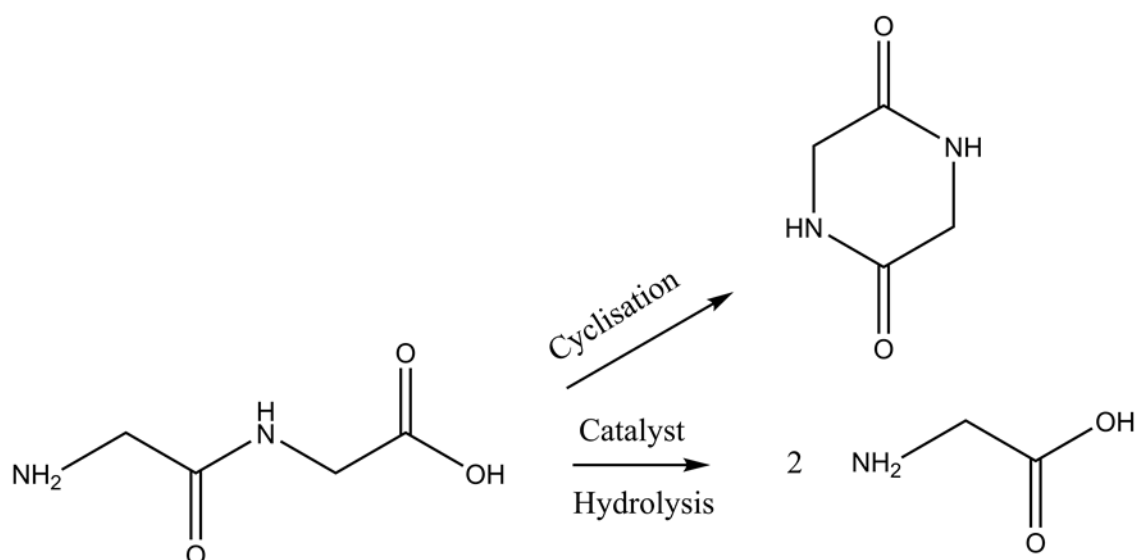
Figure 2.32 Reaction scheme for the hydrolysis of diglycine to glycine with the formation of the cyclisation-glycine side product.

The ^{1}H NMR spectra in the hydrolysis of diglycine shows two singlets around 3.65-3.75 ppm to indicate the diglycine, a singlet at around 3.4 ppm to indicate glycine and a singlet at around 3.9 ppm to indicate the cyclisation product of glycine. Both MOF-808 and the polyHIPE-MOF worked as catalysts in the hydrolysis of diglycine, but they both achieved reaction rates under different conditions. The first example of this is the use of solvent, in the first instance D$_2$O was used.

Figure 2.33 Hydrolysis plots of diglycine comparing the catalytic effects of MOF-808 to the polyHIPE-MOF in D_2O. Error bars calculated from standard deviation, this was taken from 3 repeats of the hydrolysis experiment.

Figure 2.33 compares the hydrolysis of diglycine in D_2O using two different quantities of MOF-808 and the polyHIPE-MOF. The polyHIPE-MOF in this instance was ineffective as a catalyst due to their being no solvent used which the polymer can absorb. Therefore, the D_2O used is only able to interact with the MOF particles on the surface of the polyHIPE. This explains the much lower catalytic activity of the polyHIPE-MOF when compared to the MOF on its own.

On the other hand when a solvent such as THF is added to the solvent mix, which the polyHIPE-MOF can swell up to 40 times its original mass in, the MOF catalyst inside the polymer network can then interact with the solvent mix containing diglycine.
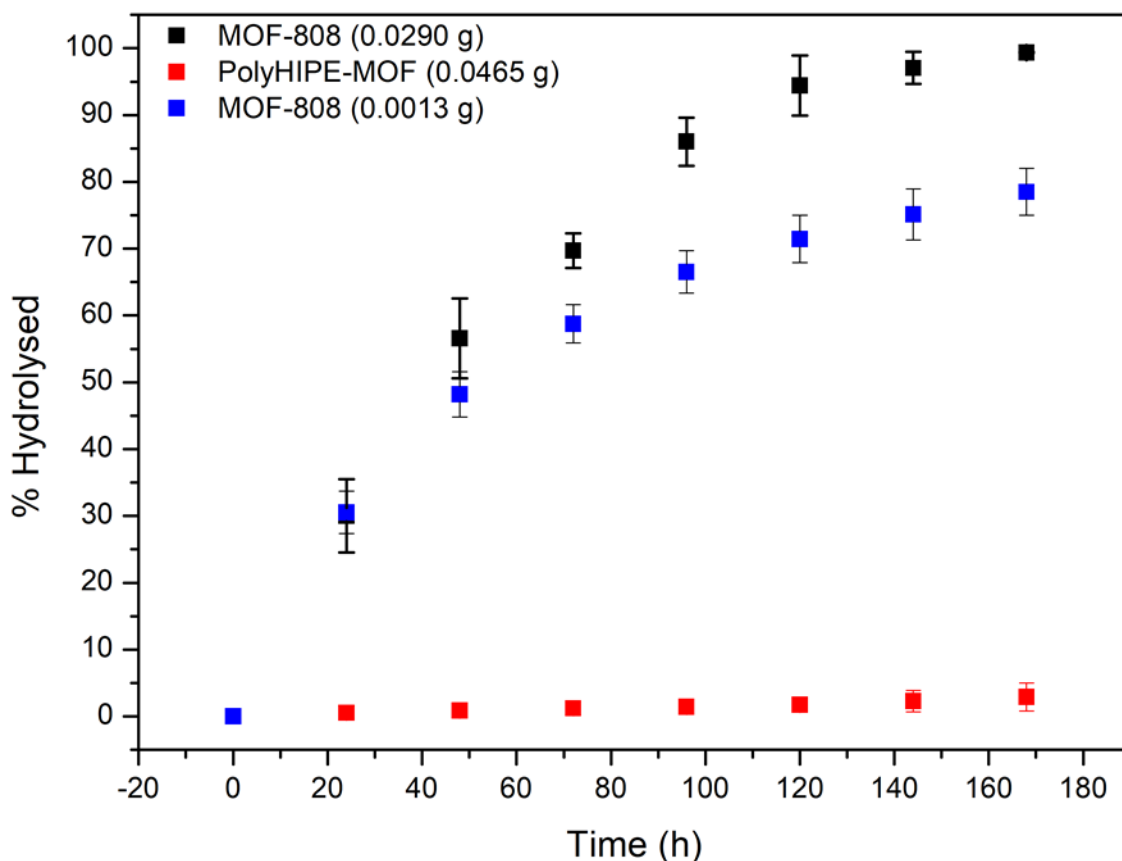
Figure 2.34 Hydrolysis plots of diglycine comparing the catalytic effects of MOF-808 to the polyHIPE-MOF in a D$_2$O/THF mix. Error bars calculated from standard deviation, this was taken from 3 repeats of the hydrolysis experiment.

As expected the polyHIPE-MOF has had a much greater effect on the hydrolysis reaction when in a D$_2$O/THF solvent mix (shown in Figure 2.34). MOF-808 once again acts as a much more effective MOF outside of the polymer network, this is potentially due to the dispersion of the MOF throughout the polyHIPE not being completely uniform. Also in this study MOF-808 (0.028 mmol) is used whereas only 7×10^{-3} and 7.6×10^{-4} mmol of MOF-808 in the polyHIPE are used. Due to the swellable nature of the polyHIPE, a smaller quantity has to be used as when it swells it expands to a point where the solvent is completely absorbed.

To counteract this issue, the polymer was ground into a powder, this also exposes the MOF catalyst as it is released from within the polymer matrix.

Figure 2.35 Hydrolysis plots of diglycine comparing the catalytic effects of MOF-808 to the polyHIPE-MOF (powdered and un-powdered) in a D₂O/THF mix after 7 days. Error bars calculated from standard deviation, this was taken from 3 repeats of the hydrolysis experiment.

Once again, there was an improvement in the polyHIPE-MOFs catalytic activity (shown in Figure 2.35), in this case the powdered form didn't absorb all of the solvent. The MOF within the polymer matrix originally has been released resulting in a much higher hydrolysis conversion. Once again in this comparison there is a major difference in the molar ratio between MOF-808 and diglycine (1:2) when compared to the molar ratio between the polyHIPE and diglycine (1:50), which can be attributed to the MOF content. The polyHIPE contained 7.6×10^{-4} mmol of MOF-808 compared to the as-synthesised MOF-808 0.028 mmol. This difference in quantity of catalyst provides a potential explanation for the difference in percentage hydrolysis between the powdered polyHIPE-MOF and MOF-808.

Another possible way of counteracting the limitations of the polyHIPE hydrolysis reaction within an NMR tube was to scale the reaction up and use a larger vessel for the reaction. This meant a larger quantity of the polyHIPE-MOF in an excess of solvent.
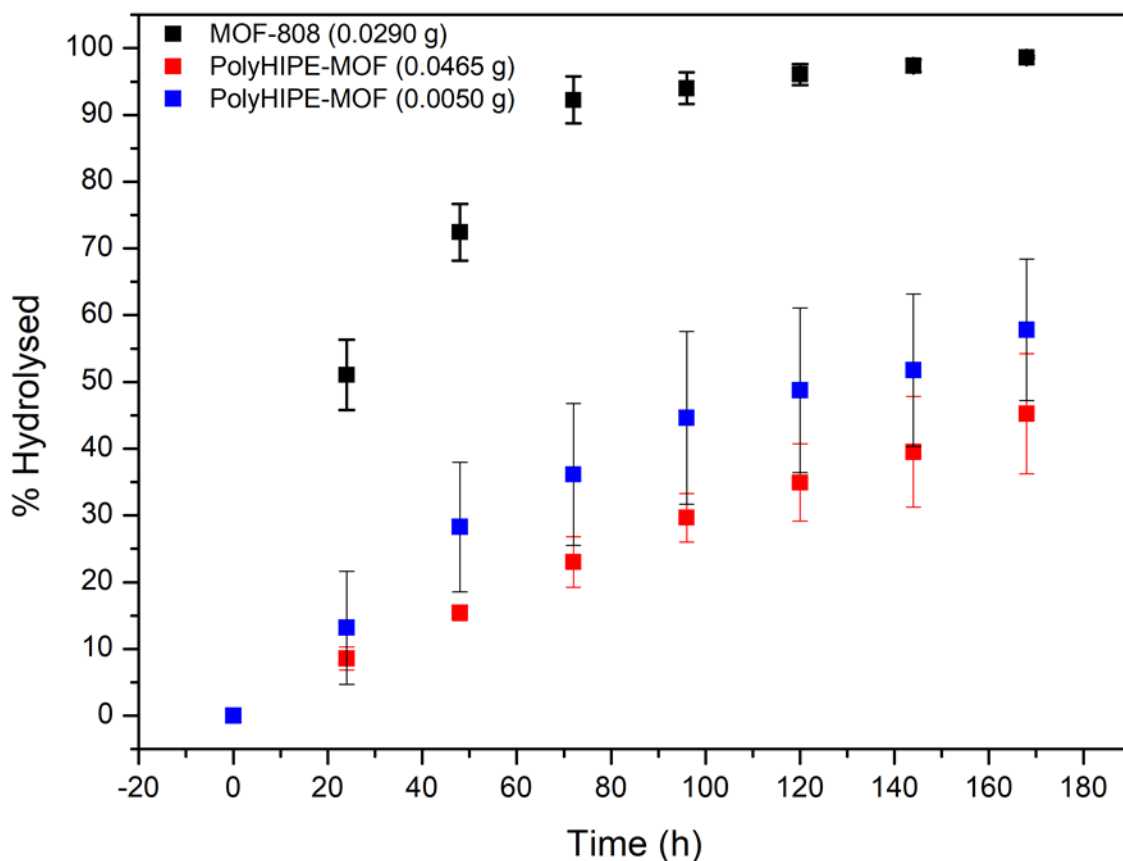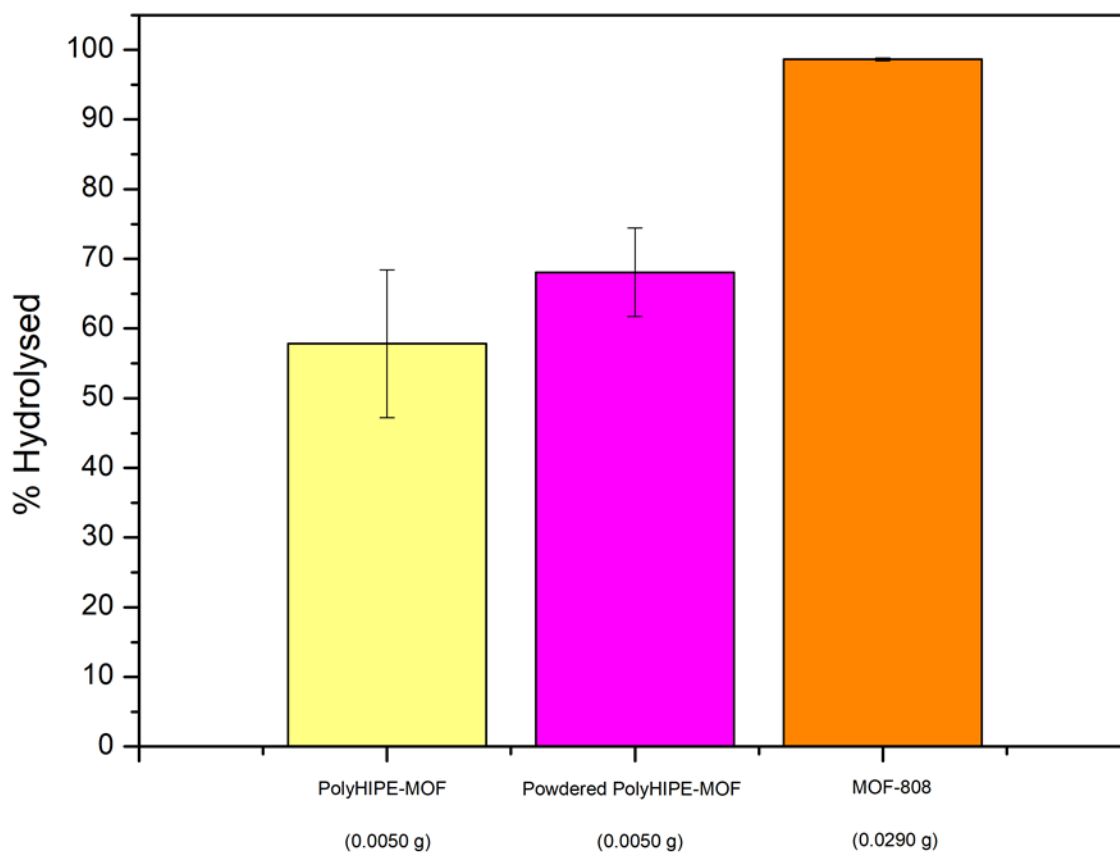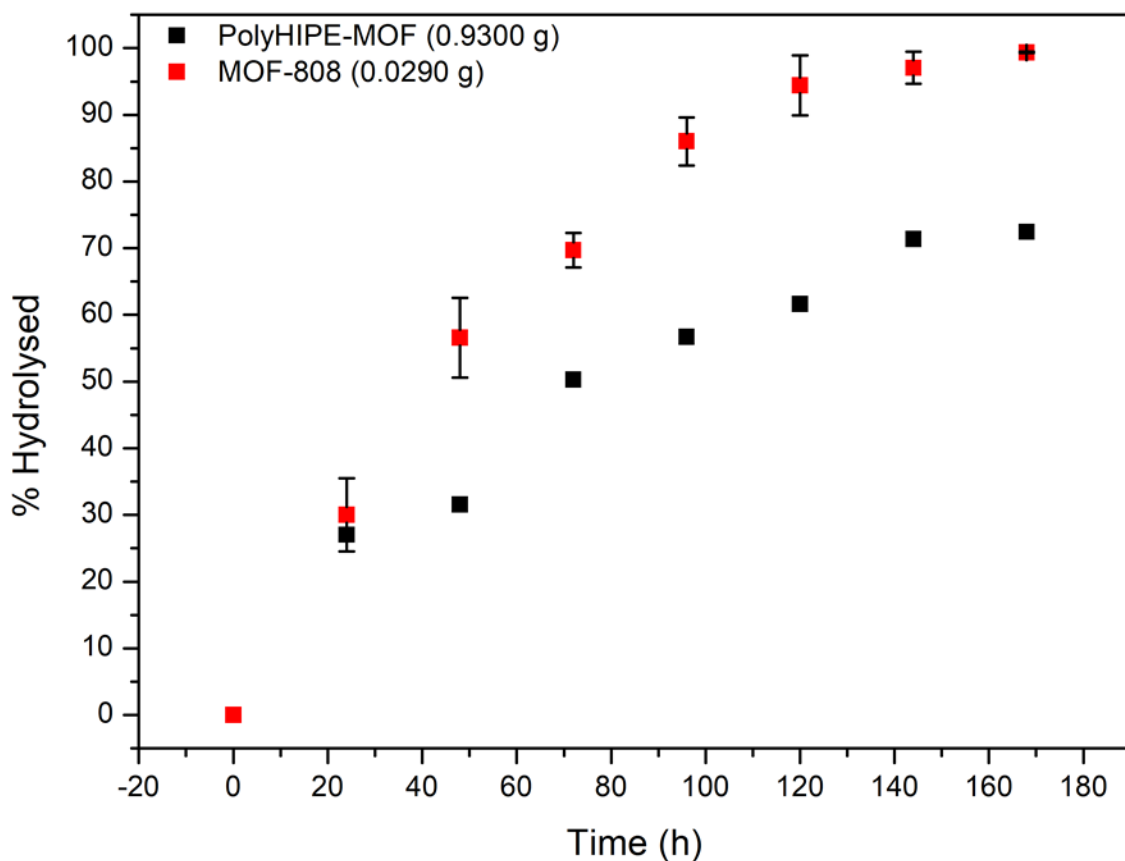
Figure 2.36 Hydrolysis plots of diglycine comparing the catalytic effects of MOF-808 to the polyHIPE-MOF (scale-up) in a D$_2$O/THF mix. Error bars calculated from standard deviation, this was taken from 3 repeats of the hydrolysis experiment.

The scale-up reaction (shown in Figure 2.36) provided similar improvements to the study using the powdered form of the polymer. Allowing the polyHIPE to reach its maximum absorption capacity in an excess of solvent allowed the active catalyst within its matrix to act as it would if it was as a crude powder. The important difference between the two results shown are the molar ratios between the catalyst and diglycine. MOF-808 is in a 1:2 molar ratio with diglycine whereas the polyHIPE-MOF is in a 1:4 molar ratio. The additional quantity of diglycine in the reaction with the polyHIPE can compensate for the difference in percentage hydrolysis.
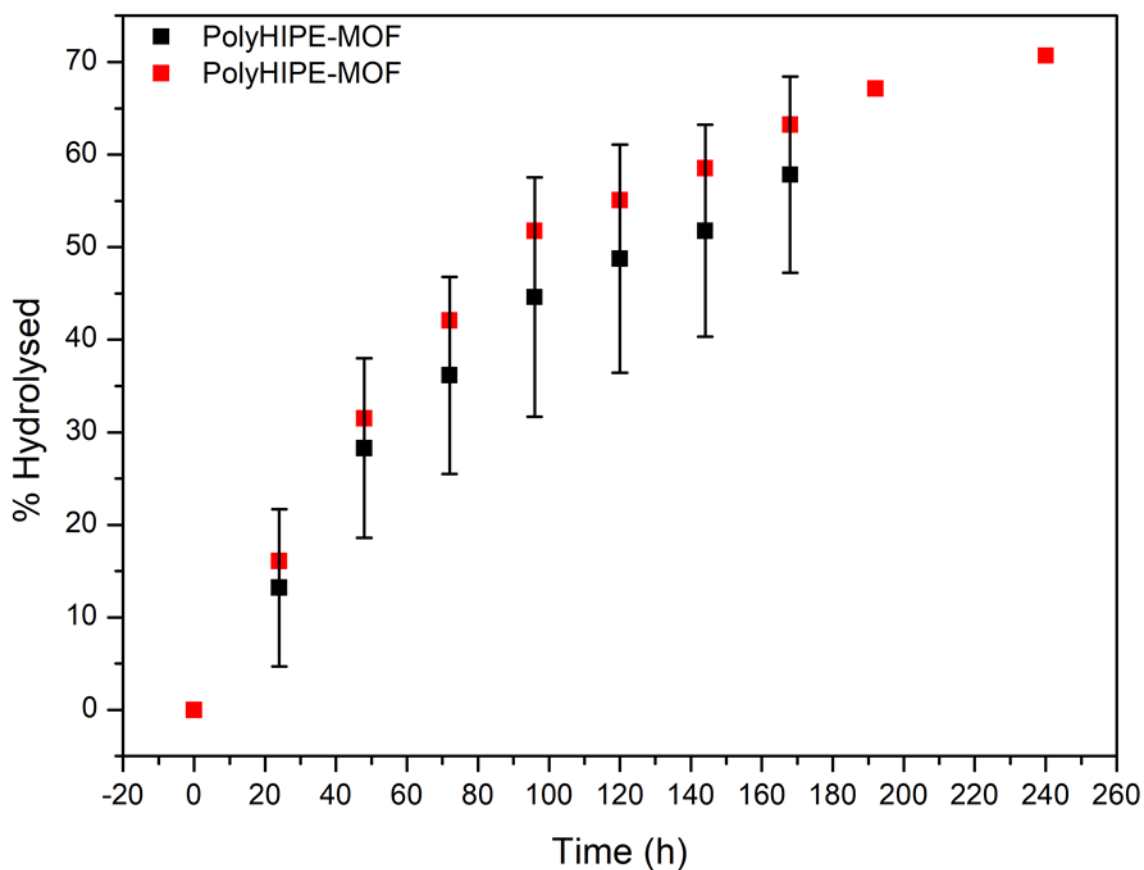
Figure 2.37 Hydrolysis plots of diglycine using the polyHIPE-MOF as a catalyst with one study extended to 10 days. Error bars calculated from standard deviation, this was taken from 3 repeats of the hydrolysis experiment.

The extended study of the polyHIPE-MOF as a catalyst (shown in Figure 2.37) showed a continued linear progression of the hydrolysis of diglycine (indicated by the red points in Figure 2.37).

During the hydrolysis of diglycine the cyclisation form of glycine forms as a by-product. With some MOF catalysts there isn't always a selectivity towards a specific product when there are 2 possible products. Therefore, the percentage cyclisation for each reaction was calculated to ensure the MOF had selectivity for the desired product in a hydrolysis reaction. Further to this, does the MOF retain this potential selectivity when embedded within a polymer network.
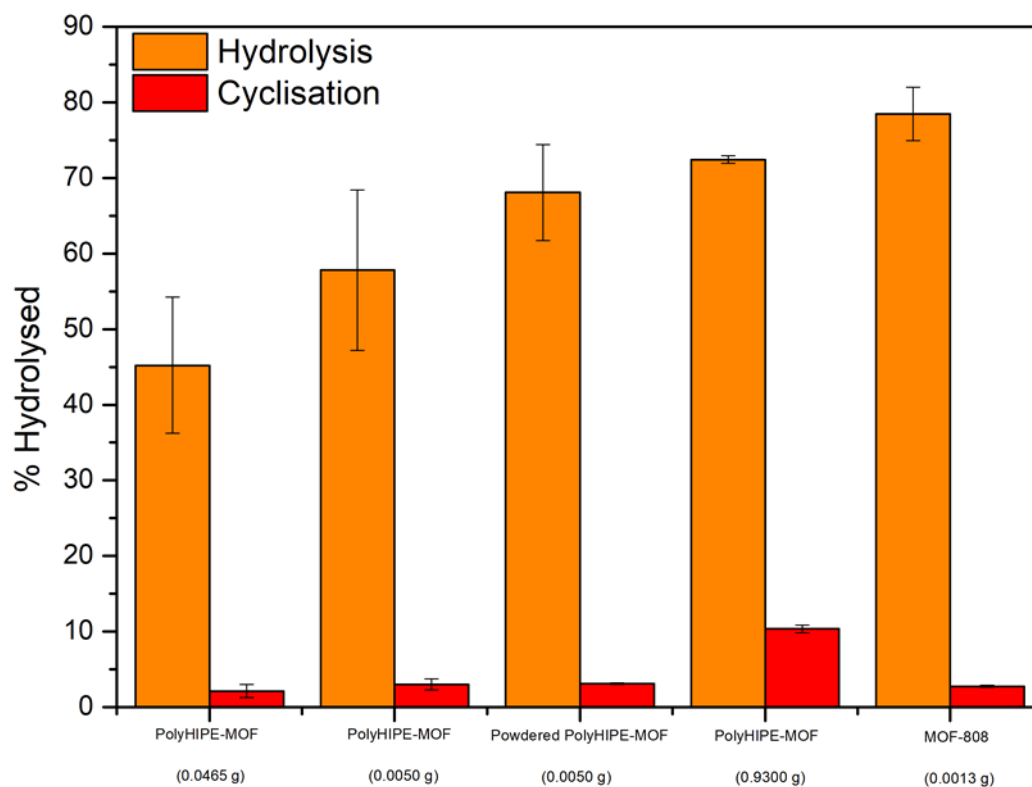
Figure 2.38 Plots showing the comparison of hydrolysis against cyclisation after 7 days using the polyHIPE-MOF and MOF-808 as catalysts. Error bars calculated from standard deviation, this was taken from 3 repeats of the hydrolysis experiment.

The results of each study (shown in Figure 2.38) shows that both the MOF and the polyHIPE-MOF have selectivity towards the hydrolysis product. This refers to multiple forms of the polyHIPE and in different quantities.

2.3.6 The Effect of Ball Milling

Samples of MOF-808 were ball milled to produce variable particle sizes to determine if smaller particle sizes would change the catalytic activity of the MOF.
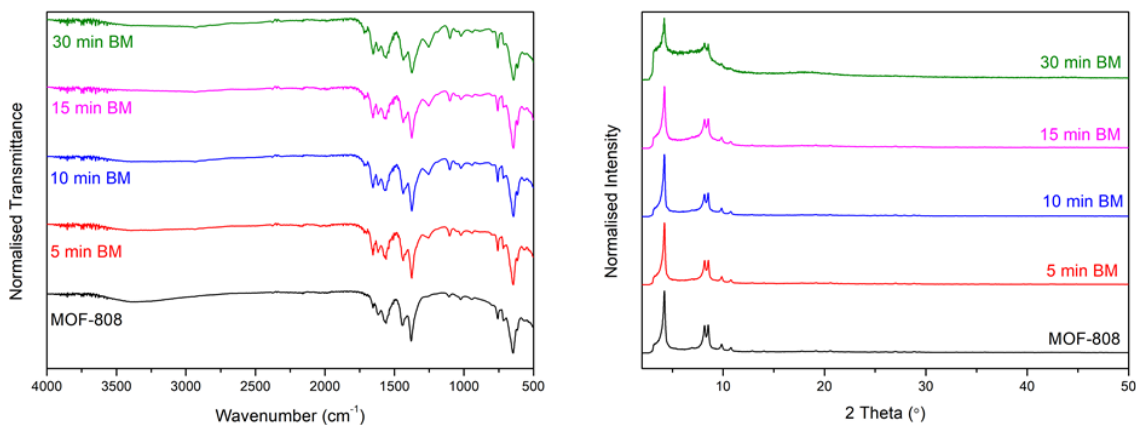
Figure 2.39 Infrared spectra overlay of MOF-808 and the ball milled MOF-808 samples (left) and PXRD overlay (right) of MOF-808 and the ball milled MOF-808 samples.

The infrared spectra of all of the ball milled MOF-808 samples (shown in Figure 2.39) suggests that there is no change in the functional groups on the framework. However, the PXRD patterns suggest that the longer the MOF is subjected to ball milling the crystallinity of the material decreases. The most obvious example of this is the sample that was ball milled for 30 minutes, as the defined sharp peaks in the as-synthesised MOF-808s PXRD have lost definition and have broadened suggesting that the framework has become amorphous.
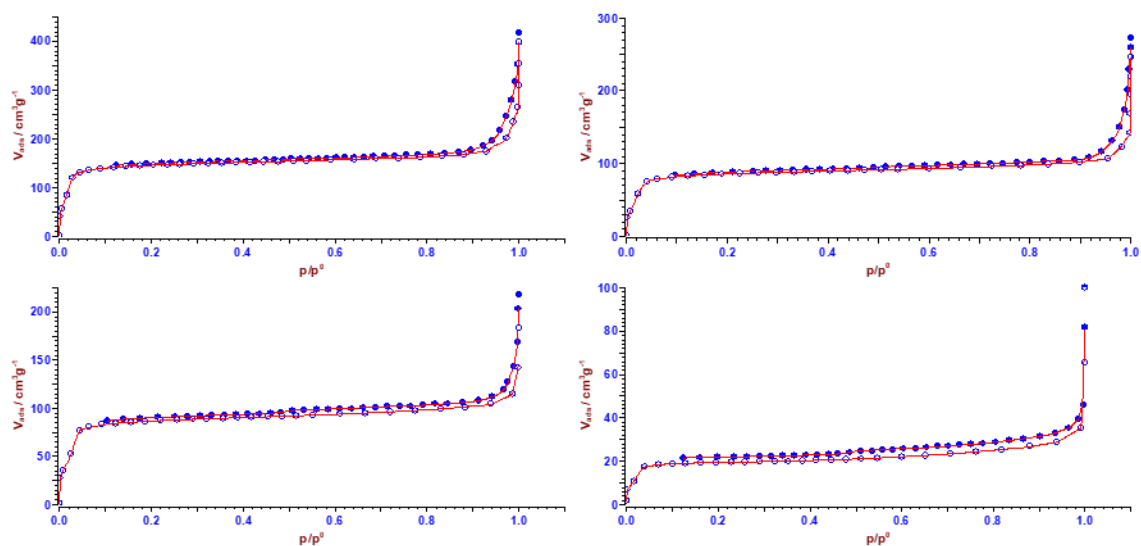
Figure 2.40 BET isotherms of the ball milled MOF-808 samples. Top left (5 min BM), top right (10 min BM), bottom left (15 min BM) and bottom right (30 min BM).

The BET isotherms of the 5, 10 and 15 minute ball milled MOF-808 samples (shown in Figure 2.40) show that they are mesoporous, this is indicated by the slight hysteresis within the adsorption and desorption curves. The 30 minute ball milled sample shows a similar curve but the adsorption and desorption curves don't form the hysteresis loop.[21]
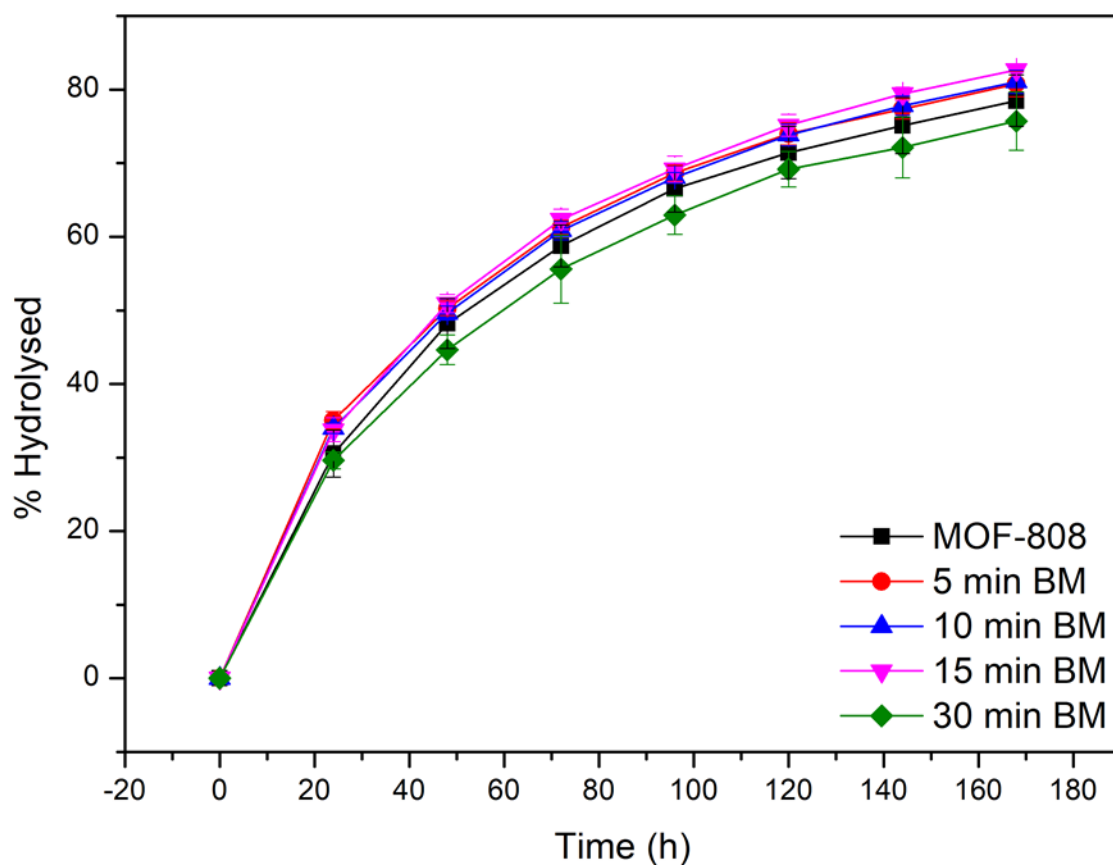
Figure 2.41 Hydrolysis plots of diglycine using MOF-808 and its subsequent ball milled samples as catalysts. Error bars calculated from standard deviation, this was taken from 3 repeats of the hydrolysis experiment.

The ball milling of MOF-808 was used to attain smaller particles of the MOF to then have more surfaces for collisions to occur, therefore increasing reaction rate. Conversely, the results of the hydrolysis studies for MOF-808 and its ball milled counterparts (shown in Figure 2.41) suggest there is no real change in reaction rate when the samples are ball milled.

	MOF-808	5 min BM	10 min BM	15 min BM	30 min BM
Particle size (microns)	4.78 ± 3.70	4.42 ± 3.76	3.57 ± 3.27	2.80 ± 3.14	6.52 ± 4.73

Table 7 A table showing the particle sizes for MOF-808 and its subsequent ball milled samples.

Particles sizes were determined by measuring 50 separate particles on an SEM image and calculating the average size. The particle size data for each of the samples suggests that there is no major difference in particle size after ball milling. This goes some way to explaining why there is no change in reaction rate. It also confirms that the breakdown of the MOF structure

when it is ball milled for 30 minutes increases the particle size slightly which has a knock on effect on its catalytic activity in the hydrolysis studies.

	MOF-808	5 min BM	10 min BM	15 min BM	30 min BM
Surface area (m^2g^{-1})	584.27	559.92	345.35	371.95	78.82
Pore volume (cm^3/g)	6.76	4.03	2.67	2.35	0.10

Table 8 A table showing the surface area and pore volume values for MOF-808 and its subsequent ball milled samples.

The surface area values for MOF-808 are much lower than in literature due to the conditions for the degassing process not being optimised. The surface area and pore volume shows a gradual decrease in both values the longer they are ball milled. Conversely, this data does not follow the trend that suggests a higher pore volume will result in greater catalytic activity.

2.4 Conclusions

Overall, the incorporation of MOF-808 into the polyHIPE network gave a promising result when compared to MOF-808 alone in the hydrolysis of diglycine when subjected to a solvent mix with a D_2O and THF 50/50 mix (by volume). Hydrolysis results however indicated that it is ultimately ineffective when just D_2O is used. Certain alterations to the composition of the polyHIPE-MOF provided improvements to its catalytic activity. When in the form of a powder and when placed into a larger vessel in a scale up reaction, around 20% more diglycine was converted to glycine. The absorption capabilities of the polyHIPE and polyHIPE-MOF were also compared, the incorporation of the MOF into the polymer did not affect the capabilities of the polyHIPE to absorb solvent, which as discussed originally was vital for hydrolysis. The MOFs catalytic activity was also still prominent even when it was embedded within a polymer network. To further study the capabilities of the polyHIPE-MOF as a catalyst, different compositions of the D_2O/THF solvent mixes could be tested, 60, 70, 75, 80 and 90% THF mixes may improve the hydrolysis further as the amount of solvent absorbed increases.

2.5 References

1   H. Q. Zheng, C. Y. Liu, X. Y. Zeng, J. Chen, J. Lü, R. G. Lin, R. Cao, Z. J. Lin and J. W. Su, *Inorg. Chem.*, 2018, **57**, 9096–9104.

2   A. H. Valekar, K. H. Cho, S. K. Chitale, D. Y. Hong, G. Y. Cha, U. H. Lee, D. W. Hwang, C. Serre, J. S. Chang and Y. K. Hwang, *Green Chem.*, 2016, **18**, 4542–4552.

3   E. Plessers, G. Fu, C. Y. X. Tan, D. E. De Vos and M. B. J. Roeffaers, *Catalysts*, 2016, **6**, 7.

4   Y. Liu, R. C. Klet, J. T. Hupp and O. Farha, *Chem. Commun.*, 2016, **52**, 7806–7809.

5   X. Yan, K. Wang, X. Xu, S. Wang, Q. Ning, W. Xiao, N. Zhang, Z. Chen and C. Chen, *Inorg. Chem.*, 2018, **57**, 8033–8036.

6   M. G. Schwab, I. Senkovska, M. Rose, M. Koch, J. Pahnke, G. Jonschker and S. Kaskel, *Adv. Eng. Mater.*, 2008, **10**, 1151–1155.

7   T. Zhang and Q. Guo, *Chem. Eng. J.*, 2017, **307**, 812–819.

8   J. B. Decoste and G. W. Peterson, *Chem. Rev.*, 2014, **114**, 5695–5727.

9   H. G. T. Ly, G. Fu, A. Kondinski, B. Bueken, D. De Vos and T. N. Parac-Vogt, *J. Am. Chem. Soc.*, 2018, **140**, 6325–6335.

10   X. Ma, L. Zhang, M. Xia, X. Zhang and Y. Zhang, *J. Hazard. Mater.*, 2018, **355**, 65–73.

11   M. J. Katz, S. Y. Moon, J. E. Mondloch, M. H. Beyzavi, C. J. Stephenson, J. T. Hupp and O. K. Farha, *Chem. Sci.*, 2015, **6**, 2286–2291.

12   J. E. Mondloch, M. J. Katz, W. C. Isley, P. Ghosh, P. Liao, W. Bury, G. W. Wagner, M. G. Hall, J. B. Decoste, G. W. Peterson, R. Q. Snurr, C. J. Cramer, J. T. Hupp and O. K. Farha, *Nat. Mater.*, 2015, **14**, 512–516.

13   S. Y. Moon, Y. Liu, J. T. Hupp and O. K. Farha, *Angew. Chemie - Int. Ed.*, 2015, **54**, 6795–6799.

14   W. Liang, H. Chevreau, F. Ragon, P. D. Southon, V. K. Peterson and D. M. D'Alessandro, *CrystEngComm*, 2014, **16**, 6530–6533.

15   J. Jiang, F. Gándara, Y. B. Zhang, K. Na, O. M. Yaghi and W. G. Klemperer, *J. Am. Chem. Soc.*, 2014, **136**, 12844–12847.

16   J. M. Williams and D. A. Wrobleski, *Langmuir*, 1988, **4**, 656–662.

17   C. Le Calvez, M. Zouboulaki, C. Petit, L. Peeva and N. Shirshova, *RSC Adv.*, 2016, **6**, 17314–17317.

18   K. Healey, W. Liang, P. D. Southon, T. L. Church and D. M. D'Alessandro, *J. Mater. Chem. A*, 2016, **4**, 10816–10819.

19   H. Furukawa, F. Gándara, Y. B. Zhang, J. Jiang, W. L. Queen, M. R. Hudson and O. M. Yaghi, *J. Am. Chem. Soc.*, 2014, **136**, 4369–4381.

20   S. Bates, G. Zografi, D. Engers, K. Morris, K. Crowley and A. Newman, *Pharm. Res.*, 2006, **23**, 2333–2349.

21   R. Matshitse, *Rhodes Univ. Natl. Res. Found., 2010.*

22   P. C. Raman, T. Handbook, R. C. Frequencies, O. Molecules, A. Press, S. Diego, S. R. I. Im-, M. Excel, C. Trichloromethane, B. Toluene, E. Acetone, T. Dimethylacetamide, A. References and A. Chemicals, .

23   C. M. Cai, T. Zhang, R. Kumar and C. E. Wyman, *Green Chem.*, 2013, **15**, 3140–3145.

2.6 Appendix
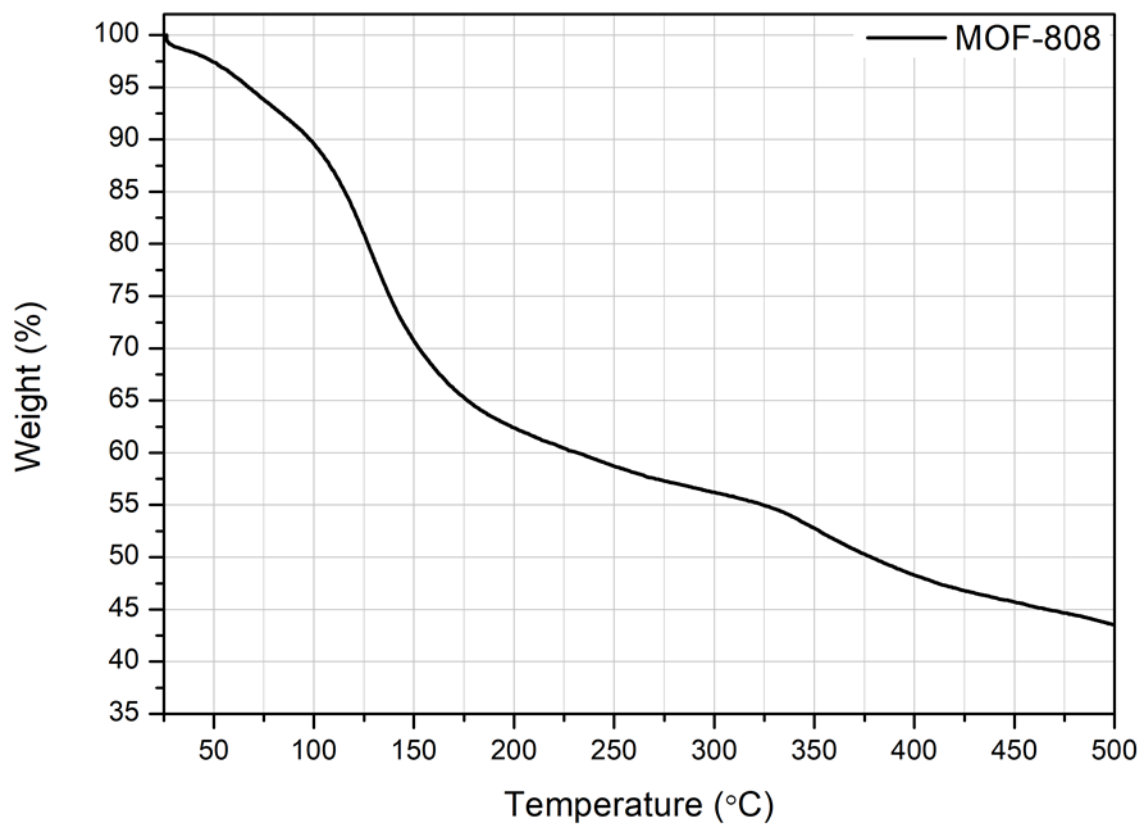
Figure 2.42 TGA of MOF-808.
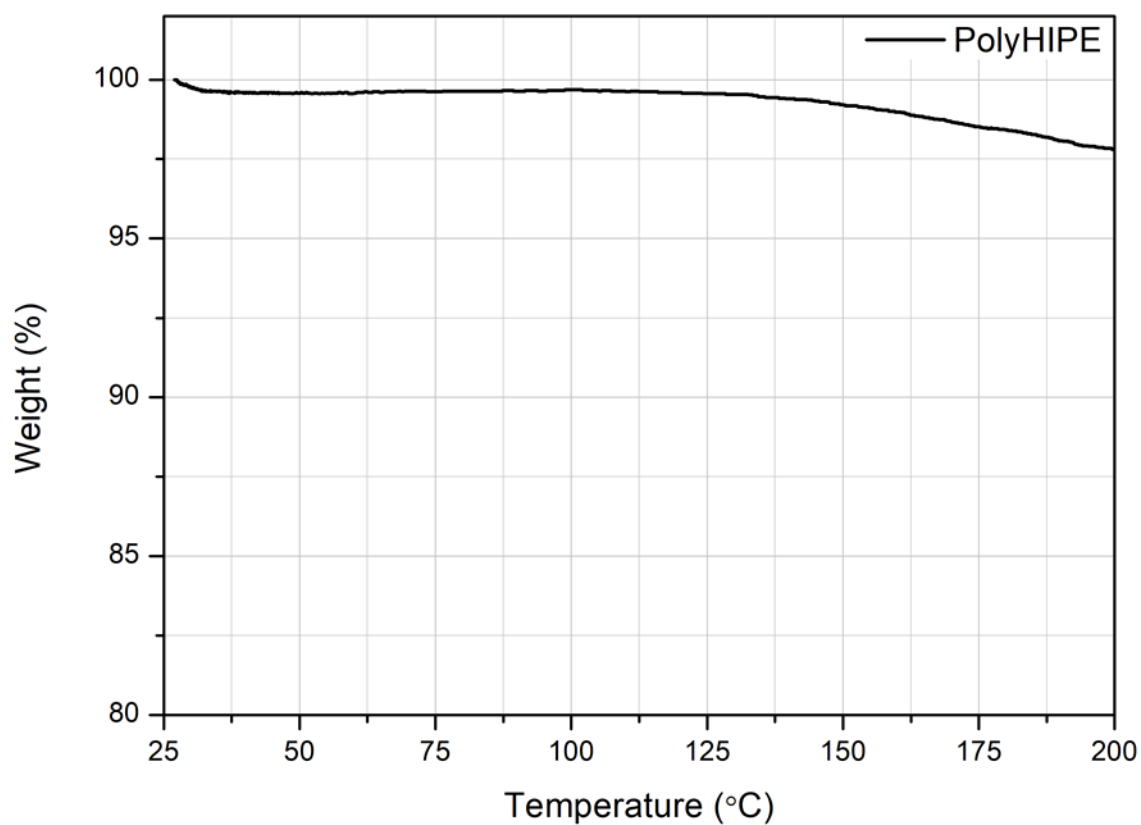
Figure 2.43 TGA of the polyHIPE-MOF.
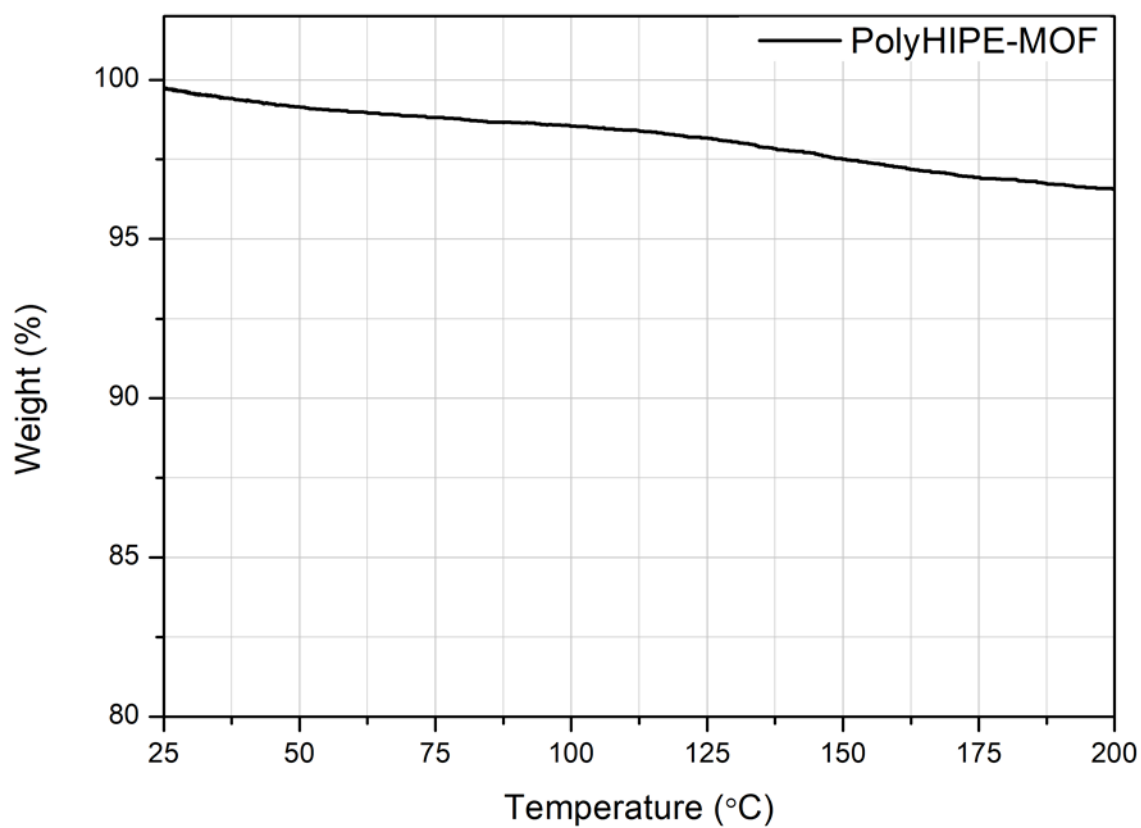
Figure 2.44 TGA of the polyHIPE-MOF.

Chapter 3 – Investigation of Alternative MOFs for the Hydrolysis of Diglycine

3.1 Introduction

The aims of the research described in this chapter were to synthesise a number of different metal organic frameworks (MOFs) and use them as catalysts in the hydrolysis of diglycine. The purpose of these MOFs was to compare them to the highly catalytically active MOF-808, the materials synthesised would differ in the number of connections, the ligand used and even using a different metal centre. The main metal centre used in this work was zirconium, but titanium was also studied as previous studies have suggested that a MOF with a titanium metal centre has issues with structural stability in water.[1] This implies that the use of a titanium MOF in a hydrolysis reaction would be near ineffective, to counteract this the formation of a bimetallic MOF with zirconium were tested. Zirconium MOFs are known to be more thermally and chemically stable, but the photoactive property that a titanium metal centre would provide could be advantageous in a hydrolysis reaction.[2,3] The robust nature of the Zr-oxo clusters combines with the Ti-oxo clusters (shown in Figure 3.1) to prevent the formally sensitive nature to reaction conditions of the Ti-MOF.[4]
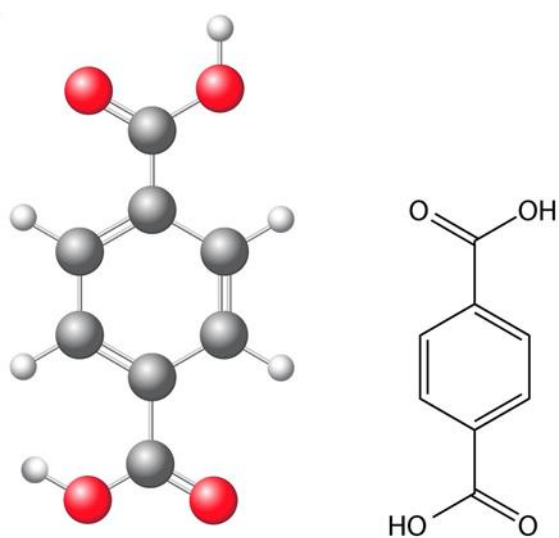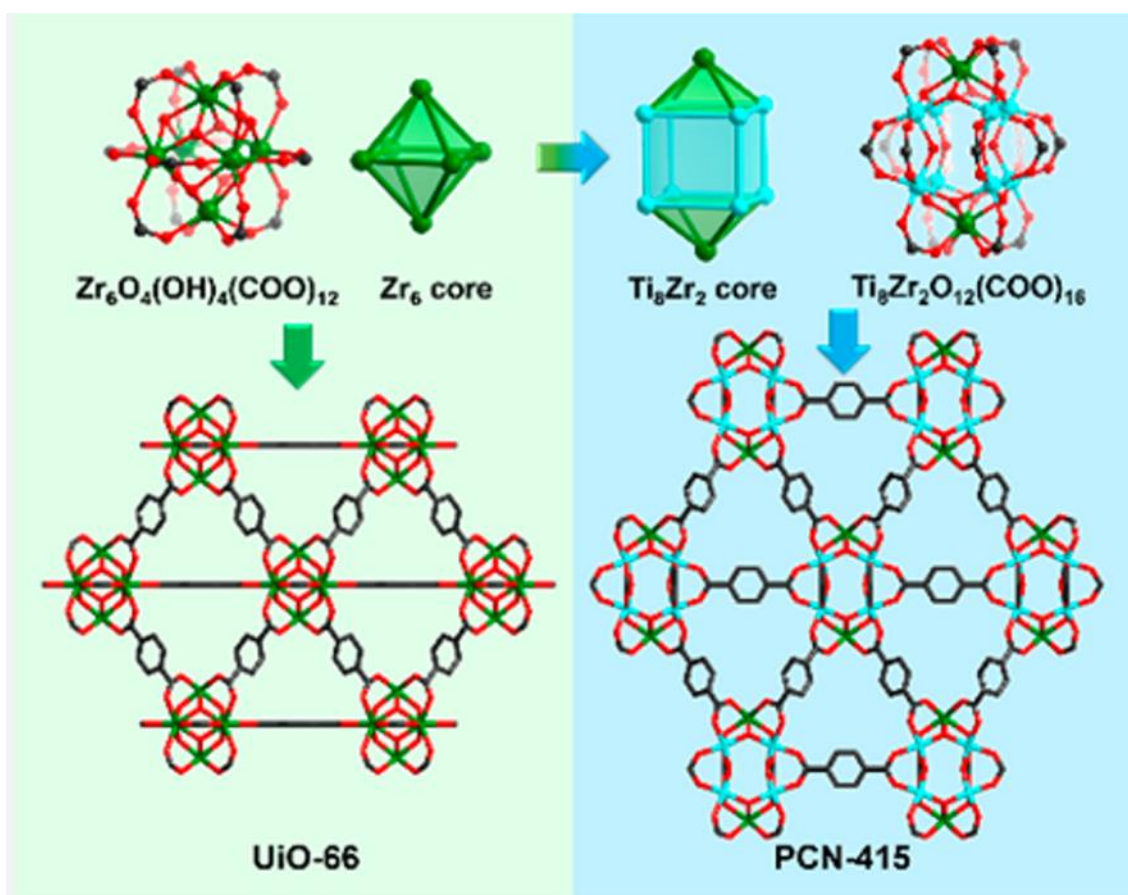
Figure 3.1 Schematic illustrating the combination of a zirconium and titanium core to form the bimetallic MOF PCN-415 and their organic linker terephthalic acid. Reprinted with permission from Ref.[5]

3.1.1 Hydrolysis

As mentioned in the previous chapter hydrolysis is one of the many reaction pathways in

which MOFs can be utilised as catalysts. In the hydrolysis of dipeptides, the procedure works

by the addition of water splitting the bond between O=C and N-H to form two separate

peptide bonds (shown in Figure 3.2).
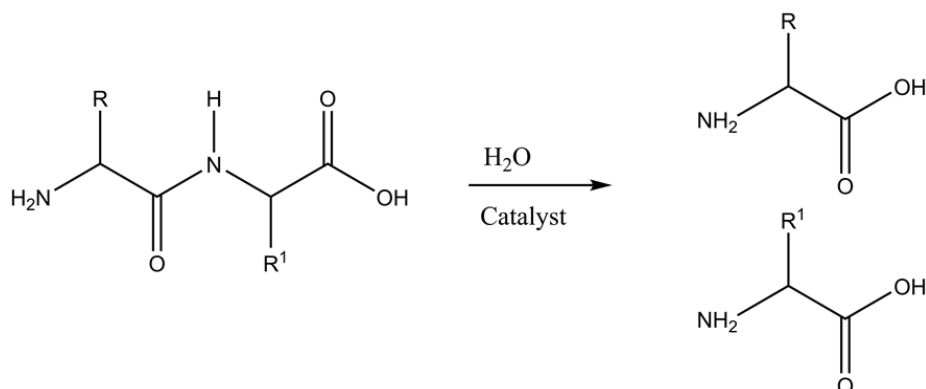
Figure 3.2 Schematic outlining the hydrolysis of a dipeptide.

The use of a MOF as the catalyst in a hydrolysis reaction is attributed in part to its extensive

porosity which is caused by the number of uncoordinated M^{IV} sites.[6] The extent of each MOFs

catalytic activity is determined by the number of active sites within their framework.[7] The

number of active sites in a framework depends on the choice of organic ligand and metal

cluster/ion, these factors determine the number of connections within the structure.[8] The

Lewis-acidic M^{IV} ionic sites within the M_6 node on the MOF are a major factor for their

catalytically efficacy.[9] MOFs with a connectivity lower than 12 or with site defects are said to

have a greater number of active sites due to a greater number of uncoordinated M^{IV} sites.[10]

Therefore, the synthesis of a variety of MOFs with different connections, metal clusters/ions

and ligands will outline the difference in catalytically activity.

3.2 Experimental

3.2.1 Materials

Alpha, alpha'-azoisobutyronnitrile (98%, Molekula), sorbitan monooleate (Alfa aesar), divinylbenzene, (80%, Alfa aesar, mixture of isomers, stab. with 1000ppm 4-tert-butylcatechol), potassium sulfate (99+%, Acros, for analysis, anhydrous powder), deuterium oxide (99.9%, Goss), GLY-GLY (99%, Sigma), tetrahydrofuran-d8 (Cambridge isotope laboratories), tetrahydrofuran (99%, Fisher) were all used without further purification, styrene (99 %, Acros) was passed through an alumina column before use to remove the inhibitor.

3.2.2 Equipment

Infra-red spectroscopy was carried out at room temperature on a Shimadzu IRAffinity-1S, with an ATR gate, a sweep of 500 - 4000 cm^{-1}, a resolution of 2 cm^{-1} and 64 scans.

Electron micrographs were obtained using a Hitachi S-3400 scanning electron microscope. The pHIPE samples were prepared for SEM by cutting into thin square slices with a completely flat surface. The chamber was set to full vacuum, with an electron beam voltage of 20 kV and an emission current of 80 mA. Detections were carried out with the backscatter electron detector. SEM-EDX was carried out using the backscatter electron detector in the analysis mode, the spectrum range for the analysis was 0-20 keV, with 10 frames processed over a livetime of 10 seconds.

^{1}H NMR spectra were acquired on a Bruker Avance Neo NMR, running a proton frequency of 400 MHz at room temperature (22 °C), with 16 scans and D_2O and/or d-THF used as solvents.

PXRD analysis was conducted by placing the powdered sample of MOF onto a zero-background sample holder and analysed in a Rigaku Miniflex 600 desktop XRD. The polyHIPE was cut into flat thin slice and placed into the centre of a zero-background sample holder.

Thermal analyses of samples were performed using a Netzsch STA 409 PC25 instrument and an aluminium crucible was used for all thermogravimetric analyses at a heating rate of 10 °C min^{-1} under nitrogen, from 25 °C to 500 °C.

Surface area and porosity measurements were carried out on a Surfer gas adsorption porosimeter. MOF and polyHIPE samples were prepared as powders, the degassing process was at 60 °C for 10 hours at 1×10^{-3} torr. The analysis process was carried out at 77 K under nitrogen atmosphere, the analysis time varied for each sample.

3.2.3 Synthesis of MOF-808

MOF-808 was synthesised following a previously reported method.[11] ZrCl$_4$ (1.281 g, 5.50 mmol) and 1,3,5-benzenetricarboxylic acid (0.3883 g, 1.85 mmol) were added to DMF (110 ml) and acetic acid (61.6 ml, 964.91 mmol). The reaction mixture was then sonicated for 20 minutes. The solution was then sealed in a duran flask and placed into a preheated oven at 135°C for 24 hours. The flask was removed from the oven and allowed to cool to room temperature at which point a white precipitate was visible at the bottom of the flask. Once cooled, the solution was vacuum filtered using a Buchner funnel before being washed with DMF (3 x 20 ml), methanol (3 x 20 ml) and acetone (3 x 20 ml). The solid was then dried under vacuum for 48 hours to yield a white microcrystalline powder. The synthesised MOF-808 was characterised using PXRD and IR by comparison to a literature pattern and spectrum.

Yield 1.028 g (61.6 %) **FT-IR**: 645.1 cm^{-1}, 1444.3 cm^{-1}, 1657.5 cm^{-1}.

3.2.4 Synthesis of DUT-52

DUT-52 was synthesised following a previously reported method.[12] ZrCl$_4$ (0.230 g, 0.99 mmol) and DMF (20 ml) were added into a duran flask and sonicated for 5 minutes. 2,6-Naphthalenedicarboxylic acid (0.216 g, 1 mmol) and acetic acid (3 ml, 52.45 mmol) were added to the reaction mixture and it was sonicated for a further 15 minutes. The solution was sealed in the duran flask and placed into a preheated oven at 120°C for 24 hours. The flask was

removed from the oven and allowed to cool to room temperature at which point a white precipitate was visible at the bottom of the flask. Once cooled, the solution was vacuum filtered using a Buchner funnel before being washed with DMF (3 x 20 ml) and ethanol (3 x 20 ml). The solid was then dried under vacuum for 48 hours to yield a white microcrystalline powder. The synthesised DUT-52 was characterised using PXRD and IR by comparison to a literature pattern and spectrum.

Yield 0.35 g (78.5 %) **FT-IR**: 654.5 cm^{-1}, 1411.9 cm^{-1}, 1652.3 cm^{-1}.

3.2.5 Synthesis of DUT-68

DUT-68 was synthesised following a previously reported method.[13] $ZrCl_4$ (0.230 g, 0.99 mmol) and DMF (25 ml) were added into a duran flask and sonicated for 10 minutes. 2,5-Thiophenedicarboxylic acid (0.258 g, 1.50 mmol) was added to the reaction mixture and it was sonicated for a further 10 minutes. Finally, acetic acid (11 ml, 192.33 mmol) was added before the solution was sonicated for an additional 10 minutes. The solution was sealed in the duran flask and placed into a preheated oven at 120°C for 72 hours. The flask was removed from the oven and allowed to cool to room temperature at which point a white precipitate was visible at the bottom of the flask. Once cooled, the solution was vacuum filtered using a Buchner funnel before being washed with DMF (3 x 20 ml) and acetone (3 x 20 ml). The solid was then dried under vacuum for 48 hours to yield a white microcrystalline powder. The synthesised DUT-68 was characterised using PXRD and IR by comparison to a literature pattern and spectrum.

Yield 0.260 g (53.3 %) **FT-IR**: 648.5 cm^{-1}, 1390.8 cm^{-1}, 1652.3 cm^{-1}.

3.2.6 Synthesis of DUT-84

DUT-84 was synthesised following a previously reported method.[12] $ZrCl_4$ (0.285 g, 1.22 mmol), 2,6-Naphthalenedicarboxylic acid (0.250 g, 1.16 mmol) and DMF (60 ml) were added into a duran flask and sonicated for 10 minutes. Acetic acid (25 ml, 437.12 mmol) was added to the

reaction mixture and it was sonicated for a further 10 minutes. The solution was sealed in the duran flask and placed into a preheated oven at 120°C for 24 hours. The flask was removed from the oven and allowed to cool to room temperature at which point a white precipitate was visible at the bottom of the flask. Once cooled, the solution was vacuum filtered using a Buchner funnel before being washed with DMF (3 x 20 ml) and ethanol (3 x 20 ml). The solid was then dried under vacuum for 48 hours to yield a white microcrystalline powder. The synthesised DUT-84 was characterised using PXRD and IR by comparison to a literature pattern and spectrum.

Yield 0.336 g (62.8 %) **FT-IR**: 659.8 cm^{-1}, 1417.2 cm^{-1}, 1652.3 cm^{-1}.

3.2.7 Synthesis of UiO-66

UiO-66 was synthesised following a previously reported method.[14] ZrCl$_4$ (0.212 g, 0.91 mmol), terephthalic acid (0.136 g, 0.82 mmol) and DMF (106 ml) were added into a duran flask and sonicated for 15 minutes. The solution was sealed in the duran flask and placed into a preheated oven at 120°C for 24 hours. The flask was removed from the oven and allowed to cool to room temperature at which point a white precipitate was visible at the bottom of the flask. Once cooled, the solution was vacuum filtered using a Buchner funnel before being washed with DMF (3 x 20 ml) and ethanol (3 x 20 ml). The solid was then dried under vacuum for 48 hours to yield a white microcrystalline powder. The synthesised UiO-66 was characterised using PXRD and IR by comparison to a literature pattern and spectrum.

Yield 0.313 g (89.9 %) **FT-IR**: 659.8 cm^{-1}, 1396.1 cm^{-1}, 1652.3 cm^{-1}.

3.2.8 Synthesis of PCN-415

PCN-415 was synthesised folllowing a previously reported method.[5] ZrCl$_4$ (0.05 g, 0.21 mmol), titanium (IV) isopropoxide (0.1 ml, 0.34 mmol) and DMF (5 ml) were added into a duran flask and sonicated for 5 minutes. Acetic acid (0.5 ml, 8.74 mmol) was added to the reaction mixture and it was sonicated for a further 10 minutes. The solution was sealed in the duran flask and

placed into a preheated oven at 100°C for 24 hours. The flask was removed from the oven and terephthalic acid (0.8 g, 4.82 mmol), trifluoroacetic acid (1 ml, 13.07 mmol) and DMF (10 ml) were subsequently added before the reaction mixture was sonicated for 10 minutes. The flask was once again sealed and placed into a preheated oven at 140°C for a further 24 hours. The flask was removed from the oven and allowed to cool to room temperature at which point a white precipitate was visible at the bottom of the flask. Once cooled, the solution was vacuum filtered using a Buchner funnel before being washed with DMF (3 x 20 ml) and ethanol (3 x 20 ml). The solid was then dried under vacuum for 48 hours to yield a white microcrystalline powder. The synthesised PCN-415 was characterised using PXRD and IR by comparison to a literature pattern and spectrum.

Yield 0.638 g (67.2 %) **FT-IR**: 686.2 cm^{-1}, 1396.1 cm^{-1}, 1652.3 cm^{-1}.

3.2.9 Synthesis of MIL-125

MIL-125 was synthesised following a previously reported method.[15] Titanium (IV) isopropoxide (2.558 g, 9 mmol), terephthalic acid (2.492 g, 15 mmol), DMF (45 ml) and methanol (5 ml) were added into a duran flask under continuous stirring for 20 minutes. The flask was sealed and placed into a preheated oven at 150°C for 16 hours. The flask was removed from the oven and allowed to cool to room temperature at which point a white precipitate was visible at the bottom of the flask. Once cooled, the solution was vacuum filtered using a Buchner funnel before being washed with DMF (3 x 20 ml) and methanol (3 x 20 ml). The solid was then dried under vacuum for 48 hours to yield a white microcrystalline powder. The synthesised MIL-125 was characterised using PXRD and IR by comparison to a literature pattern and spectrum.

Yield 4.14 g (82.0 %) **FT-IR**: 652.3 cm^{-1}, 1396.1 cm^{-1}, 1651.7 cm^{-1}

3.2.10 Hydrolysis Studies of Diglycine using MOF-808

D_2O (10 ml) was added to a volumetric flask with diglycine (0.106 g, 0.80 mmol, 80 mM) as a stock solution for the hydrolysis. D_2O/diglycine stock solution (0.75 ml, 80 mM gly-gly) was

added to a sample vial with D_2O (0.75 ml). D_2O (0.75 ml, 40mM gly-gly) was added to an NMR tube with MOF-808 (0.0013 g, $9.18x10^{-4}$ mmol). The NMR tube was inverted multiple times to evenly disperse the MOF, and the NMR tube was heated at 65°C for 7 days. At different time increments, an NMR was taken of the sample to monitor the progress of the hydrolysis.

3.2.11 Hydrolysis Studies of Diglycine using various MOFs

A typical procedure was as follows, D_2O (10 ml) was added to a volumetric flask with diglycine (0.106 g, 0.80 mmol, 80 mM) as a stock solution for the hydrolysis. D_2O/diglycine stock solution (0.75 ml, 80 mM gly-gly) was added to a sample vial with D_2O (0.75 ml). D_2O (0.75 ml, 40 mM gly-gly) was added to an NMR tube with DUT-52 (0.0018 g, $9.18x10^{-4}$ mmol). The NMR tube was inverted multiple times to evenly disperse the MOF, and the NMR tube was heated at 65°C for 7 days. At different time increments, an NMR was taken of the sample to monitor the progress of the hydrolysis.

MOF	Mass (g)	Molar ratio (MOF:gly-gly)
MOF-808	0.0013	1:50
DUT-52	0.0018	1:50
DUT-68	0.0013	1:50
DUT-84	0.0014	1:50
UiO-66	0.0015	1:50
PCN-415	0.0031	1:50
MIL-125	0.0010	1:50

Table 9 A table outlining the amount of each MOF used in each hydrolysis study.

3.2.12 Photocatalytic Studies of MIL-125 and PCN-415

A typical procedure was as follows, D_2O (10 ml) was added to a volumetric flask with diglycine (0.106 g, 0.80 mmol, 80 mM) as a stock solution for the hydrolysis. D_2O/diglycine stock solution (0.75 ml, 80 mM gly-gly) was added to a sample vial with D_2O (0.75 ml). D_2O (0.75 ml, 40 mM gly-gly) was added to an NMR tube with MIL-125 (0.0010 g, $9.18x10^{-4}$ mmol). The NMR

tube was inverted multiple times to evenly disperse the MOF, and the NMR tube was heated

at 65°C and covered with foil for 7 days for the study in the dark, or the reaction was carried

out under UV light with a UV lamp aimed at the reaction whilst covered in a dark box. At

different time increments, an NMR was taken of the sample to monitor the progress of the

hydrolysis.

3.3 Results and Discussion

3.3.1 Characterisation

3.3.1.1 Infrared Spectra
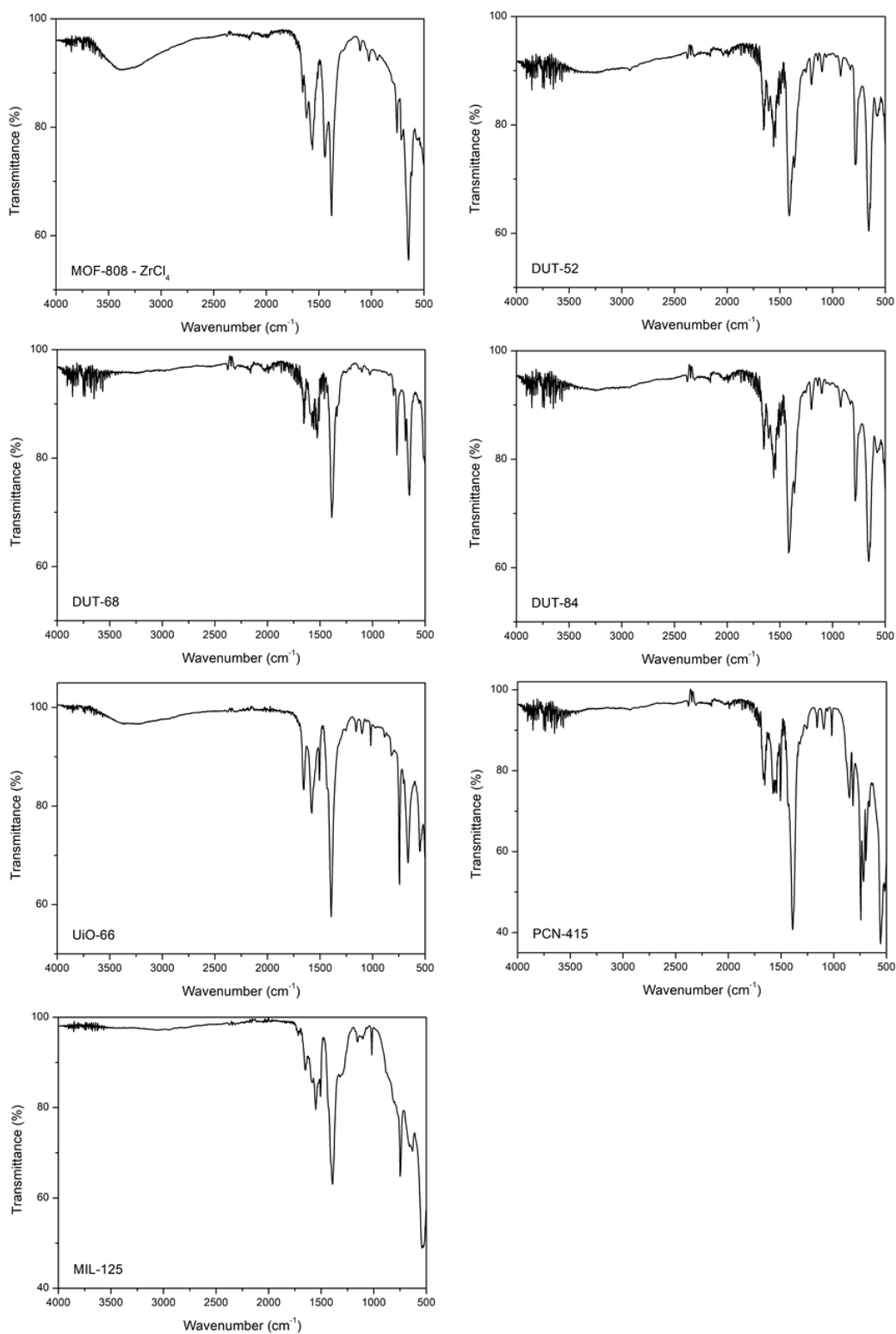
Figure 3.3 Infrared spectra of MOF-808, DUT-52, DUT-68, DUT-84, UiO-66, PCN-415 and MIL-125.

The MOFs synthesised in this chapter were also synthesised following published procedures. The as-synthesised infrared spectra for each MOF were compared to literature spectra.[5,11,12,13,14,15] The synthesised MOFs infrared spectra had the characteristic C=O peak at around 1650 cm^{-1} indicative of the carboxylic acid group on the MOF and the peak at around 1400 cm^{-1} indicative of the aromatic group.

3.3.1.2 PXRD
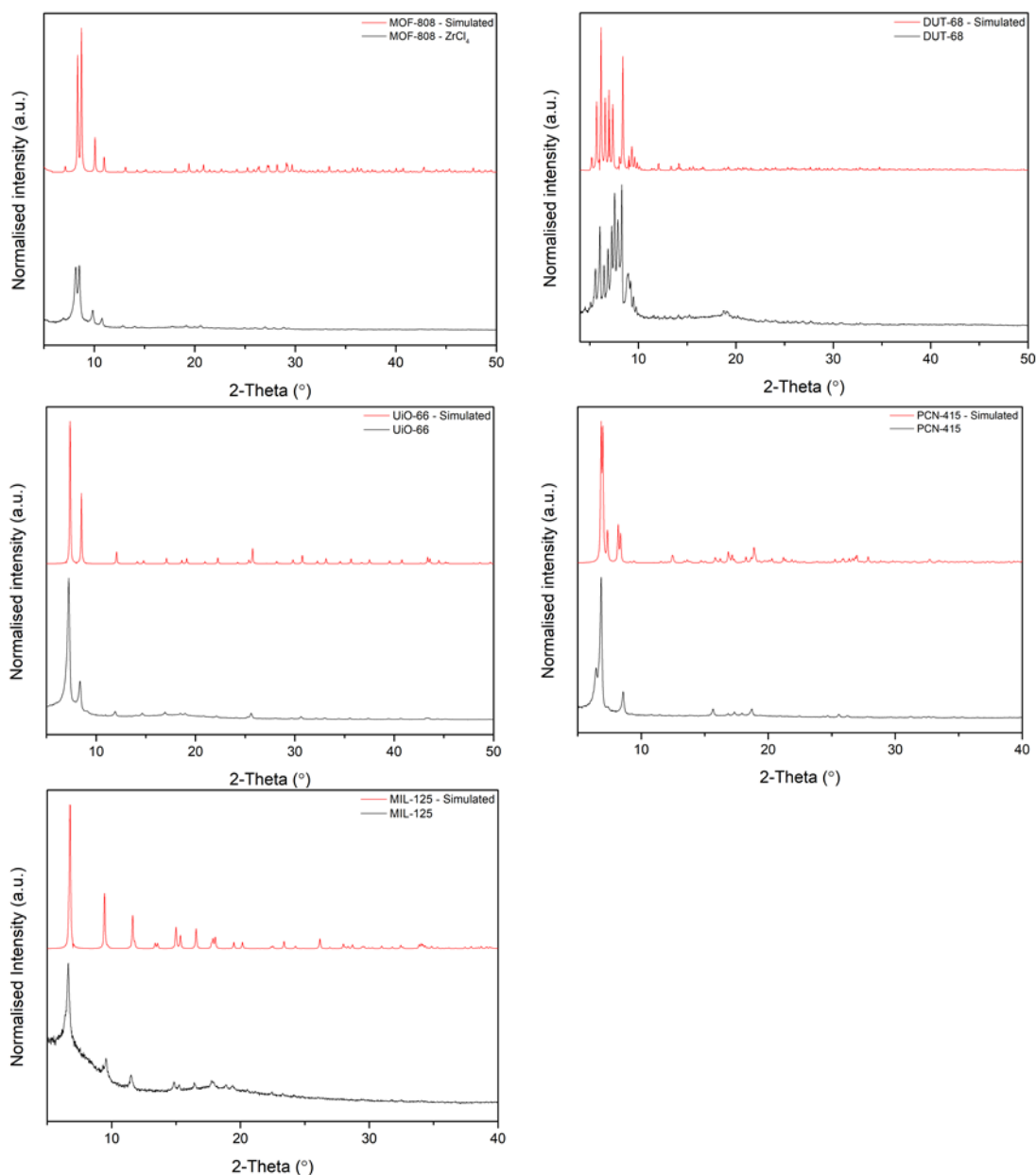
Figure 3.4 PXRD of MOF-808, DUT-68, UiO-66, PCN-415 and MIL-125 compared to their simulated patterns. Adapted with permission from Refs.[5,13,16,17,18]

As aforementioned, the MOFs synthesised in this chapter were also synthesised following published procedures. The as-synthesised PXRDs for each MOF were compared to simulated

patterns (shown in Figure 3.4).[5,13,16,17,18] The PXRD for MOF-808 has two peaks at around 8-9°

which is comparable to the simulated pattern. DUT-68 has a cluster of peaks between 5-10°

which is comparable to the simulated pattern. UiO-66 has two peaks at around 7-9° which is

comparable to the simulated pattern. PCN-415 has a peak at around 7° which has a small

shoulder peak and a smaller peak at around 9° which is comparable to the simulated pattern.

MIL-125 has a peak at around 6° and a further two smaller peaks at around 9° and 11° which is

comparable to the simulated pattern.

Figure 3.5 PXRD of DUT-52 and DUT-84 and their literature patterns. Adapted with permission from Ref.[12]

DUT-52 and DUT-84s patterns had similar peaks when compared to the simulated patterns

(shown in Figure 3.5) but they were not completely crystalline. The peaks did not have a

defined sharpness suggesting that the product is slightly amorphous.[12]
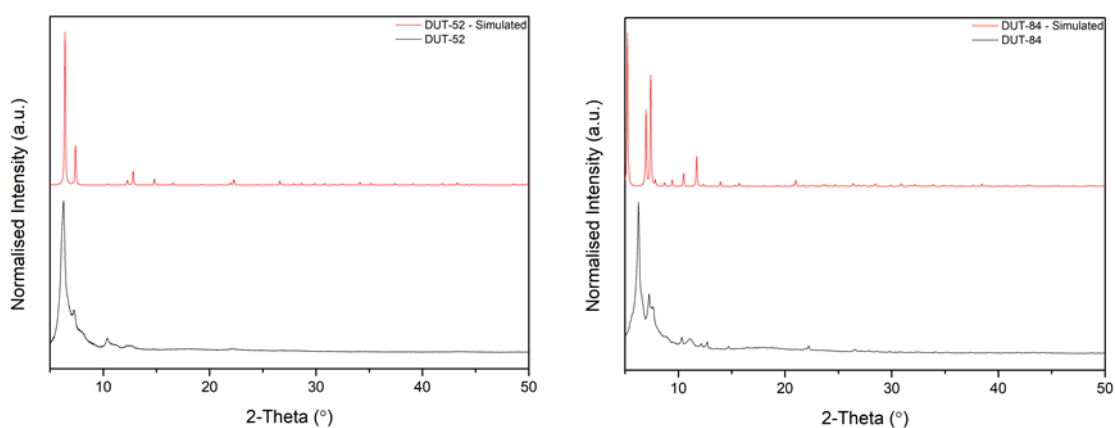
3.3.1.3 Surface Area and Porosity
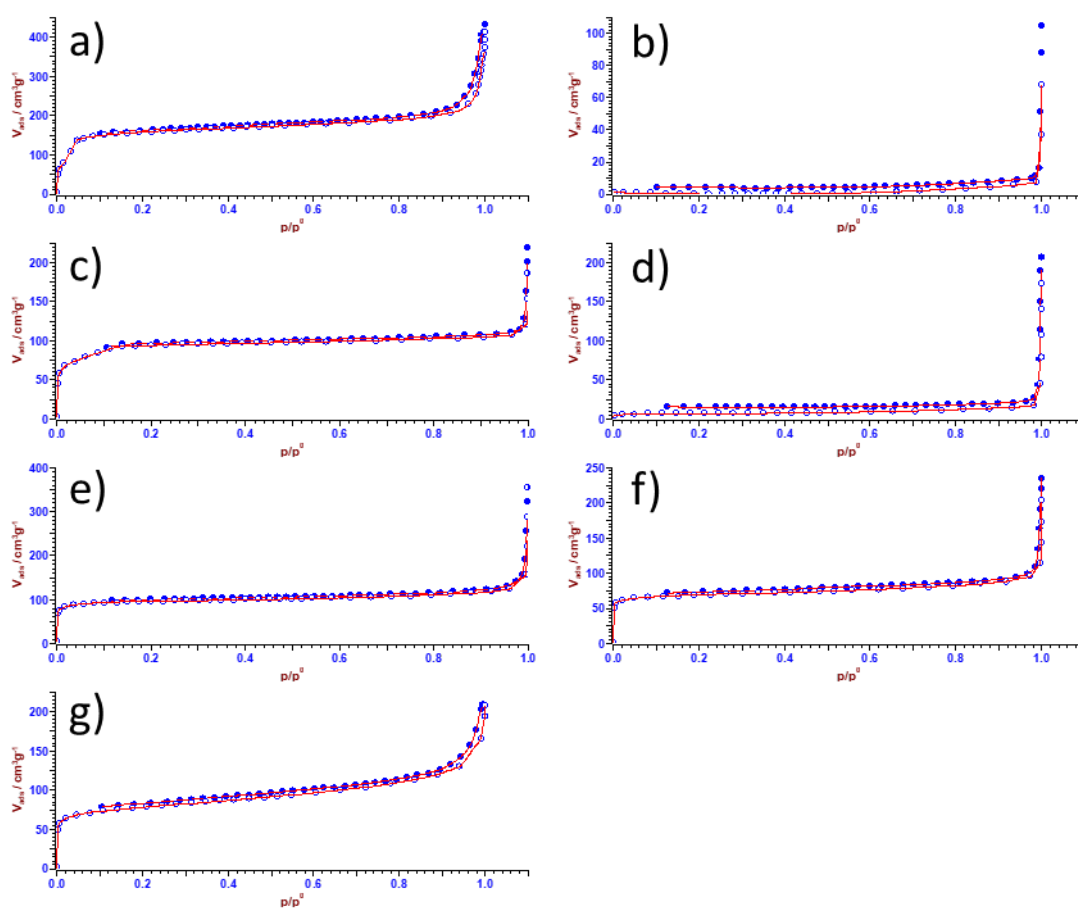
Figure 3.6 BET isotherms of MOF-808, DUT-52, DUT-68, DUT-84, UiO-66, PCN-415 and MIL-125 (a,b,c,d,e,f and g).

The porosity for all synthesised MOFs were recorded on a Surfer gas adsorption porosimeter; the resulting isotherms are shown in Figure 3.6. The isotherms for MOF-808, DUT-68, UiO-66, PCN-415 and MIL-125 confirm that they are mesoporous, as in these isotherms the capillary condensation is accompanied by hysteresis.[19] However, DUT-52 and DUT-84s isotherms show they are non-porous, as in these isotherms there is unrestricted mono-multilayer adsorption which results in complete monolayer coverage.[19] This was not expected as these MOFs are known for having extensive porosity, the reason for this can be attributed to the non-crystalline structures both MOFs formed as shown in their PXRDs. [6]

MOF	Surface Area (m²g⁻¹)	Pore Volume (cm³/g)	Literature Surface Area (m²g⁻¹)	Literature Pore Volume (cm³/g)
MOF-808	719	0.34	1606	0.78
DUT-52	<1	0.01	1399	0.57
DUT-68	404	0.16	891	0.41
DUT-84	30	0.02	637	0.29
UiO-66	416	0.19	1187	0.52
PCN-415	292	0.14	1050	0.47
MIL-125	313	0.21	935	0.44

Table 10 A table showing the surface area and pore volume of all the synthesised MOFs and previously reported literature values.[5,11,12,13,20,21]

The experimental surface areas and pore volumes can be compared to literature values, all the experimental values were much lower than reported in literature. The conditions for the degassing of each sample may offer an explanation to this, all the surface area measurements performed in this thesis were degassed at 60°C for 10 hours under nitrogen atmosphere. The optimal conditions for degassing were not stated in literature so using thermogravimetric analysis (TGA), the degassing temperature was determined in order to ensure each MOF was stable against the degassing conditions. The TGA suggested that the majority of the MOFs percentage weight began to decrease almost instantaneously (as shown in figure 3.7) due to loss of H_2O and then solvent evaporation, therefore a lower temperature for degassing was essential for structural stability. However, DUT-52 and DUT-84 have non-porous structures, their low surface areas may be attributed to their non-crystalline structure as illustrated in their PXRDs. Alternatively, the temperature used in the degassing may have been too harsh and broke down the structure of these frameworks affecting their porosity. In order to obtain more accurate values for pore volume and surface area, the conditions used on the porosimeter would need to be optimised.
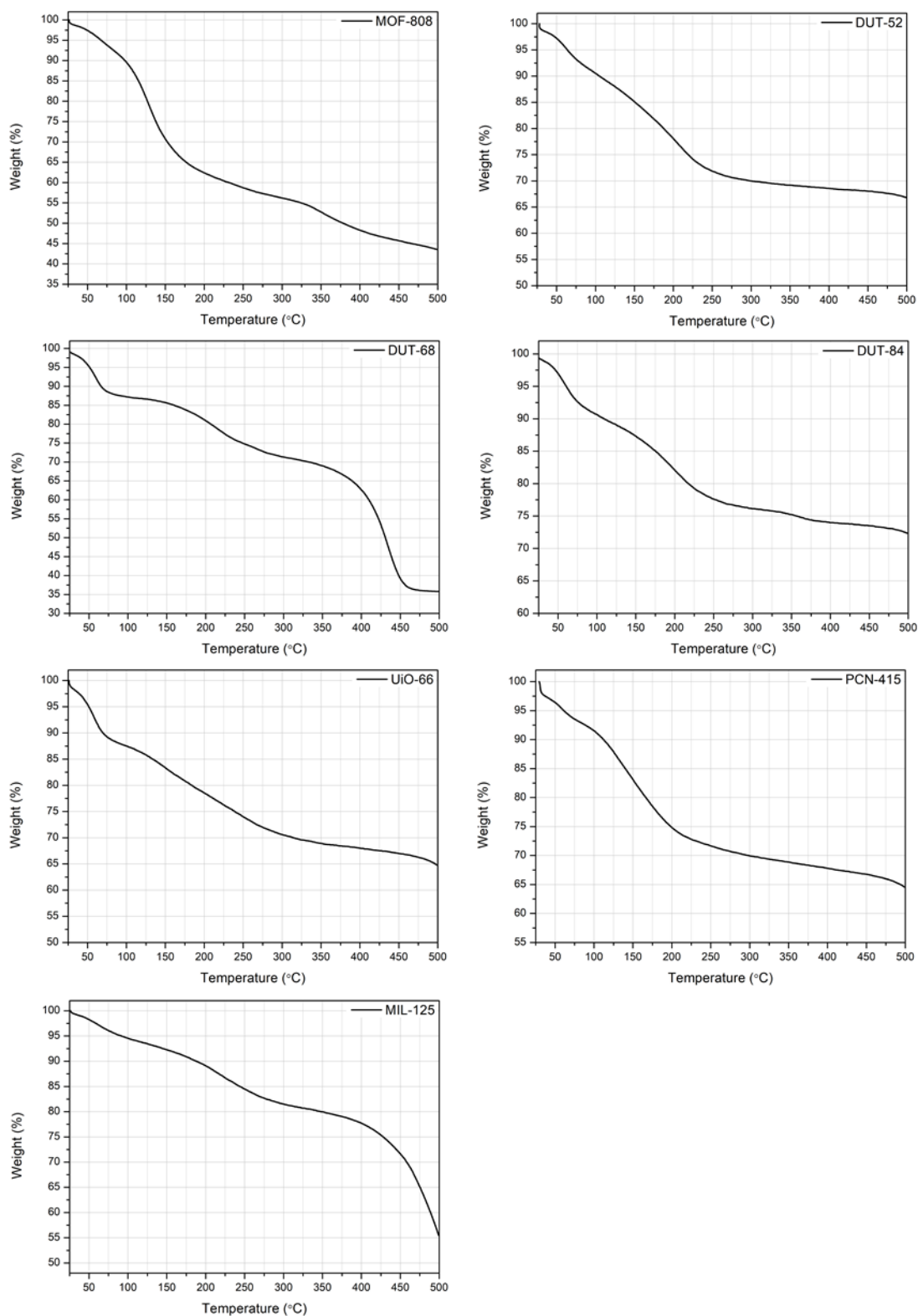
Figure 3.7 TGA of MOF-808, DUT-52, DUT-68, DUT-84, UiO-66, PCN-415 and MIL-125.

3.3.2 Hydrolysis

	MOF (g)	Diglycine (g)	Molar ratio (MOF:gly-gly)
MOF-808	0.0013	0.0080	1:50
DUT-52	0.0018	0.0080	1:50
DUT-68	0.0013	0.0080	1:50
DUT-84	0.0014	0.0080	1:50
UiO-66	0.0015	0.0080	1:50
PCN-415	0.0031	0.0080	1:50
MIL-125	0.0010	0.0080	1:50

Table 11 A table showing the reaction parameters for this section.

All reactions were carried out in 0.75 ml of D_2O at a concentration of 40 mM diglycine at 65°C.

This section will look at the effects of different MOFs in this hydrolysis reaction and the activity

of each MOF. The difference in the MOFs used were the metal centres (Zr, Ti and Zr/Ti), the

organic linkers and the connected nodes (6, 8 and 12) which all have an effect on the number

of active sites. The hydrolysis of diglycine was carried out following a previously reported

procedure. The reaction was followed using NMR. The use of a MOF as a catalyst in the

hydrolysis of diglycine has been previously studied using MOF-808, with nearly 100 %

hydrolysis after 3 hours.[22] Diglycine and MOF-808 were in a 1:1 molar ratio in the previous

study with a diglycine concentration of 40 mM at 60°C in an NMR tube. The reaction does not

achieve 100 % conversion to glycine as the cyclisation form of glycine is formed as a by-

product in this reaction, cyclisation will be discussed further in 3.3.6. The reaction conditions

used in the hydrolysis studies within this chapter are identical to the temperature and

concentrations used in literature but the molar ratio between the catalyst and diglycine differ.

The molar ratio in literature was 1:1, compared to 1:50 in this chapter, the difference in molar

ratio was due to the feasibility of using such a large quantity of catalyst in an NMR tube. The

hydrolysis in literature took place over 3 hours whereas all reactions shown in this thesis were
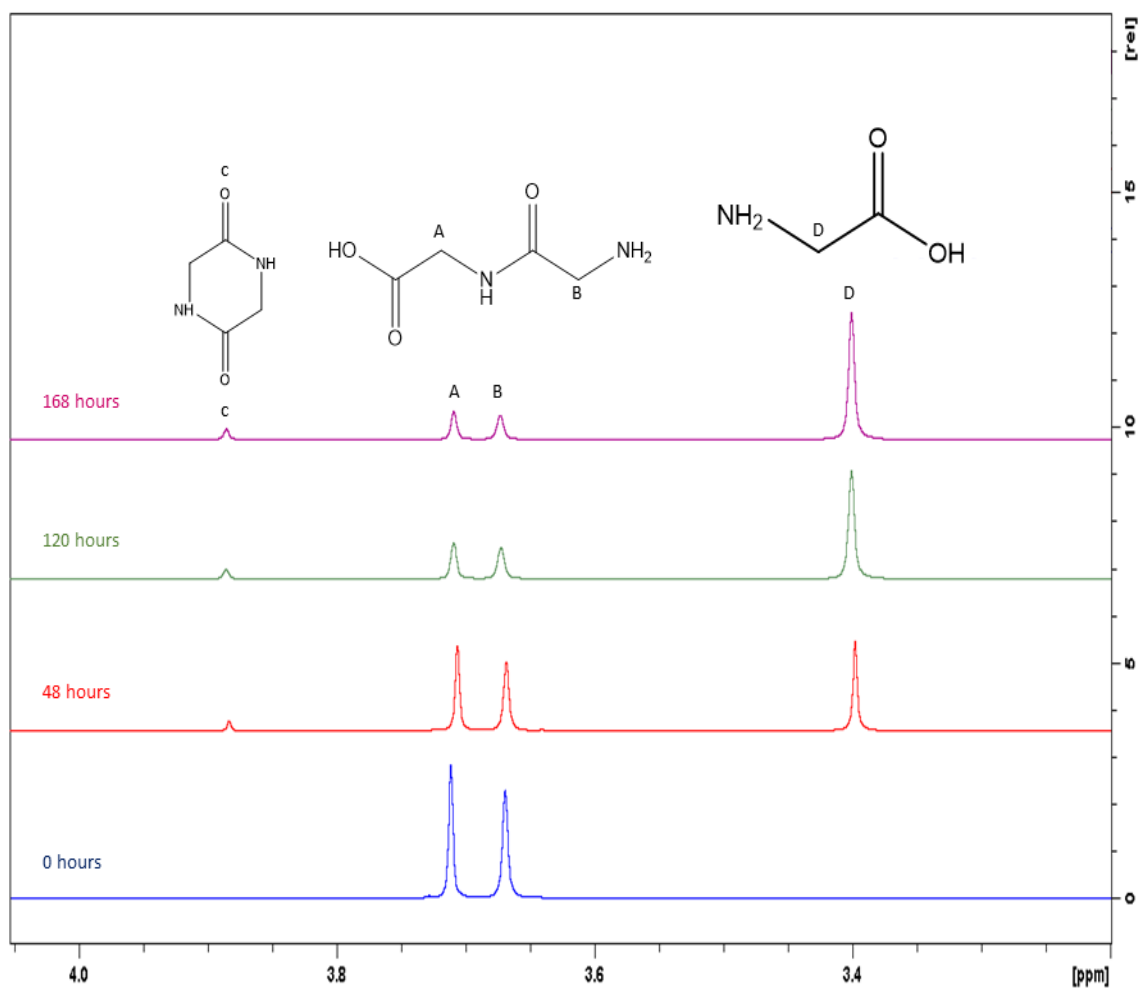
over 7 days.

Figure 3.8 NMR spectra overlay showing the hydrolysis of diglycine after 0, 48, 120 and 168 hours.

The peak at around 3.4 ppm is due to glycine, the peaks at around 3.65-3.75 ppm are due to

the two diglycine peaks and the peak at around 3.9 ppm is due to the cyclised form of glycine.
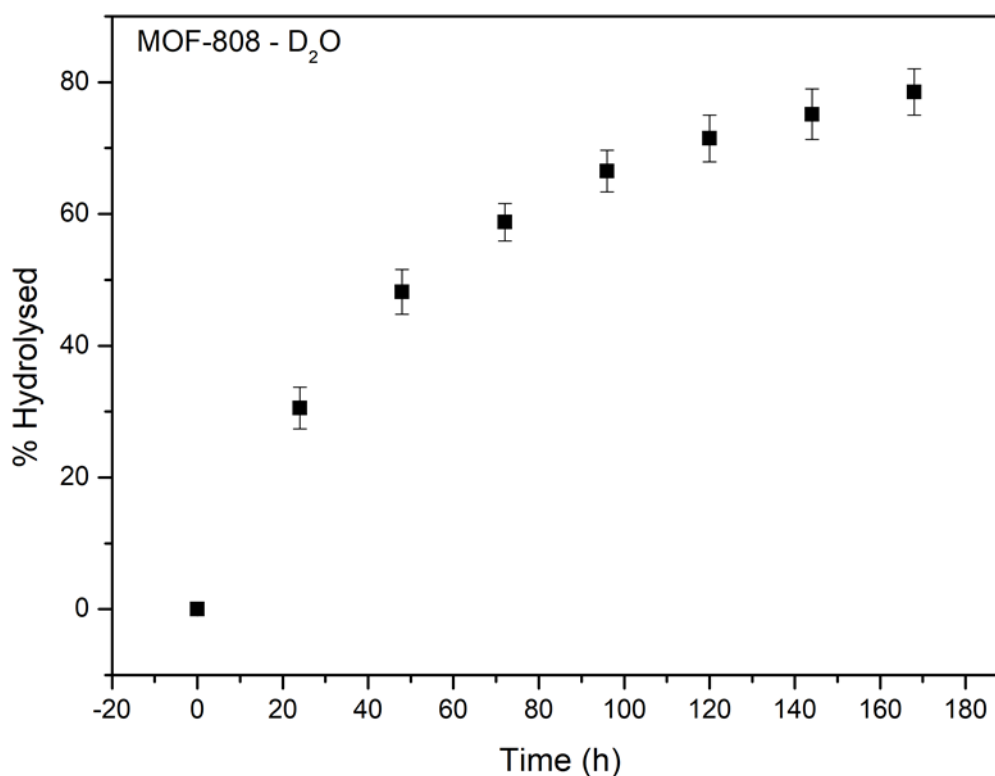
3.3.2.1 MOF-808

MOF-808 - D$_2$O

Figure 3.9 Hydrolysis plot of diglycine in D$_2$O using MOF-808 as a catalyst. Error bars calculated from standard deviation, this was taken from 3 repeats of the hydrolysis experiment.

The hydrolysis of diglycine using MOF-808 as a catalyst was extensively studied in chapter 2. In this hydrolysis reaction, it is proposed that gly-gly binds to two Zr (IV) metal centres in the Zr$_6$O$_8$ core via the oxygen atom of the amide group and the N-terminus. Furthermore, the amine nitrogen and oxygen atoms coordinate to Zr (IV), polarising the peptide bond, making it more vulnerable for nucleophilic attack by water, although the actual reaction mechanism is not confirmed and work into it is ongoing.[22] The hydrolysis reached around 80% completion after 7 days. The results from chapter 2 indicated that MOF-808 shows good catalytic activity in both a 1:2 and 1:50 diglycine:MOF-808 molar ratio. MOF-808 showing catalytic activity in a 1:50 molar ratio with diglycine indicates its propensity for catalysis. The other MOFs used in this study will work using the proposed mechanism above, the only MOF previously published for hydrolysis studies other than MOF-808 was UiO-66. UiO-66 was used as a catalyst in phosphate-ester hydrolysis, UiO-66 did work as a catalyst in this reaction but was more effective when amino-functionalised.[23] As aforementioned, the MOFs catalytic activity in

hydrolysis reactions is in part attributed to its extensive porosity. Previously reported literature values have shown that the MOFs used in this study are all porous with their surface areas and pore volumes shown in table 2. Surface area values do not correlate with catalytic activity as expected, this will be explained in more detail in the next section.

3.3.3 Comparison of MOF-808 to Alternative MOFs
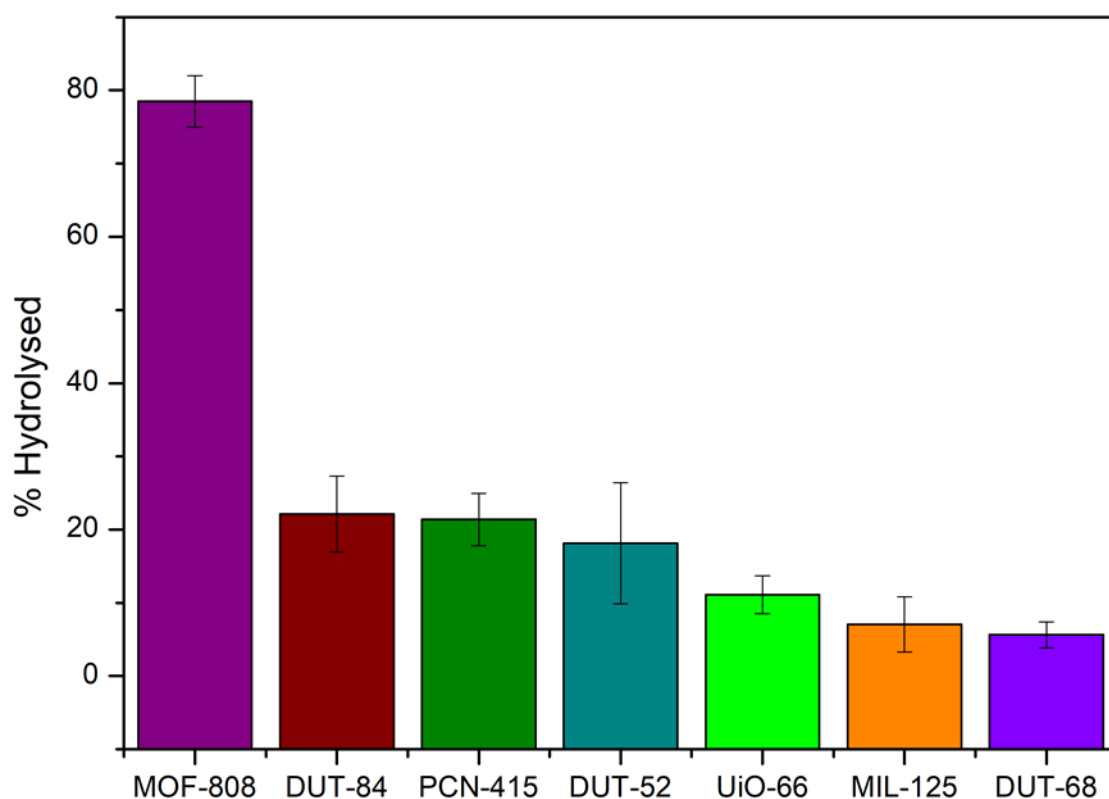
Figure 3.10 Hydrolysis plots of diglycine comparing the catalytic activity of a number of MOFs after 7 days. Error bars calculated from standard deviation, this was taken from 3 repeats of the hydrolysis experiment.

All the MOF catalysts used in this study were used in a 1:50 molar ratio (MOF: diglycine). The results of the hydrolysis of diglycine show the superiority of MOF-808s catalytic activity, this can be attributed to it having a greater number of active sites and a larger pore volume.

3.3.3.1 Connectivity
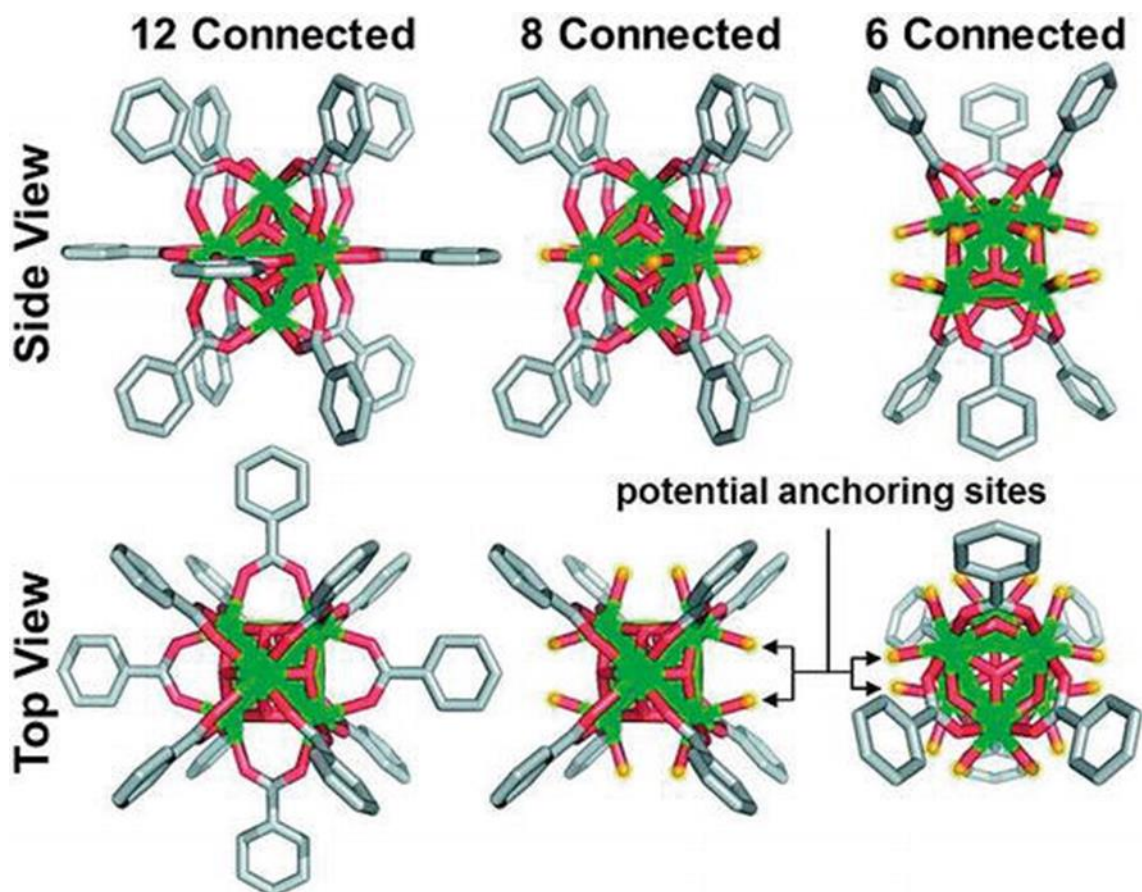
Figure 3.11 Illustration showing 6,8 and 12 connected nodes from both a top and side-on view. Adapted with permission from Ref.[24] Carbon (grey), oxygen (red), zirconium (green) and active sites (yellow).

MOF-808 and DUT-84 are 6-connected so they have a greater number of active sites than any MOFs with 8 or 12-connections. DUT-68 is 8-connected so has fewer active sites than 6-connected but a greater number than 12-connected MOFs. PCN-415, DUT-52, UiO-66 and MIL-125 have 12-connected nodes, they have fewer active sites and rely on defects within their frameworks for these sites. Figure 3.11 shows the potential active sites for 6 and 8-connected nodes but indicates that those sites aren't present on the 12-connected framework, this explains the need for defects within the structure to form these active sites.

3.3.3.2 Organic Linkers

Figure 3.12 Illustration showing the organic linkers used in each of the MOFs.

The difference in the size of the organic linker can also affect the catalytic activity of the MOF.

MOF-808s linker is trimesic acid which is a tricarboxylic acid, UiO-66, MIL-125 and PCN-415

have a terephthalic acid linker which is a dicarboxylic acid. DUT-52 and DUT-84s organic linker
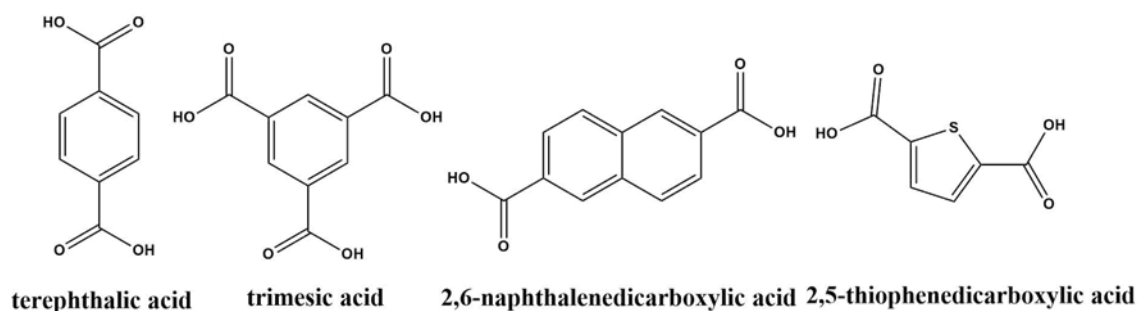
is 2,6-naphthalenedicarboxylic acid and DUT-68s is 2,5-thiophenedicarboxylic acid. The size of

these organic linkers differ which subsequently effects the activity of each MOF, the

relationship between the organic linker used and the connectivity of the MOF alters their

catalytic properties.

3.3.3.3 Porosity

MOF	Pore Volume (cm^3/g)	Literature Pore Volume (cm^3/g)
MOF-808	0.34	0.78
DUT-52	0.01	0.57
DUT-68	0.16	0.41
DUT-84	0.02	0.29
UiO-66	0.19	0.52
PCN-415	0.14	0.47
MIL-125	0.21	0.44

Table 12 A table showing the pore volume of all the synthesised MOFs and previously reported literature values.[5,11,12,13,20,21]

The porosity of each MOF is expected to show a correlation with active sites, and therefore

catalytic activity. However, this correlation isn't witnessed in the results of the hydrolysis. This

can be attributed to the effects of both connectivity and organic linkers ultimately altering

active sites and the surface area of each MOF. In some experimental porosity values, it is also due to the non-crystalline nature of the MOF.

3.3.3.4 Hydrophobicity

The hydrophobicity of a MOFs structure will also affect the activity of a MOF in a hydrolysis reaction. Hydrophobic surfaces have an apparent contact angle greater than 90° in relation to water.[25] The dipeptide embeds into the pores of the MOF in a highly hydrophobic material, therefore inhibiting the hydrolysis of the dipeptide. The more hydrophobic the MOF, the greater the inhibition of hydrolysis.[26] Trimesic acid and terephthalic acid have been used in hydrophobic MOFs in previous studies.[27,28] However, these previous studies include the post modification of these MOFs, suggesting that in some cases post modification is required in order to induce the hydrophobicity of these materials. Post modification is not always essential as sometimes hydrophilic groups are added in this step.

3.3.3.5 Buffer

Buffers have been used in previously reported procedures to give a more neutral pH and optimise conditions.[22,23] The pH when a buffer was used was 7.4, a neutral pH was determined to be the optimal value for hydrolysis reactions. MOF-808s pH was measured previously in chapter 2, it was 3.64 in the hydrolysis reaction with D_2O. The literature study suggests a more acidic pH decreases reaction rate as the acidic conditions inhibit the active sites (Zr-O to Zr-OH), so therefore without a buffer a slower reaction rate for all MOFs is expected. This is due to the acidic conditions inhibiting active sites

3.3.3.6 Overall Effects on Hydrolysis Results

MOF-808 is 6-connected so it has a greater number of active sites than any MOFs with 8 or 12-connections. DUT-84 is the only other MOF used with a 6-connected node, where it varies from MOF-808 is there difference in organic linker. DUT-84 has 2,6-napthalenedicarboxylic acid (2,6-ndc^{2-}) as its organic linker, MOF-808s organic linker is 1,3,5-benzenetricarboxylic acid (btc^{3-}). btc^{3-} is a larger linker than 2,6-ndc^{2-} as it has wider tetrahedral and octahedral cavities,

so therefore it produces a greater amount of porosity as a result of these larger cavities. MOF-808s pore size was 0.34 compared to 0.02 in DUT-84, which inherently improves catalytic activity due to its larger porosity.[29] The difference between MOF-808 and PCN-415, DUT-52, UiO-66 and MIL-125 is their 12-connected nodes, they have less active sites and rely on defects within their frameworks for these sites. The difference between PCN-415, UiO-66 and MIL-125 will be explained in more depth in the following section. The varying catalytic activity in the zirconium 12-connected MOFs DUT-52 and UiO-66 could be their difference in organic linker. In this case DUT-52s linker 2,6-ndc^{2-} is larger than UiO-66s 1,4-benzenedicarboxylic acid (bdc^{2-}) linker. The MOF with the least catalytic activity in this study was DUT-68, which has an 8-connected node and 2,5-thiophenedicarboxylic acid (tdc^{2-}) as its organic linker. Previous reports show that 12-connected MOFs show the lowest catalytic activity and there is an increase to the 8 and then 6-connected MOFs, however the results in this chapter do not follow that trend.[9,10] UiO-66 has a slightly larger surface area and pore volume than DUT-68 as shown in Table 2, which could explain the slight increase in catalytic activity in UiO-66.[20] The results of the hydrolysis studies using DUT-52 and DUT-84 was affected by them being non-porous during synthesis, so their catalytic activity was greatly affected.

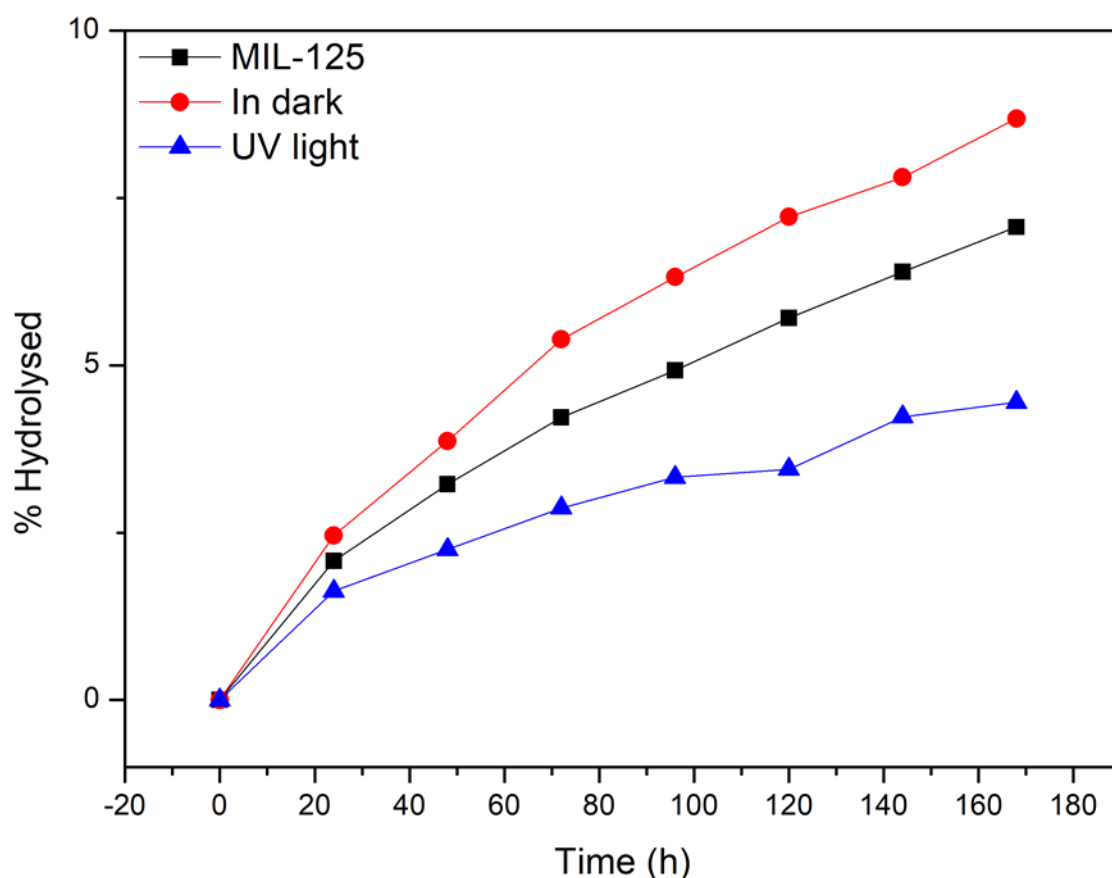## 3.3.4 Titanium and Bimetallic (Ti/Zr) MOFs

3.3.4.1 MIL-125

Figure 3.13 Hydrolysis plot of diglycine in D_2O using PCN-415 as a catalyst under visible light, UV light and in the dark.

MIL-125 is a titanium-based MOF with a terephthalic acid organic linker, and it has a 12-connected Ti-node. The hydrolysis studies in the previous section showed poor catalytic activity for all the MOFs other than MOF-808. Therefore, the titanium-MOF was looked at in more detail due to its potential as a light-activated catalyst at 350 nm as transient excited states are formed.[30] MIL-125 was tested under UV light and in the dark using the same conditions as shown in 3.2.11, but UV light was used (320-400 nm) and the NMR tube was covered with tin foil to achieve dark conditions. The results shown in figure 3.13 show no real photocatalytic activity under either condition, which was expected for the reaction in the dark as it wasn't photoactivated. However, the use of a photocatalyst was expected to cause a chemical reaction that involves the absorption of light by one or more reacting species

accelerating a photoreaction.[31] Previous studies have shown that in some cases the MOF

needs to be amino functionalised to initiate its photoactivity.[32] Although there was very little

difference in the percentage hydrolysis in all three reaction conditions, the reaction in the dark

did prove the most effective whereas under UV light it appeared to be the least effective of the

three conditions.

3.3.4.2 PCN-415
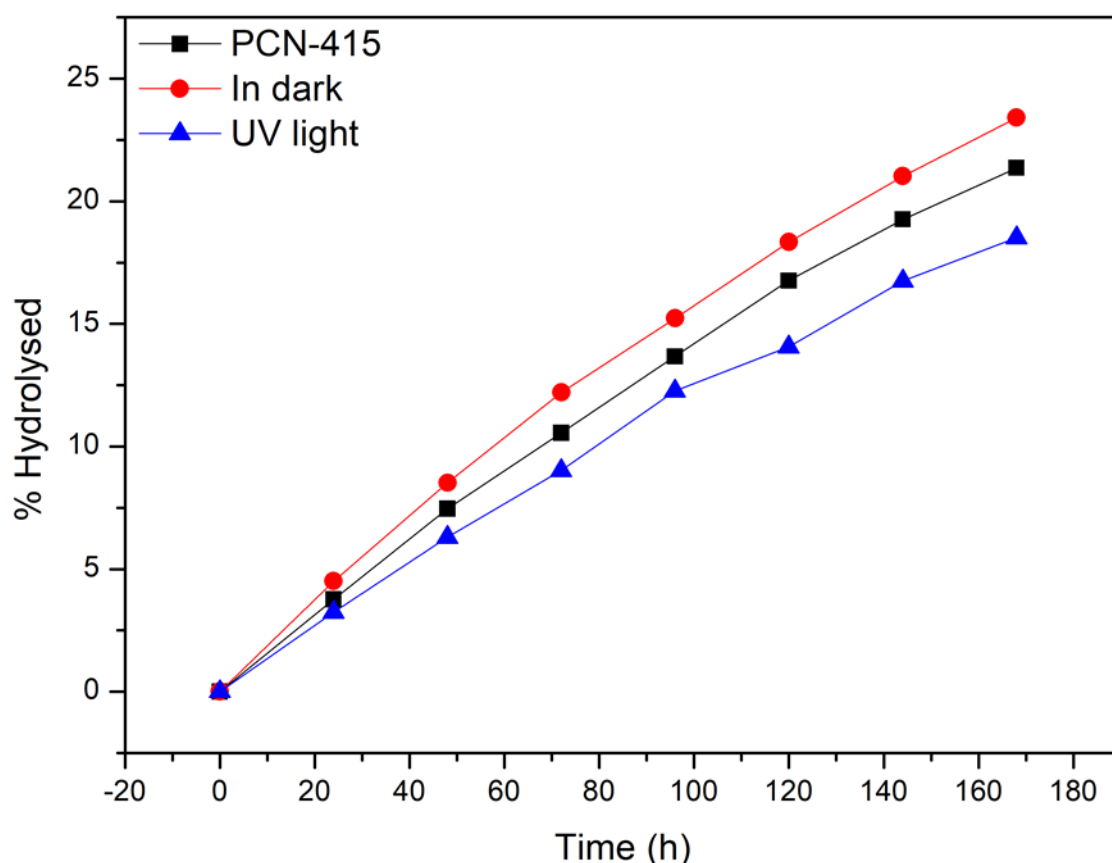
Figure 3.14 Hydrolysis plot of diglycine in D$_2$O using PCN-415 as a catalyst under visible light, UV light and in the dark.

PCN-415 is a bimetallic MOF combining zirconium and titanium metal centres with a

terephthalic acid organic linker, and it has a 12-connected node. The hydrolysis studies have

previously shown poor catalytic activity for all the MOFs other than MOF-808. Therefore, the

bimetallic MOF was looked at in more detail due to its potential as a photocatalyst at 350 nm

as transient excited states are formed.[30]. PCN-415 was tested under UV light and in the dark

using the same conditions as shown in 3.2.11, but UV light was used (320-400 nm) and the

NMR tube was covered with tin foil to achieve dark conditions. The results shown in figure 3.14 show no real photocatalytic activity under either condition, which was expected for the reaction in the dark as it wasn't photoactivated. Previously, studies have shown that the MOF may need to be amino functionalised to initiate its photoactivity.[32] Once again there was very little difference in the percentage hydrolysis in all three reaction conditions, the reaction in the dark did prove the most effective whereas under UV light it appeared to be the least effective of the three conditions.

3.3.5 Comparison of 12-connected MOFs
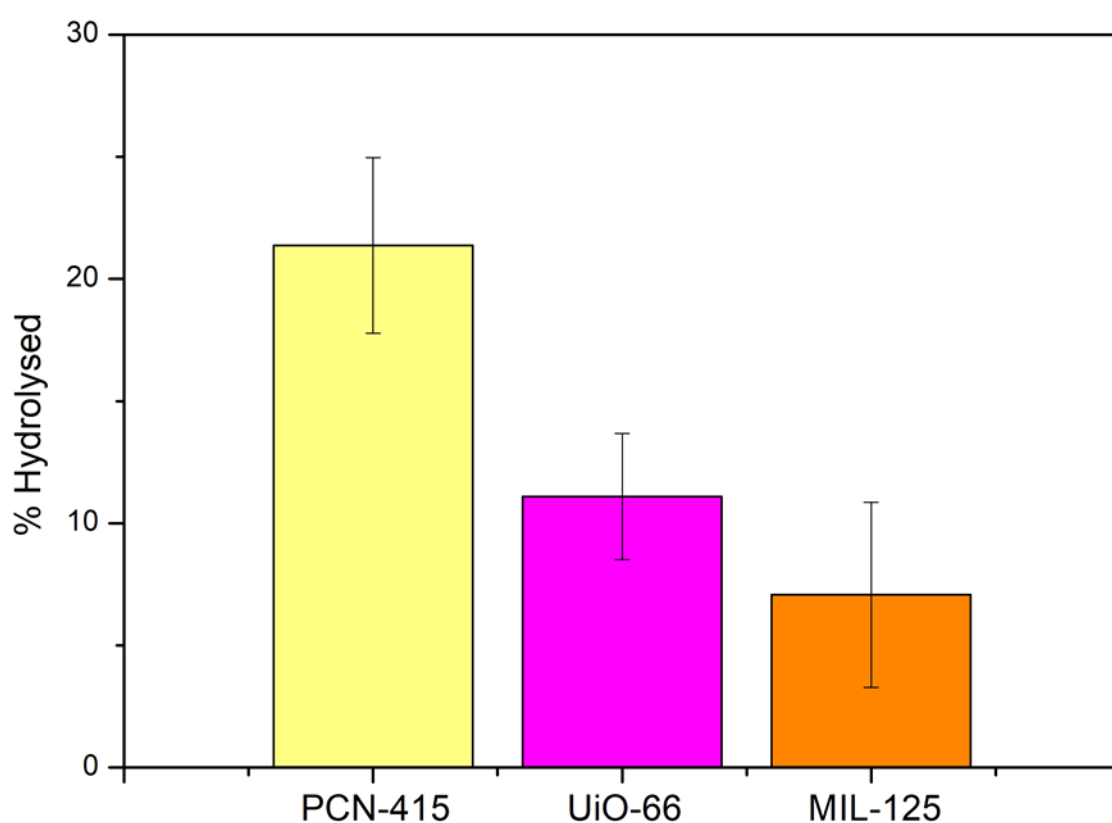
Figure 3.15 Hydrolysis plots of diglycine comparing the 12-connected UiO-66 (Zr), MIL-125 (Ti) and PCN-415 (Zr/Ti) MOFs after 7 days. Error bars calculated from standard deviation, this was taken from 3 repeats of the hydrolysis experiment.

PCN-415, UiO-66 and MIL-125 all have the same 12-connected node and organic linker bdc^{2-}. The difference in these MOFs is their metal centres, UiO-66 has a zirconium metal centre, MIL-125 has titanium and PCN-415 has zirconium/titanium bimetallic. Titanium-MOFs are generally sensitive to reaction conditions, which correlates to a lower catalytic activity. UiO-66 is

zirconium based so it is more stable in the reaction and therefore the amount of hydrolysis that occurs is greater. In PCN-415, the combination of zirconium and titanium combines their desirable characteristics, titanium based MOFs generally have larger surface areas and higher porosity and zirconium MOFs have greater stability.[4] Subsequently, the stable bimetallic MOF formed has greater catalytic activity which is shown in the graph above, there is a significant increase in percentage hydrolysis.

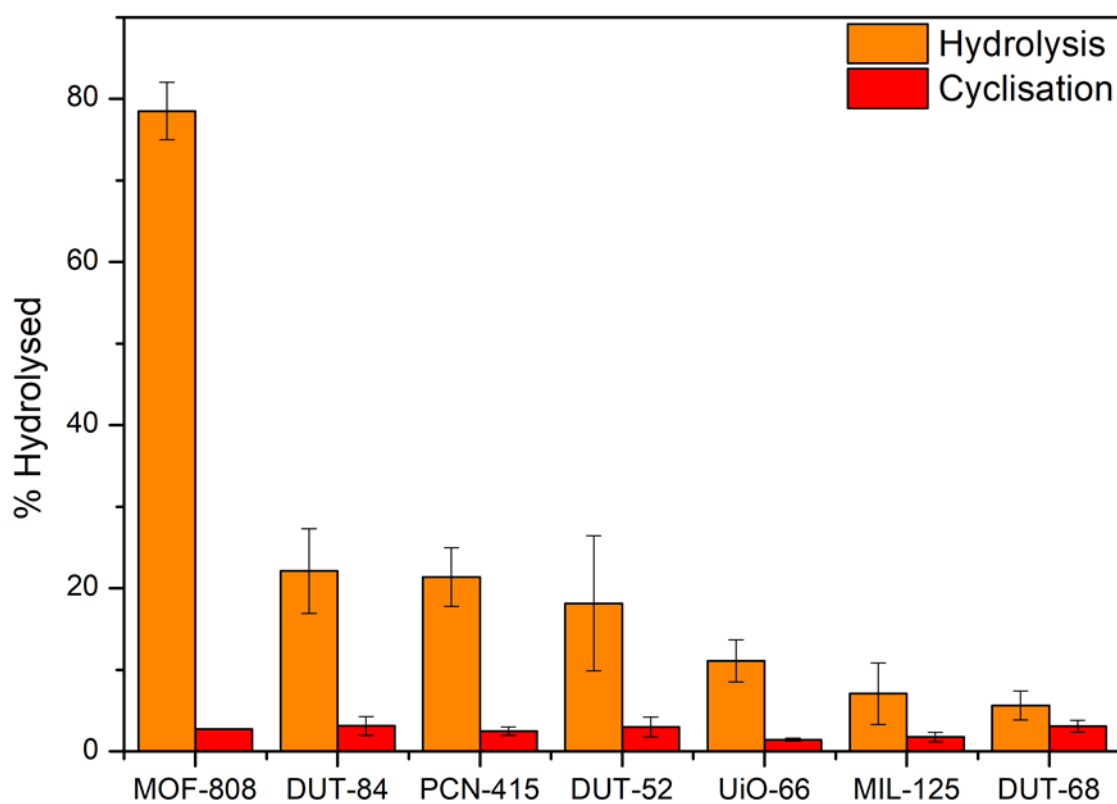## 3.3.6 Comparison of Hydrolysis and Cyclisation Products

Figure 3.16 Plots showing the comparison of hydrolysis against cyclisation using the MOFs as catalysts after 7 days. Error bars calculated from standard deviation, this was taken from 3 repeats of the hydrolysis experiment.
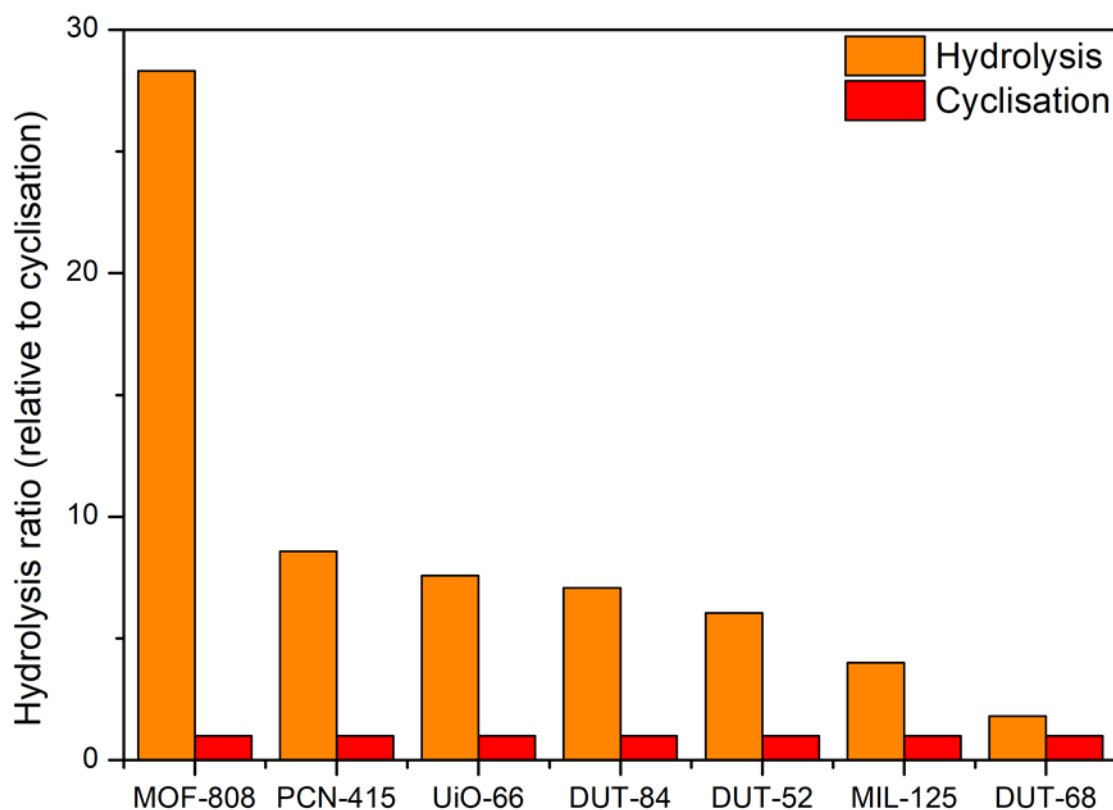
Figure 3.17 Plot showing the ratio of hydrolysis product against cyclisation with increasing 'preference' for the cyclisation product.

MOFs show a selectivity towards the preferred product, in this study all the MOFs show a general selectivity towards the hydrolysis product. However, DUT-68 is less selective towards the production of glycine and produces a significant amount of the cyclisation product of glycine. This is due to the number of strong Zr Lewis acid sites within the framework being greater, so therefore it is unable to inhibit the interaction with the diglycine bond that needs to be split to form glycine molecules as effectively.[33]

3.4 Conclusions

The original aims of this section were to synthesise a number of MOFs to use as catalytic comparisons to the well reported MOF-808. Originally several Zr-MOFs were synthesised, but to broaden the research MOFs with a different metal centre (Ti) and a combination of two metal centres (Ti/Zr) were synthesised. The synthesis of these two MOFs led to further comparisons being made, not just ones with MOF-808. The way the different metal centres act in catalysis is clear due to their reported properties. Ti-MOFs are sensitive to reaction

conditions but have good reactivity properties when stable, Zr-MOFs are said to have high thermal and chemical stability.[2,4] This led to the simple conclusion that the combination of these two metal centres could result in a highly reactive stable MOF. The results of the hydrolysis supported this theory as the bimetallic MOF showed much greater activity when compared to its equivalent Zr and Ti-MOFs. To further investigate the efficacy of a bimetallic MOF, the equivalent to MOF-808, which was the most effective catalytic MOF in this study, could be synthesised. If the catalytic activity of the bimetallic equivalent to MOF-808 follows the same trend as in this study, the proposed MOF would be able to achieve high levels of catalytic activity. The overall comparison of MOFs showed that MOF-808 has greater catalytic activity when compared to the other synthesised MOFs. The reason for this was clearly defined in literature as a difference in connections changing the activity of the MOF, and the larger the ligand used the more porous the framework is.[29] Comparison of the other MOFs to one another also followed this trend, as porosity of samples can be found in literature and correlated to the level of hydrolysis from these studies. The outcome of this study clearly showed that MOF-808 is the best option as a catalyst in hydrolysis studies, but there is potential for improvement in a bimetallic framework.

3.5 References

1   C. Li, H. Xu, J. Gao, W. Du, L. Shangguan, X. Zhang, R. B. Lin, H. Wu, W. Zhou, X. Liu, J. Yao and B. Chen, *J. Mater. Chem. A*, 2019, **7**, 11928–11933.

2   M. Kandiah, M. H. Nilsen, S. Usseglio, S. Jakobsen, U. Olsbye, M. Tilset, C. Larabi, E. A. Quadrelli, F. Bonino and K. P. Lillerud, *Chem. Mater.*, 2010, **22**, 6632–6640.

3   L. Zou, D. Feng, T. F. Liu, Y. P. Chen, S. Yuan, K. Wang, X. Wang, S. Fordham and H. C. Zhou, *Chem. Sci.*, 2016, **7**, 1063–1069.

4   D. Sun and Z. Li, *Chinese J. Chem.*, 2017, **35**, 135–147.

5   S. Yuan, J. S. Qin, H. Q. Xu, J. Su, D. Rossi, Y. Chen, L. Zhang, C. Lollar, Q. Wang, H. L. Jiang, D. H. Son, H. Xu, Z. Huang, X. Zou and H. C. Zhou, *ACS Cent. Sci.*, 2018, **4**, 105–111.

6   J. B. Decoste and G. W. Peterson, *Chem. Rev.*, 2014, **114**, 5695–5727.

7   P. Valvekens, F. Vermoortele and D. De Vos, *Catal. Sci. Technol.*, 2013, **3**, 1435–1445.

8   S. Yuan, J. S. Qin, C. T. Lollar and H. C. Zhou, *ACS Cent. Sci.*, 2018, **4**, 440–450.

9   J. E. Mondloch, M. J. Katz, W. C. Isley, P. Ghosh, P. Liao, W. Bury, G. W. Wagner, M. G. Hall, J. B. Decoste, G. W. Peterson, R. Q. Snurr, C. J. Cramer, J. T. Hupp and O. K. Farha, *Nat. Mater.*, 2015, **14**, 512–516.

10   S. Y. Moon, Y. Liu, J. T. Hupp and O. K. Farha, *Angew. Chemie - Int. Ed.*, 2015, **54**, 6795–6799.

11   W. Liang, H. Chevreau, F. Ragon, P. D. Southon, V. K. Peterson and D. M. D'Alessandro, *CrystEngComm*, 2014, **16**, 6530–6533.

12   V. Bon, I. Senkovska, M. S. Weiss and S. Kaskel, *CrystEngComm*, 2013, **15**, 9572–9577.

13   V. Bon, I. Senkovska, I. A. Baburin and S. Kaskel, *Cryst. Growth Des.*, 2013, **13**, 1231–1237.

14   F. Vermoortele, B. Bueken, G. Le Bars, B. Van De Voorde, M. Vandichel, K. Houthoofd, A. Vimont, M. Daturi, M. Waroquier, V. Van Speybroeck, C. Kirschhock and D. E. De Vos, *J. Am. Chem. Soc.*, 2013, **135**, 11465–11468.

15   S. N. Kim, J. Kim, H. Y. Kim, H. Y. Cho and W. S. Ahn, *Catal. Today*, 2013, **204**, 85–93.

16   H. Furukawa, F. Gándara, Y. B. Zhang, J. Jiang, W. L. Queen, M. R. Hudson and O. M. Yaghi, *J. Am. Chem. Soc.*, 2014, **136**, 4369–4381.

17   L. Valenzano, B. Civalleri, S. Chavan, S. Bordiga, M. H. Nilsen, S. Jakobsen, K. P. Lillerud and C. Lamberti, *Chem. Mater.*, 2011, **23**, 1700–1718.

18   M. Dan-Hardi, C. Serre, T. Frot, L. Rozes, G. Maurin, C. Sanchez and G. Férey, *J. Am. Chem. Soc.*, 2009, **131**, 10857–10859.

19   R. Matshitse, *Rhodes Univ. Natl. Res. Found.*

20   Y. Bai, Y. Dou, L. H. Xie, W. Rutledge, J. R. Li and H. C. Zhou, *Chem. Soc. Rev.*, 2016, **45**, 2327–2367.

21   N. D. McNamara, G. T. Neumann, E. T. Masko, J. A. Urban and J. C. Hicks, *J. Catal.*, 2013, **305**, 217–226.

22   H. G. T. Ly, G. Fu, A. Kondinski, B. Bueken, D. De Vos and T. N. Parac-Vogt, *J. Am. Chem. Soc.*, 2018, **140**, 6325–6335.

23   M. J. Katz, S. Y. Moon, J. E. Mondloch, M. H. Beyzavi, C. J. Stephenson, J. T. Hupp and O. K. Farha, *Chem. Sci.*, 2015, **6**, 2286–2291.

24   T. F. Liu, N. A. Vermeulen, A. J. Howarth, P. Li, A. A. Sarjeant, J. T. Hupp and O. K. Farha, *Eur. J. Inorg. Chem.*, 2016, **2016**, 4266.

25   K. Jayaramulu, F. Geyer, A. Schneemann, Š. Kment, M. Otyepka, R. Zboril, D. Vollmer and R. A. Fischer, *Adv. Mater.*, 2019, **31**, 1–31.

26   C. Montoro, F. Linares, E. Quartapelle Procopio, I. Senkovska, S. Kaskel, S. Galli, N. Masciocchi, E. Barea and J. A. R. Navarro, *J. Am. Chem. Soc.*, 2011, **133**, 11888–11891.

27   W. Zhang, Y. Hu, J. Ge, H. L. Jiang and S. H. Yu, *J. Am. Chem. Soc.*, 2014, **136**, 16978–16981.

28   N. Ding, H. Li, X. Feng, Q. Wang, S. Wang, L. Ma, J. Zhou and B. Wang, *J. Am. Chem. Soc.*, 2016, **138**, 10100–10103.

29   A. M. Ebrahim, B. Levasseur and T. J. Bandosz, *Langmuir*, 2013, **29**, 168–174.

30   J. Bedia, V. Muelas-ramos, M. Peñas-garz, G. Almudena, J. J. Rodr and C. Belver, Catal., 2019, **9**, 52.

31   C. Xu, P. Ravi Anusuyadevi, C. Aymonier, R. Luque and S. Marre, *Chem. Soc. Rev.*, 2019, **48**, 3868–3902.

32   Y. Fu, D. Sun, Y. Chen, R. Huang, Z. Ding, X. Fu and Z. Li, *Angew. Chemie - Int. Ed.*, 2012, **51**, 3364–3367.

33   F. Vermoortele, A. Vimont, C. Serre and D. De Vos, *Chem. Commun.*, 2011, **47**, 1521–1523.

Chapter 4 – Thesis Conclusions and Future Work

The aims of this thesis were to synthesise a MOF with high catalytic activity for hydrolysis studies with a dipeptide. In addition, the MOF was encapsulated within a polymer network to form a swellable composite with a stable catalyst embedded within it. The polymer would then be tested for its recyclability and reusability as a catalyst. A number of other well known MOFs with different metal centres and organic linkers were studied alongside the originally selected MOF. A comparison of all of the MOFs catalytic abilities would be monitored through dipeptide hydrolysis. A swellable composite was useful as it was able to encapsulate the dipeptide to swelling degrees up to $Q = 40$, and then subsequently hydrolyse the dipeptide. The use of a solid support catalyst like a polyHIPE is that it provides mechanical stability that is not as prominent in just a powder form.

Chapter 2 described the incorporation of MOF-808 with the polyHIPE to form the polyHIPE-MOF. Following swelling studies of both the polyHIPE and polyHIPE-MOF it was shown that the hydrolytic proficiency of the composite had not reduced. MOF-808 and the polyHIPE-MOF were then used as catalysts in the hydrolysis of diglycine. For MOF-808, there were changes in the variables for this reaction such as the molar ratio between catalyst and diglycine and the temperature. In a molar ratio of 1:50 diglycine:MOF-808, the MOF still showed impressive catalytic activity with an 80% conversion over 7 days, compared with 1:1 in literature which reached complete conversion after 3 hours and 1:2 in this study which reached complete conversion after 7 days. During, the studies with MOF-808, THF was also used as a solvent as it became clear during the swelling studies of the polyHIPE-MOF that an organic solvent was required to be absorbed into the polymer matrix to enable accessibility to the catalyst. Therefore, the hydrolysis studies with the polyHIPE-MOF could be compared with MOF-808 to see if the MOFs proficiency as a catalyst was maintained within the polymer. In a D_2O/THF solvent mix the polyHIPE-MOF in a molar ratio of 1:50 diglycine:polyHIPE-MOF, the hydrolysis reaches around 60% conversion indicating the MOF has maintained its propensity as a catalyst within the polymer. Furthermore, the important of THF and the subsequent swelling of the polymer was demonstrated in the study using just D_2O as the solvent, with only 3% conversion

to glycine achieved proving that an organic solvent is required to absorb into the polymer enabling access to the catalyst. Further studies with the polyHIPE-MOF included a scale-up reaction with almost 1 g of polyHIPE being used compared to 0.0050 g of polyHIPE used in studies in an NMR tube, and the potential recyclability and reusability of the material. In the scale up reaction, the conversion to glycine was 70% implying that in a large scale reaction, the polymer is just as effective. After 3 cycles in a recyclability/reusability study, the hydrolysis conversion was largely consistent. Initial results suggest it can be recycled and reused, however further investigation will be required to confirm that consistent results are achieved and that the polymer-supported catalyst is truly reusable.

Chapter 3 described investigations into the use of alternative MOFs in the hydrolysis of diglycine, with MOFs containing a variety of organic linkers, connectivity and metal centres/ions studied. All of the MOFs used were compared to MOF-808 as it was the only MOF previously used in the hydrolysis of diglycine. UiO-66 (12-connected), PCN-415 (12-connected), DUT-52 (12-connected), MIL-125 (12-connected), DUT-68 (8-connected) and DUT-84 (6-connected) were used alongside MOF-808 (3,6-connected) in this study. The importance of connections, metal centre and organic linker were highlighted in this study. As a general trend, 6-connected MOFs have the greatest catalytic activity followed by 8-connected and then 12-connected which rely on structural defects for active sites. 6 and 8-connected MOFs have a number of active sites present within their structures after synthesis. MOF-808 was the most porous of the MOFs in this study and it had the largest surface area. MOF-808 showed the greatest catalytic activity which is expected due to its 6-connected nodes. However, DUT-68 which is 8-connected showed the least catalytic activity in these hydrolysis studies, this can be attributed to UiO-66 having a slightly larger surface area and pore volume than DUT-68. The difference in reactivity between metal centres was compared between UiO-66 (Zr), MIL-125 (Ti) and PCN-415 (Zr/Ti). The bimetallic MOF, PCN-415 showed the greatest catalytic activity out of the three different metal centres. Ti-MOFs are generally sensitive to reaction conditions,

which correlates to a lower catalytic activity whereas Zr-MOFs are generally more stable. However, the combination of zirconium and titanium metal centres combines their desirable characteristics, titanium based MOFs generally have larger surface areas and higher porosity and zirconium MOFs have greater stability. Subsequently, PCN-415 has greater catalytic activity than both UiO-66 and MIL-125, which is outlined in the hydrolysis results. Finally, the selectivity of each MOF showed that all of the MOFs had a selectivity for glycine over the cyclisation form of glycine but in vastly different degrees.

Overall, the aims of this thesis were met with MOF-808 being synthesised and then incorporated into the polyHIPE. An understanding of the polyHIPE-MOFs swelling capabilities were studied showing the importance of an organic solvent in the subsequent hydrolysis studies. Both MOF-808 and the polyHIPE-MOF were effective in hydrolysis studies with diglycine and the scalability and recyclability/reusability showed promising properties. The other MOFs synthesised indicated the superiority of MOF-808s structural design with a stable zirconium metal centre and an organic linker, which resulted in large surface areas and high porosity, which were pivotal in catalytic reactions. The formation of a bimetallic MOF produced interesting results, which can be further studied to provide a potentially highly catalytic, stable MOF.

Further work of this project would look at different solvent mixes used in the hydrolysis studies, as the swelling value of the polyHIPE-MOF increases with greater THF content, although the ideal solvent mix would be to use as little organic solvent as possible. Further testing of the polyHIPE-MOF when scaled up and recycled/reused would be required to prove they it can be used on a larger scale efficiently and to ensure that the material can be used for a number of cycles with just as effective catalytic activity. Finally, the promising properties of the bimetallic MOF suggested that if the perfect combination of organic linker and connected node were found, they could be used with the stable zirconium and titanium metal centre. The

resulting MOF may prove to be even more efficient than MOF-808 in catalytic studies if it

follows the same trend as with UiO-66 and PCN-415.